HIGH-PRESSURE OPTICAL STUDIES OF III-V SEMICONDUCTORS USING THE DIAMOND ANVIL CELL.

Jonathan L. Sly

A thesis submitted to the Faculty of Science at the University of Surrey for the degree of Doctor of Philosophy.

Department of Physics

University of Surrey

August 1995.

ABSTRACT.

High pressure photoluminescence techniques have been used to investigate bulk and heterostructure properties in a number of III-V semiconductor materials systems. The results are reported in this thesis along with a description of the experimental procedures.

The indirect band-gaps of a series of $In_xGa_{1-x}Sb/GaSb$ quantum-wells have been measured. The results have been extrapolated to zero indium content to give the indirect band-gaps of bulk GaSb; values quoted in the literature vary widely. We obtain results consistent with accepted values but cannot refine them due to experimental errors arising from using ruby as a pressure gauge. A development of the experimental technique is proposed which would eliminate this source of error.

The low-temperature Γ and X band-gaps have been determined in bulk $(Al_xGa_{1-x})_{0.5}In_{0.5}P$ as functions of composition; we obtain $E_g(\Gamma)=(1.985+0.61x)$eV and $E_g(X)=(2.282+0.085x)$eV respectively. Lower limits have been put on the position of the L minima in this system and 1% compressively strained $Ga_{0.38}In_{0.62}P$. Band offsets have been determined in unstrained (y=0.5) and 1% (y=0.62) compressively strained $Ga_{1-y}In_yP/(Al_xGa_{1-x})_{0.5}In_{0.5}P$; we obtain $\Delta E_v(\text{meV})=63x+157x^2$ and $\Delta E_c(\text{meV})=547x-157x^2$ for the unstrained system and $\Delta E_v(\text{meV})=72+63x+157x^2$ and $\Delta E_c(\text{meV})=72+547x-157x^2$ for the strained system. Effects of atomic ordering on the conduction band of $Ga_{0.5}In_{0.5}P$ have been investigated.

An investigation of anomalous pressure coefficients in strained $In_xGa_{1-x}As$ has been carried out. A strain-related reduction in pressure coefficients (similar to that reported for $In_xGa_{1-x}As/GaAs$) is found in $In_{0.67}Ga_{0.33}As/InGaAsP$ quantum-wells grown on [001]

substrates, but not in InGaAs/GaAs grown on [111] substrates. Preliminary results from tensile samples show evidence of *increased* pressure coefficients. A new X-ray powder-diffraction technique is described for direct investigation of the elastic behaviour of strained InGaAs.

Acknowledgements.

I would like to thank all of the staff of the Physics Department at the University of Surrey for the help I have received during the course of this research; particular thanks go to Andy Prins and Alistair Meney. I also gratefully acknowledge the financial support of the EPSRC. Above all, though, I am grateful to Dave Dunstan for his excellent supervision, timely encouragement and for always having an answer (not always *the* answer, but always *an* answer)!

Finally, I am especially grateful to Dr A.T.Meney for carrying out the band structure calculations used throughout this work (see chapters 4, 5 and 6).

Publications.

1. "High Pressure Determination of AlGaInP Band Structure", A.D.Prins, J.L.Sly, A.T.Meney, D.J.Dunstan, E.P.O'Reilly, A.R.Adams and A.Valster, *J. Phys. Chem. Solids* **56**, 349 (1995)

2. "Direct Measurement of Band Offsets in GaInP/AlGaInP Using High Pressure", A.D.Prins, J.L.Sly, A.T.Meney, D.J.Dunstan, E.P.O'Reilly, A.R.Adams and A.Valster, *J. Phys. Chem. Solids* **56**, 423 (1995)

3. "Determination of the Band Structure of Disordered AlGaInP and its Influence on Visible-Laser Characteristics", A.T.Meney, A.D.Prins, A.F.Phillips, J.L.Sly, E.P.O'Reilly, D.J.Dunstan, A.R.Adams and A.Valster, *IEEE Journal of Selected Topics in Quantum Electronics* **1**, 697 (1995)

4. "Band Structure Measurements of AlGaInP", A.D.Prins, J.L.Sly, A.T.Meney, D.J.Dunstan, E.P.O'Reilly, A.R.Adams and A.Valster, *Proc. 22nd Int. Conf. Phys. Semicond.*, Vancouver, Canada, August 15th-19th, (1994)

5. "Direct Determination of Band Offsets in GaInP/AlGaInP Heterostructures", A.D.Prins, J.L.Sly, A.T.Meney, D.J.Dunstan, E.P.O'Reilly, A.R.Adams and A.Valster, *Proc. 22nd Int. Conf. Phys. Semicond.*, Vancouver, Canada, August 15th-19th, (1994)

6. "Pressure Induced Shallow-Deep A_1 Transition For Sn Donor In GaAs Observed in Diamond Anvil Cell Photoluminescence Experiment", J.E.Dmochowski, R.A.Stradling, J.L.Sly, D.J.Dunstan, A.D.Prins and A.R.Adams, *Acta Physica Polonica A* **87**, 457 (1995)

CONTENTS.

CHAPTER 1.

Introduction.

With modern semiconductor growth techniques such as Metal-Organic Vapour-Phase Epitaxy (MOVPE) and Molecular Beam Epitaxy (MBE) the design, fabrication and application of optoelectronic devices is becoming evermore widespread. For example, a great deal of research is currently being carried out with the aim of optimising the efficiency and operating-wavelength of semiconductor lasers both at long wavelengths, for fibre-optic communication applications, and at visible wavelengths, for optical data-storage applications.

Fundamental to the successful design of any optoelectronic device is a full and accurate knowledge of the electronic band-structure and material parameters of the constituent materials. In addition, in the case of quantum-well (QW) and other such heterostructure devices, a knowledge of the line-up of the band-structures at the interfaces between the constituent materials (the band offsets) is particularly important.

The application of hydrostatic pressure to a crystal structure causes a reduction in the lattice constant of the material but maintains the symmetry of the crystal. Even relatively small changes in lattice constant can give rise to substantial perturbations in the band-structure of a semiconductor. By using optical measurement techniques such as photoluminescence and absorption, carried out as a function of pressure in the diamond anvil cell (DAC), it is possible to obtain accurate and unambiguous information about band-structure and materials parameters in both bulk and heterostructure systems.

This thesis is arranged as follows:

Chapter 2 contains a brief summary of the behaviour of bulk and heterostructure semiconductor systems under the influence of hydrostatic pressure. Included in this is a discussion of the way in which photoluminescence techniques can be used, in conjunction with high pressures, to determine a variety of parameters.

In chapter 3 the experimental details and techniques used and developed throughout the course of this work are described in full.

Chapter 4 contains details of a programme of work in which the indirect band-gaps of a number of $In_xGa_{1-x}Sb/GaSb$ quantum-well structures have been measured for the first time. Using these results, a method is described for determining accurately the indirect band-gaps of bulk GaSb; the values of which are currently a matter of some debate.

Chapter 5 is the result of a comprehensive investigation of the AlGaInP semiconductor materials system. Bulk band-structure measurements have been made, including a determination of the compositional dependence of the conduction-band Γ and X energies in $(Al_xGa_{1-x})_{0.5}In_{0.5}P$. Band offsets have been measured, also as functions of composition, in both the unstrained and compressively strained $GaInP/(Al_xGa_{1-x})_{0.5}In_{0.5}P$ systems. Effects of atomic ordering on the conduction band of $Ga_{0.5}In_{0.5}P$ have been investigated. This represents the most complete, and experimentally consistent, high pressure study of this materials system so far carried out.

In chapter 6 the results are reported from a series of high pressure photoluminescence experiments to investigate anomalous band-gap pressure coefficients in strained InGaAs. Unexpectedly low pressure coefficients have previously been reported in compressively strained InGaAs/GaAs quantum-wells. In this chapter the investigation

of this phenomenon is extended to different alloy compositions, substrate orientations and, for the first time, to InGaAs under tensile strain. A novel high-pressure X-ray powder diffraction technique has been developed to help determine whether the cause of the anomalous results is related to the elastic properties of the strained material or rather is a problem of electronic band-structure.

Finally, in chapter 7, some concluding remarks are made.

CHAPTER 2.

III-V Semiconductors Under Hydrostatic Pressure.

2.1 Introduction.

This chapter provides a brief introduction to the basic principles underlying the use of hydrostatic pressure as a perturbation technique for investigating bulk and heterostructure semiconductors. The effects of pressure on the band structure of tetrahedrally-bonded bulk semiconductors are discussed. This discussion is then extended to include heterostructure systems and the influence of hydrostatic pressure on quantum-confined states. The chapter concludes with a brief review of the technique of photoluminescence and an introduction to some of the ways in which photoluminescence, carried out as a function of pressure, can yield fundamental bulk and heterostructure properties.

2.2 The Influence of Hydrostatic Pressure on Bulk III–V Semiconductors.

The electronic band structure of a semiconductor is determined by its constituent atoms and its crystalline structure. At the most fundamental level the effect of applying hydrostatic pressure to a semiconductor is to reduce its lattice constant whilst maintaining the overall symmetry of the crystal structure. The reduction in lattice constant is small (typically ~3% for 100kbar of applied pressure) but the resulting perturbation in the band structure is highly significant[1,2,3]. The increased interaction between adjacent atomic

orbitals has two principle effects; it increases the energy separation between bonding and antibonding states and gives rise to a broadening of the bands. As will become clear below, much of the power of hydrostatic pressure as an investigative technique comes from the fact that the overall effect of the applied pressure is substantially different for energy levels at different symmetry points in the Brillouin zone. Figure 2.1 is a schematic representation of the band structure of a typical tetrahedrally bonded semiconductor. It shows the high symmetry points of the Brillouin zone and indicates the way in which hydrostatic pressure changes the energies of the conduction band Γ, X and L minima with respect to the top of the valence band. The pressure coefficients shown here for the direct and indirect band-gaps represent a reasonable guide for the whole range of tetrahedrally bonded semiconductors[4]. It should be noted that although pressure coefficients are commonly quoted purely as a linear term this is not strictly accurate. If the pressure dependence of the direct band-gap of GaAs, for example, is measured over a sufficiently wide range of pressure a definite sublinearity becomes apparent[5]. Empirically it has been found that the pressure dependence of the direct band-gap of most III–V semiconductors can be fitted with a quadratic relationship of the following form:

$$E_g(P) = E_g(0) + \alpha P + \beta P^2 \qquad (2.1)$$

where α and β are constants of the order of +10meV/kbar and $-20\text{x}10^{-3}$meV/kbar respectively. Although pressure is the experimentally controlled variable, the more fundamental variable is the resultant change in lattice constant. The change in lattice constant can be related to applied pressure by an appropriate equation of state and it is

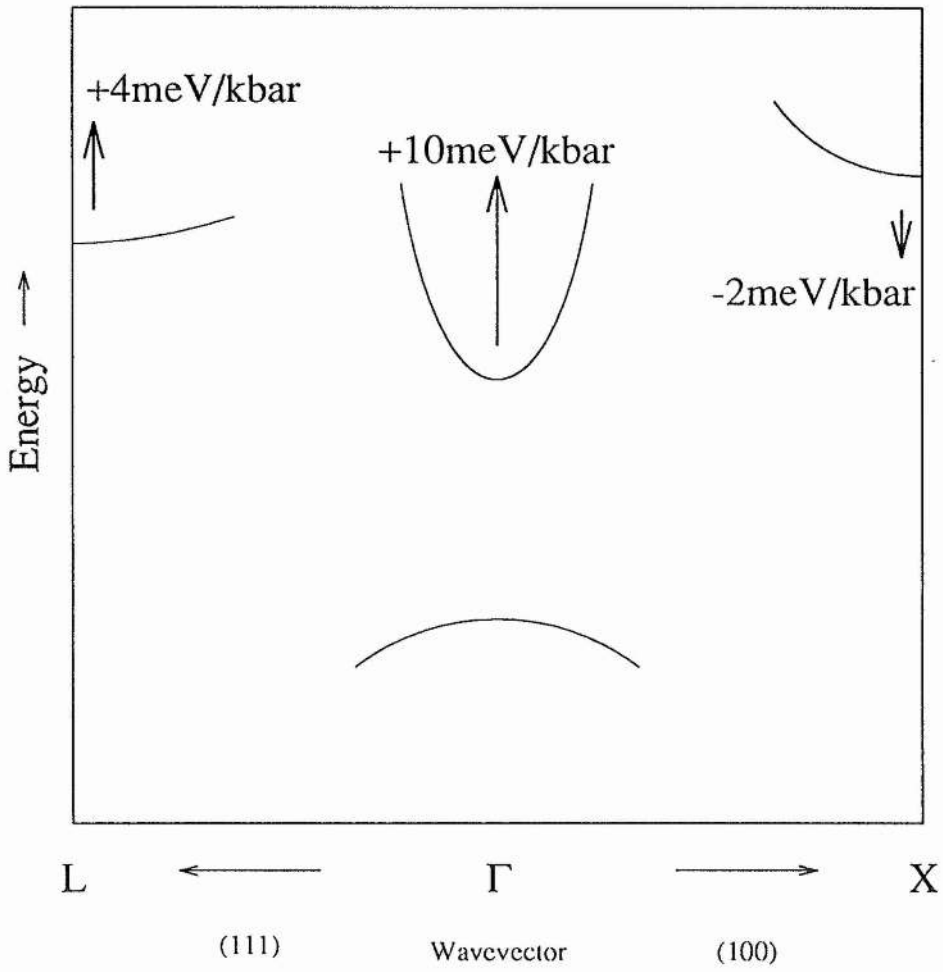

Figure 2.1 A schematic band diagram of a typical tetrahedrally bonded semiconductor showing the characteristic pressure coefficients of the high symmetry points with respect to the top of the valence band.

from here that the nonlinearity arises. This is discussed more fully in chapter 6 (section 6.4.1).

2.3 The Influence of High Pressure on Heterostructures.

Heterojunctions are formed at the interfaces between different semiconductor materials which have been grown as a single crystal. Given that the two materials have different band-gaps, there will clearly be band-edge discontinuities at the interfaces. Probably the most technologically important heterostructure is the quantum-well; essentially two back-to-back heterojunctions in which a material with a relatively small band-gap is sandwiched within a material having a larger band-gap. A crucial parameter in the design of any quantum-well device is a knowledge of the way in which this difference in band-gaps is distributed between the conduction and valence bands; the so-called band offsets. The various possible configurations for the line-up of bands at quantum-well interfaces can be classified broadly into two classes; those in which both electrons and holes are confined in the well material (Type–I) and those in which the electrons and holes are confined in different materials (Type–II)[6]. Figure 2.2 serves to illustrate this and also to define various terms and notation that will be used throughout this thesis.

If we are to apply high pressure techniques to heterostructures such as quantum-wells then, in addition to the bulk effects outlined above, we must also consider the influence of hydrostatic pressure on quantum-confined states. The important effects can be summarised as follows:

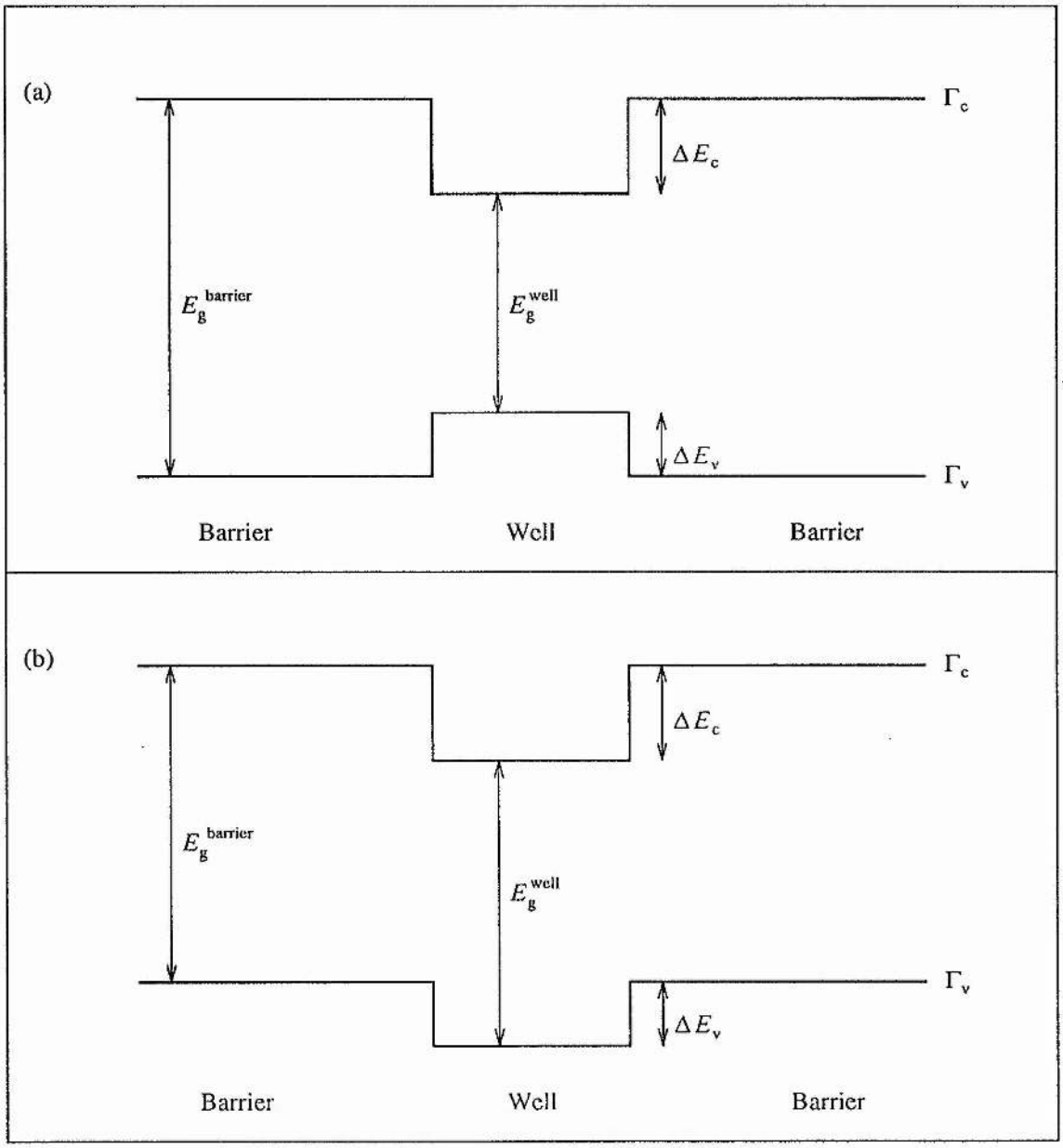

Figure 2.2 Two possible band configurations for a single quantum-well showing (a) a Type I configuration, in which electrons and holes are confined in the well material, and (b) a Type II configuration, in which electrons and holes are confined in different materials.

If the quantum-well and barrier materials have different pressure coefficients then, as pressure is applied, the confining potential will be changing. This can lead to a difference between the pressure coefficients of quantum-confined and bulk states of a material. There is also the possibility that the band offsets may vary with pressure. In particular, the electron confinement energy is sensitive to changes in the conduction-band offset (the greater effective mass of the heavy-hole makes it less sensitive to changes in the valence-band offset) and this can also lead to differences between the pressure coefficients of quantum-confined and bulk states[7]. The third effect that must be taken into consideration is the pressure dependence of the effective masses. In most III-V materials the effective masses are approximately proportional to the band-gap of the material[8] and as the band-gap increases with pressure, so do the effective masses. This linear dependence of effective mass on pressure has been measured in several materials systems including GaAs and InP[9]. These are the major effects that have to be considered in the behaviour of confined states under hydrostatic pressure. One further factor, albeit not very significant, is the physical reduction in the width of the quantum-well with hydrostatic pressure (this will tend to increase confinement energies).

2.4 Photoluminescence.

Photoluminescence (PL) is now extremely well established as a technique for the investigation and characterisation of semiconductors. Full discussions of the technique can be found elsewhere[10,11] and only the basic principle is reiterated here, along with an indication of some of the advantages of carrying out photoluminescence as a function of

hydrostatic pressure.

Optical excitation at an energy greater than that of the band-gap of a semiconductor causes the formation of electron-hole pairs. The excess energy is lost quickly by the emission of phonons as the carriers thermalise to the band edges. The electron and hole can then recombine through the emission of a photon, whose wavelength will be characteristic of the band-gap of the material. The time taken for the initial thermal relaxation of carriers ($\sim 10^{-12}$s) is considerably less than that for radiative recombination ($\geq 10^{-9}$s). This means that photoluminescence emission comes from, and so gives us information about, only the lowest energy band-gaps. It should also be noted that PL transitions only rarely occur from band-edge to band-edge[10]. In high quality material at low temperatures excitonic transitions may occur, in which case the PL energy is reduced by the exciton binding energy. Impurity related emissions may also occur, with radiative transitions from the conduction band to acceptor states or from donor states to the valence band. Finally, particularly in the case of indirect band-gap materials, the energy of PL transitions may be modified by the emission or absorption of phonons.

In general, as indicated above, photoluminescence can only give us information about the lowest-lying energy levels. However, as is obvious from section 2.1, hydrostatic pressure provides us with a means of moving the relative positions of the energy levels in a semiconductor. Indeed, depending on their initial positions it may be possible to induce crossing of the conduction-band Γ, X or L levels. By carrying out photoluminescence as a function of pressure we can follow the movement of the lowest conduction-band minimum, relative to the top of the valence band, and identify it by its characteristic pressure coefficient (see figure 2.1). So, if the energy levels cross under

pressure and the movement of the new lowest-lying minimum can be followed then it is possible to extrapolate back and determine its position at ambient pressure. High pressure photoluminescence can thus be used on certain direct band-gap semiconductors in order to determine their indirect band-gaps (see, for example, chapter 4), which would be inaccessible to conventional PL techniques. Similar methods can be applied to the problem of measuring band offsets in quantum-well structures. On applying hydrostatic pressure to a Type I quantum-well structure there is now the possibility that the conduction-band Γ minima in the well can cross with either the X minima in the well or those in the barriers. If the quantum-well Γ crosses with the barrier X then PL transitions may be observed between the barrier conduction-band and the barrier valence-band and between the barrier conduction-band and the quantum-well valence-band. Clearly the difference in energy between these two types of transition represents the energy of the valence-band discontinuity. From this, and a knowledge of the difference in barrier and well band-gaps, the conduction-band offset follows. Figure 2.3 illustrates this principle and defines notation that will be used later in this thesis. This method of determining band-offsets has been applied successfully in several materials systems[12,13] and is discussed more fully in chapter 5 in relation to the GaInP/AlGaInP heterostructure system.

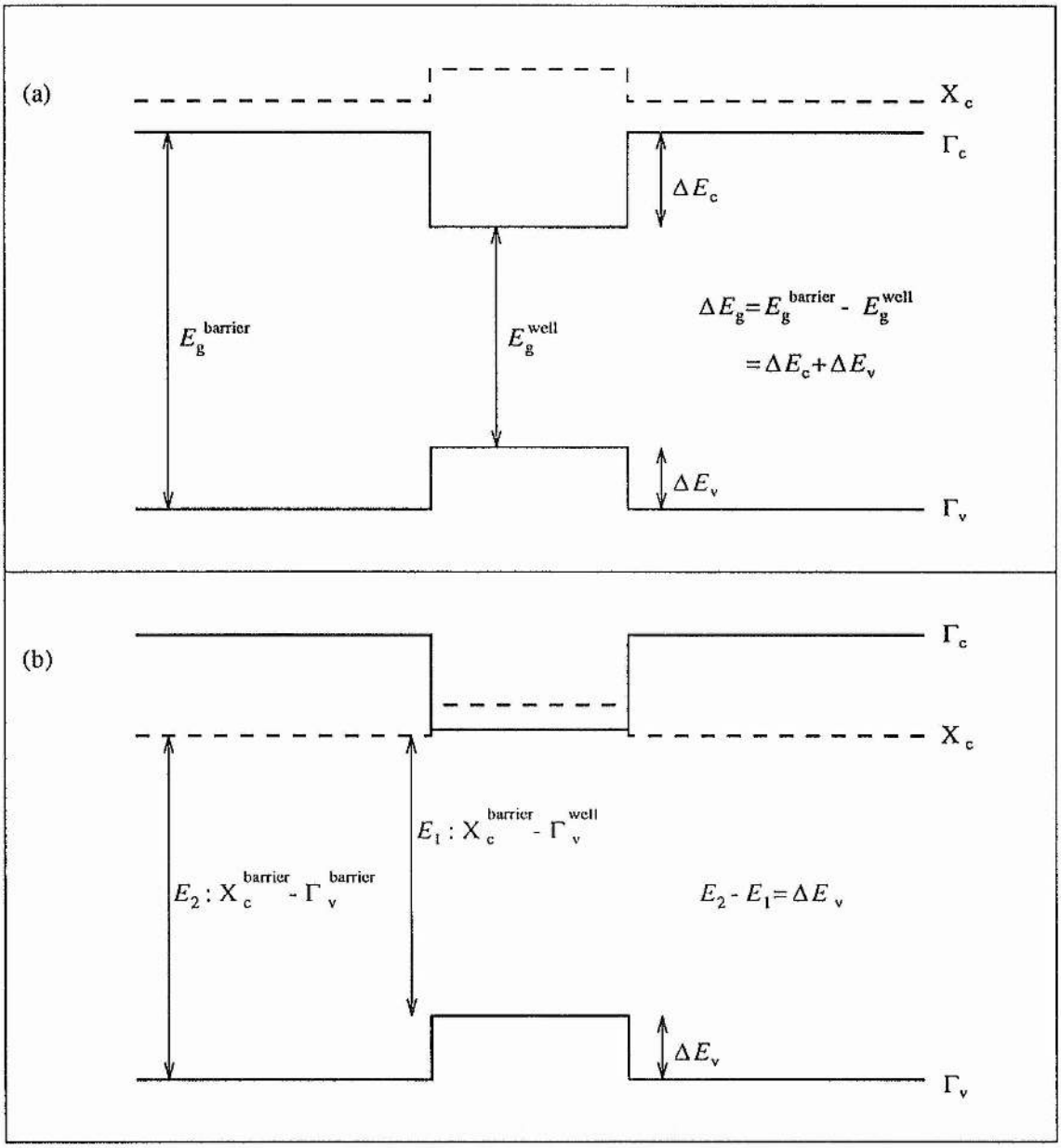

Figure 2.3 A schematic band diagram of a quantum-well structure (a) at ambient pressure, showing a Type I band line-up, and (b) under hydrostatic pressure, just at the point of crossover from Type I to Type II. This figure illustrates how high-pressure PL from such a structure can be used to determine band offsets.

2.4 References.

1. W.Paul and D.M.Warschauer, *Solids Under Pressure*, (McGraw-Hill, New York, 1963)
2. R.W.Keyes, in *Semiconductors and Semimetals*, Vol.4 page 327, edited by R.K.Williardson and A.C.Beers (Academic Press, New York, 1968)
3. D.L.Camphausen, G.A.N.Connel, W.Paul, Phys. Rev. Lett., **26**, 184 (1971)
4. W.Paul, J. Appl. Phys. Supplement to Vol. **32**, 2082 (1961)
5. A.R.Goñi, K.Strössner, K.Syassen and M.Cardona, Phys. Rev. B, **36**, 1581 (1987)
6. L.Esaki, IEEE J. Quantum Electronics, QE**22**, 1611 (1986)
7. J.D.Lambkin, A.R.Adams, D.J.Dunstan, P.Dawson and C.T.Foxon, Phys. Rev. B, **39**, 5546 (1989)
9. A.R.Adams, L.G.Shantharama, R.J.Nicholas and C.K.Sarkar, Physica **139** and **140**B, 401 (1986)
10. J.L.Pankove, *Optical Processes in Semiconductors*, (Dover Publications, New York, 1975)
11. S.Perkowitz, *Optical Characterisation of Semiconductors: Infrared, Raman, and Photoluminescence Spectroscopy*, (Academic Press, New York, 1993)
12. D.J.Wolford, T.F.Keuch, J.A.Bradley, M.A Gell, D.Ninno and M.Jaros, J. Vac. Sci. Technol., **B4**, 1043 (1986)
13. U.Venkateswaren, M.Chandrasekhar, H.R.Chandrasekhar, B.A.Vojak, F.A.Chambers and J.M.Meese, Phys. Rev. B, **33**, 8416 (1986)

CHAPTER 3.

Experimental Techniques.

3.1 Introduction.

This chapter contains details of the experimental apparatus and techniques used during the course of this work. Standard photoluminescence and optical absorption techniques are well established and so are only briefly described here, the emphasis being on how such methods have been adapted for high pressure measurements. The remainder of the chapter describes the more specialised procedures and apparatus required to produce high hydrostatic pressures at cryogenic temperatures.

3.2 Photoluminescence Techniques.

A schematic diagram of the PL system used is shown in figure 3.1. The only significant modification to a conventional PL set up is the back scattering geometry by which the emission is collected. This is necessary due to the restricted optical aperture of the diamond anvil cell.

Optical excitation is provided by an argon ion laser emitting at 514nm or 488nm, with excitation powers typically in the range 30-150mW. Laser plasma lines are filtered out with a suitable notch filter. Steering mirrors direct the laser beam through a 10cm focal length lens which focuses the beam to a spot diameter of approximately 50μm on the sample. This same lens collects the PL emission and collimates it into a near-parallel

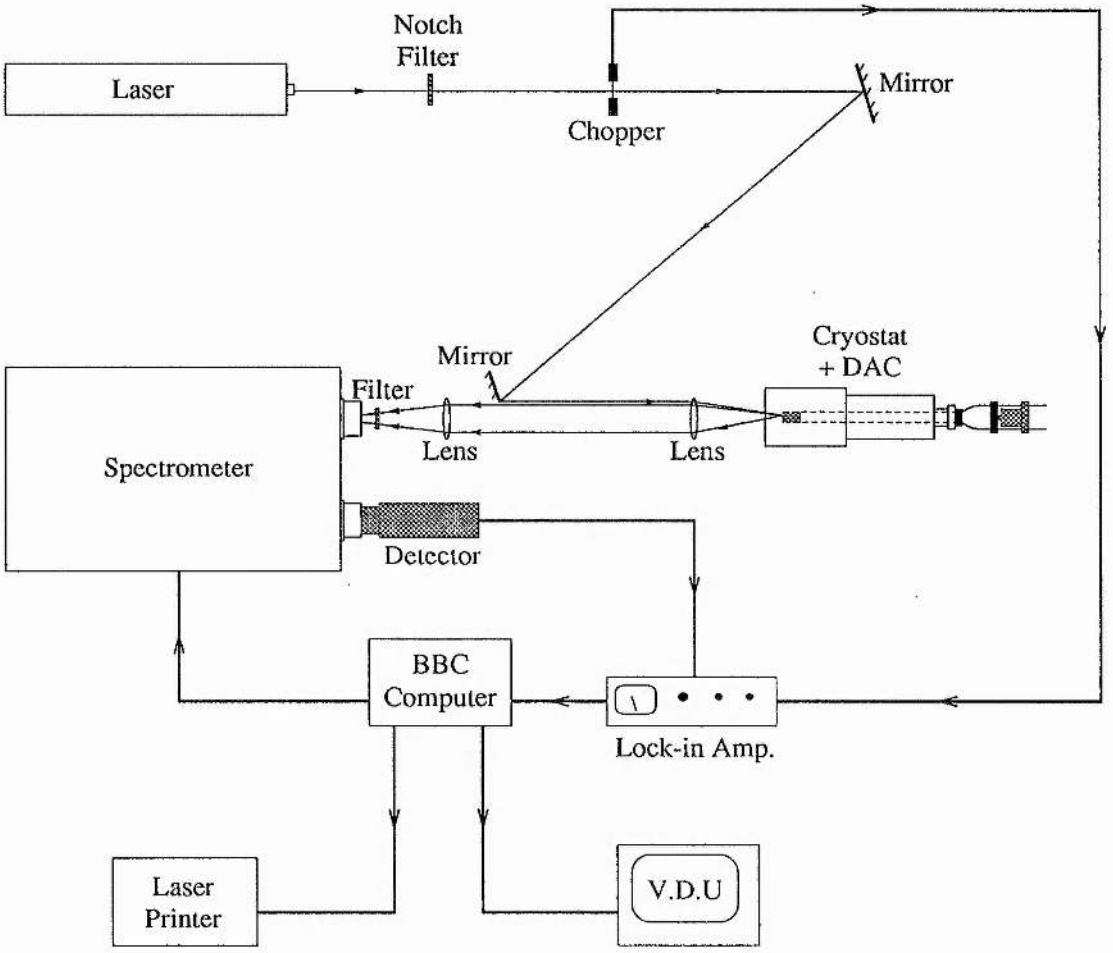

Figure 3.1 A schematic diagram of the photoluminescence apparatus used.

beam (see below) which is brought to a focus on the slits of 1 metre spectrometer by a second lens. Red-pass filters in front of the spectrometer slits reject scattered laser light and prevent second order effects from shorter wavelengths. The emission is analyzed by the spectrometer and detected with a suitable photodetector. The choice of detector is governed principally by the emission characteristics of the samples being studied. Figure 3.2 shows the range and response of the detectors used. Background noise is reduced using a phase locked detection system. The laser beam is chopped at a fixed frequency by a light chopper connected to a lock-in amplifier. The detector output is also connected to the lock-in amplifier which amplifies only those signals with the selected chopping frequency. Further noise reduction features[1] are incorporated into the software routines of the BBC microcomputer which records and displays the spectra and controls the spectrometer. The software also allows spectra to be corrected for the spectral response of the detection system.

As mentioned above, the layout of this system is such that a single lens is used to focus the laser beam onto the sample and to collect and collimate the emitted PL. It should be noted that, due to the difference in their wavelengths, the focal length of this lens for the laser light will be slightly different to that for the PL emission. Therefore, the optimum lens-to-sample distance is a compromise between focusing the laser spot and collimating the PL emission (ideally into a perfectly parallel beam). This fact, combined with the very small area of the sample (typically 50×100μm), means that accurate alignment of the optics is necessary. Consequently the lenses and, unusually, the cryostat are mounted on precision X–Y–Z stages and the steering mirrors are capable of translation and rotational adjustment. A useful aid to alignment is an optical fibre butted

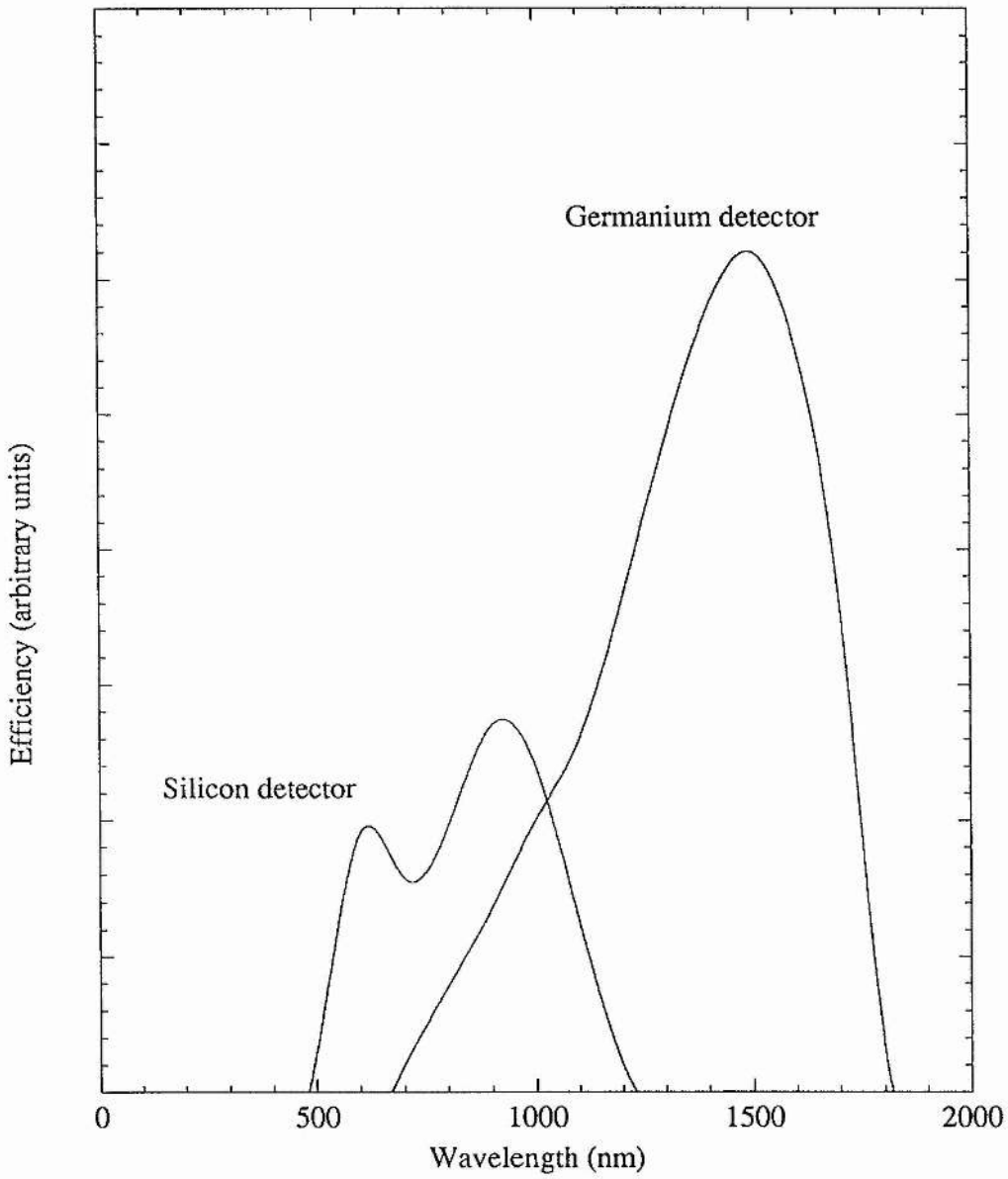

Figure 3.2 The spectral response of the photodetectors used.

up against the back diamond in the DAC. White light passed down this fibre and through the DAC gasket-hole (in which the samples are situated) allows the detection optics to be aligned. The fibre can also be used to observe the intensity of the laser light coming through the gasket hole. This assists in the initial positioning of the laser spot. Final optimisation of the optical system is carried out by monitoring the PL intensity on the lock–in amplifier, whilst systematically 'walking' the X-Y-Z adjustments of the lenses to maximise the signal. In practice it is found that, once the system has been optimised in this way, it is preferable to leave the position of the lenses fixed. Subsequent adjustment (for example, when moving the laser spot from the sample to the pressure gauge or vice versa) and minor realignment (often necessary after making a pressure change) is most simply achieved by moving the cryostat, rather than the lenses. Furthermore, the greater mass of the cryostat on its mounting, as compared to that of the lenses, makes it less prone to the instability caused by the operator whilst making X–Y–Z adjustments. Given the high precision required when trying to 'peak-up' on a sample, this is a significant advantage. Sometimes, however, precise positional adjustment of the cryostat may be difficult (particularly if it is a bath cryostat that is being used). In such cases the necessary adjustments can be carried out using the X–Y–Z movement of the lenses, though more care is required.

3.3 Optical Absorption Techniques.

Optical absorption measurements can be carried out in the diamond anvil cell with little modification necessary to the optical arrangements described above. Indeed, both

absorption and PL measurements can be made in the same high pressure run.

A tungsten lamp provides the source of light which passes through a light chopper and is guided down an optical fibre to the back of the cell. In order to prevent stray light from swamping the transmitted signal the gasket hole around the sample is masked (two methods for doing this are described, in sections 3.6.2 and 3.7). The same software routines that correct for the spectral response of the detector can also be used to compensate for the spectral response of the lamp and fibre.

Although successful experiments have been carried out in which PL and absorption measurements are made in the same pressure run[2], such experiments cannot yet be performed routinely and reliably in the diamond anvil cell in the way that PL experiments can. The main reason for this is the additional complexity of having to provide a mask to prevent light from coming around the sample. Associated with this is an increase in the precision required when loading a sample (see section 3.8) and a heightened requirement that the sample does not subsequently move (as sometimes happens when the pressure medium is introduced into the sample space). The coupling of light from the optical fibre into the back of the cell in a constant and reproducible manner also presents problems, particularly when experiments are being performed at cryogenic temperatures. Experimental techniques are being developed to try and improve the success rate of absorption experiments (see, for example, section 3.7).

3.4 Cryogenic Temperatures.

All the high pressure optical experiments described here have been performed at

low temperatures (2-10K). The design of the Dunstan miniature cryogenic diamond anvil cell[3] is such that standard cryogenic equipment and techniques can be used.

For measurements down to 4K an unmodified continuous flow cryostat is used with helium as the cryogenic fluid. Optical access is from the bottom of the cell so the cryostat is fitted with a bottom window and used horizontally, this allows direct optical access to the gasket hole.

For temperatures down to 2K a standard liquid-helium bath cryostat is used. In this case, since the bath cryostat must be used in the vertical position, a miniature 90° prism is fixed at the base of the cell to provide optical access. As well as the lower temperature, the bath cryostat has the advantage that it provides a simple means of loading helium into the gasket hole to act as the pressure medium (see section 3.9.2). Furthermore, the helium consumption is typically less than one third of that of the flow cryostat. Preparation time, however, is longer for the bath cryostat (~8 hours) than for the flow cryostat (~2 hours).

3.5 The Diamond Anvil Cell.

3.5.1 Diamond Anvil Cell Principles.

The diamond anvil cell has become established as the best method for carrying out optical studies at pressures above 10kbar. Furthermore, designs such as that of Dunstan and Scherrer[3] have made it possible for laboratories not previously specialising in high pressure work to successfully install and operate a high pressure facility.

A huge variety of DAC designs exists[4,5] but they share the same basic principles illustrated by figure 3.3. The sample, surrounded by a pressure transmitting medium, is contained within a hole in the centre of a gasket. The gasket is squeezed between the opposing faces (culets) of two diamonds. Due to the very small culet area, a moderate force applied to the back of the diamond anvils gives rise to very high stresses over the gasket and gasket hole. A pressure medium in the gasket hole causes the resultant stresses in the sample to be hydrostatic (or close to hydrostatic).

It should be noted that some mechanism is required to ensure accurate alignment of the diamonds (see section 3.5.4). The maximum pressure (P_{max}) that can be obtained depends on the stress tolerances of the gasket, diamonds and supporting components; it also depends on the culet size. In a well designed system, where this is the limiting factor, the following relation has been suggested[5]:

$$P_{max}(\text{kbar}) = 125d^{-2} \qquad (3.1)$$

where d is the culet diameter in millimetres.

3.5.2 Diamond Anvils.

The unique properties of diamond make it the ideal choice of material around which to design a high pressure cell. As well as being the hardest substance known it is transparent to photons of a wide range of energies.

A wide variety of diamond anvil designs exist and a full discussion of the design

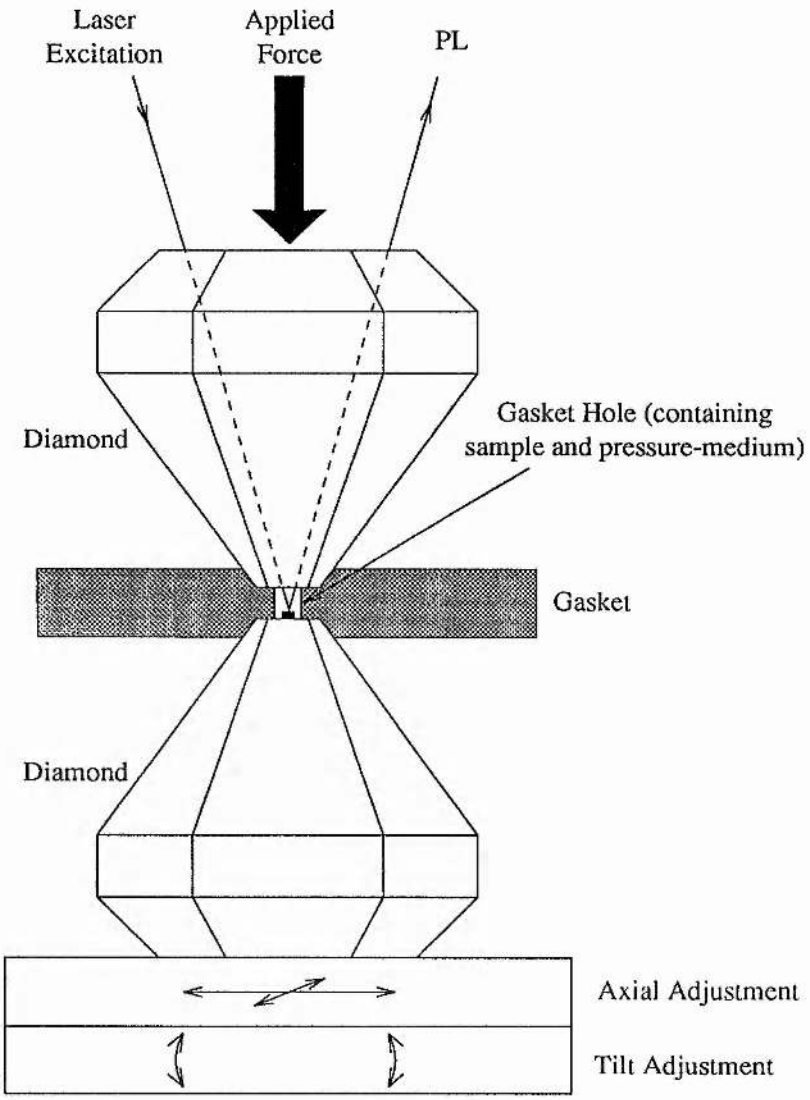

Figure 3.3 A schematic diagram illustrating the principles of the diamond anvil cell.

considerations can be found elsewhere[6]. The choice of diamond anvil depends primarily on the particular application for which it is to be used. For the optical studies described here the diamonds were cut in the Drukker Dubbledee design[6], which is a standard cut for high pressure applications. All the diamonds used were of high optical quality (type IIa) and low fluorescence. Most of the diamond anvils had culet diameters in the range 650–750μm as these had been found to give the required pressure range (up to 200kbar) without being too small to work with comfortably. One pair of diamonds, with 500μm diameter culets, was available in case higher pressures were required. Both eight-sided and sixteen-sided diamonds were used, with no significant advantages or disadvantages noted for either. Some operators have expressed a preference for one or the other (mainly with respect to the ease of axial alignment) but this seems largely a matter of personal preference or familiarity. For certain applications, such as electrical measurements in the DAC[7] or Mbar pressure studies[8], diamonds with rounded or bevelled culet-edges are commonly used. Whilst this has no particular advantage in the optical studies described here, some of the diamond anvils that have been used have had culets with single or double bevels. In these cases, as long as the bevel was uniform around the culets, then no extra difficulty was found in aligning the diamonds, or in any other aspect of their use. It is worth noting, therefore, that a small chip on the edge of a diamond can often be removed, relatively cheaply and without causing problems, by having the diamond bevelled.

3.5.3 Diamond Anvil Cell Gaskets.

In a properly designed DAC the most important factor in the success or failure of a high pressure run is the correct preparation of the gasket (a full discussion of DAC gasket behaviour is given in reference 9). In preparing a gasket the following choices have to be made; the choice of gasket material, the starting thickness of the gasket, how this thickness will be achieved (either by use of stock material of the required thickness or by preindentation) and, finally, the size of the gasket hole.

In choosing a gasket material several factors must be considered, such as ease of machining for example, but most important is the fact that the potential pressure range of the experiment will depend on the shear strength of the material[9]. For this work, using pressures ≤200kbar, standard stainless steel (British Standard 1449 T316) has been used. Other possible materials include Inconel, copper-beryllium or tool steel. For a given cell and gasket material, the biggest influence that the operator has on the experiment is in the choice of gasket thickness and whether or not to preindent. These choices will determine the pressure range of the experiment. The principle argument for preindenting gaskets is the massive support it provides to the gasket material between the culets. It has been shown[9] that this support can significantly increase the maximum pressure for a given gasket thickness. In addition preindentation provides support around the culets of the diamonds. It also means that only a single thickness of stock material is required, which can be indented to precisely the chosen thickness, rather than having to keep a variety of thicknesses in stock. Furthermore, with a preindented gasket the tricky procedure of centring the gasket hole on the diamond culet simply becomes a matter of accurately

drilling the hole in the centre of the indentation. It is thus separated from the similarly difficult procedure of placing the sample(s) at the centre of the culet, thereby making the overall task of loading the cell easier.

Regarding the choice of gasket thickness, it has been found[9] that there are essentially two regimes in which gaskets operate; the 'thick' and 'thin' regimes. In the thick regime, when the diamond anvils are advanced the flow of gasket material is outwards and the gasket hole enlarges. However, in the thin regime the material around the gasket hole extrudes inwards making the hole smaller as the pressure is increased. The thick gasket regime is unstable, exaggerating any asymmetry in the shape or position of the sample hole and ultimately threatening failure of the gasket and possible diamond breakage. For this reason DAC experiments should always be carried out in the thin gasket regime. The most simple way to determine which of these regimes is operating is to make visual observations of the gasket hole during the experiment to see whether it is getting larger or smaller. The relationship between gasket thickness and the force-pressure behaviour of the cell has to be established empirically for given culet sizes and gasket materials (several force-pressure plots are shown in figure 3.10 along with the conditions under which they were obtained).

Finally, we come to the choice of gasket-hole size. Clearly it must be big enough to accommodate one or more samples (allowing for a degree of hole contraction under pressure) but small enough that, if the hole should start to enlarge, small imperfections in symmetry or position do not lead to immediate gasket failure. These limits will depend on such factors as the choice of gasket material, the gasket thickness and the compressibility of the pressure medium used. Again, some experimentation is required

to find the optimum size for given circumstances (see figure 3.10).

3.5.4 The Miniature Cryogenic Diamond Anvil Cell.

All of the high pressure optical measurements made in the course of this work were performed using the miniature cryogenic diamond anvil cell designed by Dunstan. Full details of this particular design can be found in reference 3, so only the essential features are described here.

The cell, made from hardened Be:Cu, is illustrated in figure 3.4. It has a maximum outside diameter of 19mm enabling it to fit in the bore of a standard optical cryostat. At the heart of the system are the diamond anvils, one fixed to the piston and the other attached to a pad which rests against a base plate. The pad is held in place by three grub screws. Adjustment of these screws moves the pad around on the base plate thus providing X-Y alignment. Tilt adjustment is made by tilting the base plate itself using a system of three stand-off screws and three retaining screws. This design means that the alignment mechanisms do not have to support the working load (alternative designs in which the load is applied through the alignment mechanisms tend necessarily to be more bulky) and, once set, the alignment tends to remain stable over repeated pressure runs. When necessary, minor X–Y or tilt adjustments can be made quickly and precisely.

Figure 3.5 shows the drive mechanism used to apply force to the diamonds. Again the design is such that it will operate in a standard cryostat allowing pressure changes to be made at low temperature. The drive operates on the Bowden cable principle. Four

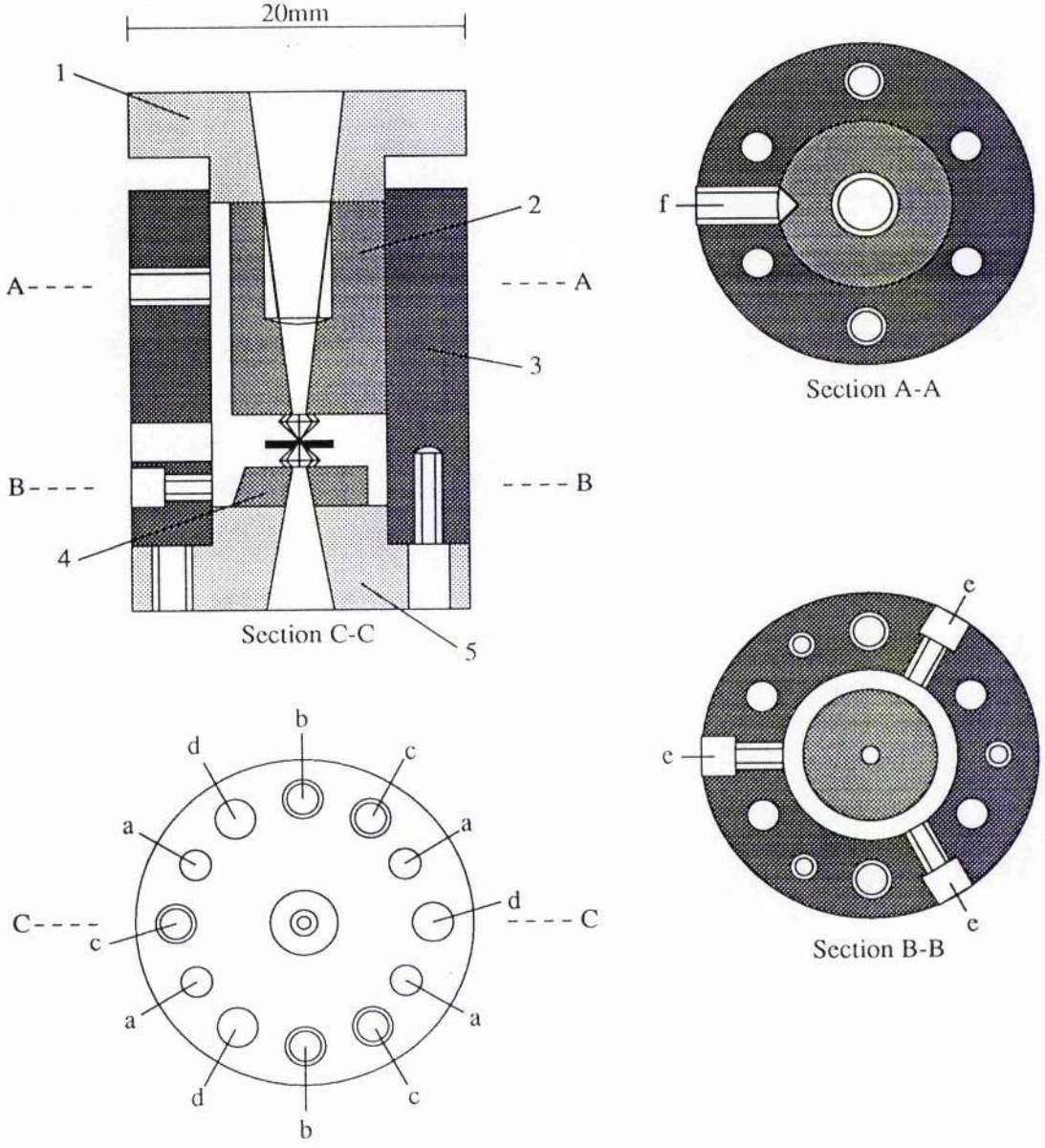

Figure 3.4 The miniature cryogenic diamond anvil cell. The components are numbered as follows: (1) Top plate (2) piston (3) cell body (4) pad (5) base plate. The holes labelled in the horizontal sections are for (a) the tension wires (b) clamp bolts (c) base-plate stand-off screws (d) base-plate securing screws (e) X-Y adjustment (and pad securing) screws and (f) the piston guide screw.

compression tubes are soldered at the top end to a thrust plate. At the bottom end they butt up against the top plate of the cell which pushes on the piston. Within the compression tubes two tension wires run down through the thrust plate, around the base of the cell and back up through the thrust plate. The ends of the wires are fitted with friction clips so that a hydraulic ram pushing against the thrust plate will pull on the wires and thus apply force to the cell. A ball bearing between the ram and the thrust plate ensures even loading. For protection the tension wires make their 180° bend around semi-circular saddles positioned against the base plate of the cell. Several heatshields placed along the length of the drive reduce thermal loading of the cryostat and O-rings are used to make a vacuum seal where the wires pass through the thrust plate. An additional tube, with an O-ring seal, passes through the cryostat plug allowing an optical fibre and electrical leads to be run down the drive to the cell.

3.5.5 Diamond Mounting and Alignment.

In operation it is essential that the diamond anvils are well aligned with respect to one another. This means that the culets must be axially aligned (X-Y alignment) and parallel to one another (tilt alignment). It is preferable for the diamonds to be mounted in such a way that the alignment remains good over repeated pressure runs. In the cells used for this work the diamonds are soldered to the pad and piston using ordinary electrical solder (60/40 tin/lead). There are many alternative mounting techniques[5] but soldering has proved the most convenient and reliable (cells typically undergoing 20-30 pressure runs before remounting is necessary). Soldering requires that the bottom of the

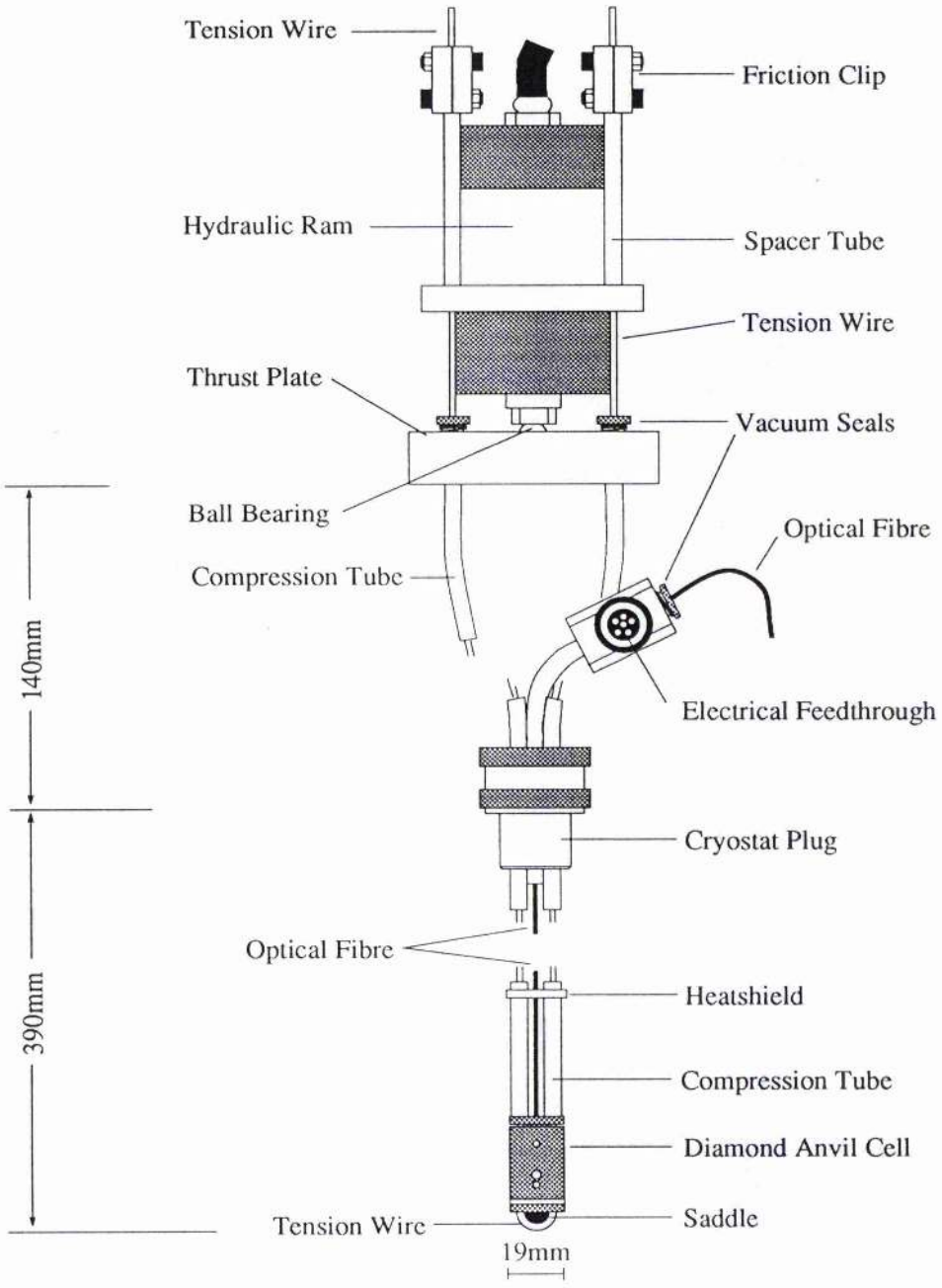

Figure 3.5 The drive mechanism for the miniature cryogenic diamond anvil cell.

diamonds are first metallised and gold-plated, but with a clear central hole left for optical access. Initial metallisation, using a succession of metals (for adhesion) and finishing with gold, is done (at little extra cost) by the diamond suppliers and subsequent re-plating is done in-house. The procedure for soldering the diamond onto the piston is as follows. The surface of the piston is cleaned and, if necessary, machined and polished perfectly flat (this is especially important when mounting diamonds in an old cell as previous pressure runs may have caused some indentation of the surface). With the piston on a hot plate (at 180°C) the diamond is positioned, by eye, centrally over the optical access hole and temporarily fixed with a small amount of solder under and around its base. The piston is then placed in a jig (see figure 3.6) which accurately centres the diamond on the piston. The jig is left on the hot plate until the whole assembly is just above the melting point of the solder (indicated by placing a small amount of solder on the jig). Force is then applied (simply by pushing with a screwdriver) to the bottom of the piston to ensure that the diamond is located centrally and that there is only a very thin layer of solder between piston and diamond (if too much solder is used the alignment will be prone to shift during pressure runs). Finally, the piston is removed and cleaned thoroughly. The procedure for soldering a diamond onto the pad is exactly the same except that the pad is first placed in an adaptor (see figure 3.6) so that it fits the mounting jig. Once both diamonds are mounted they must be aligned.

Diamond alignment is checked after every pressure run and adjusted when necessary. If drastic changes in alignment occur then the cause should be found and the fault corrected. X-Y alignment is checked by viewing the assembled cell from above, along the axis of the cell, using a microscope. With a combination of light from below

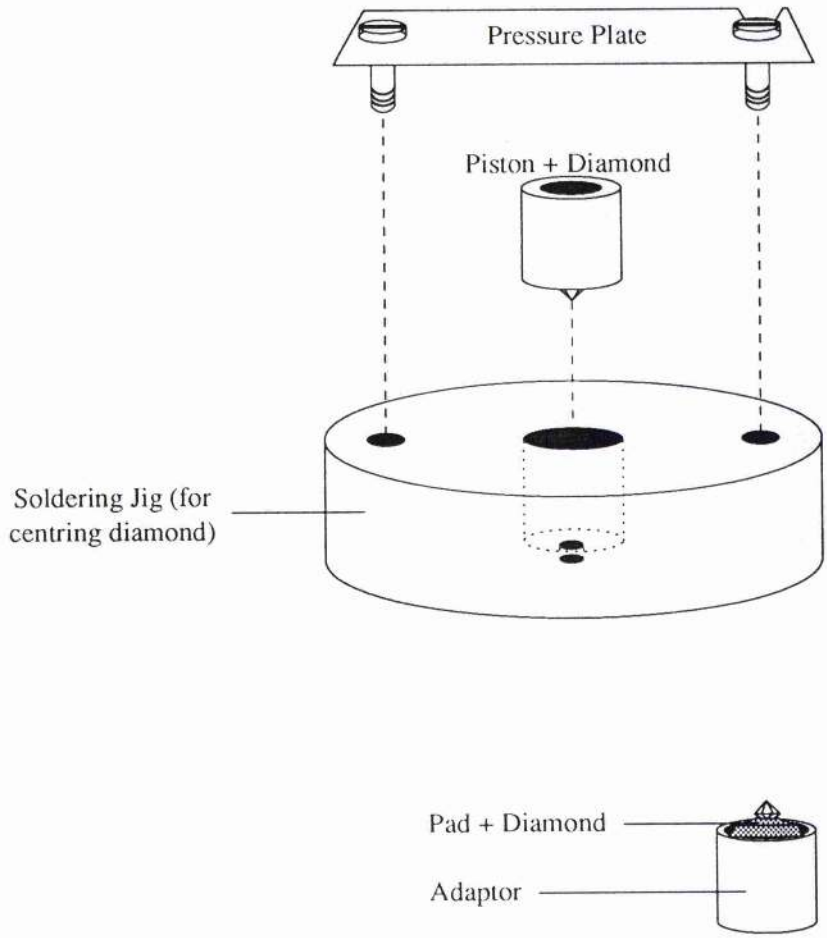

Figure 3.6 The mounting jig and adaptor for soldering diamonds into the DAC.

and from the side (through the side-access holes) it is possible to see when the culets lie exactly opposite one another. Adjustment is made using the three grub screws indicated in figure 3.4. Adjustments should not be made with the diamonds in contact and care should always be taken when bringing the diamonds together (particularly in an unaligned cell) as point contact and shear stress can cause damage. Coarse tilt alignment is carried out by directly viewing through the side-holes as the diamonds are brought together. Adjustments are made using the stand-off and securing screws shown in figure 3.4. Final tilt alignment is carried out by viewing the cell from above with a light source below. With the (clean) diamond faces in contact, coloured interference fringes should be visible across the culets. The fewer the fringes, the better the parallelism. Gently pressing on the piston causes the fringe pattern to move away from the point at which the diamonds are touching and corrections are made accordingly until there are no more than 3-4 fringes. This also provides a check on the piston-cylinder fit; when pushing on the piston at different points around its circumference there should be a change of no more than a few fringes. After alignment the stability of the cell is checked by indenting some gasket material at successively higher forces up to a typical working load. After each indentation the alignment is checked and if it remains consistently good then the cell is ready for use.

3.6 Gasket Preparation.

Two types of gasket have been used in this work. For simple photoluminescence measurements a single-piece gasket is used whereas for simultaneous photoluminescence and absorption experiments a laminated gasket is used. In both cases stainless steel

(British Standard 1449 T316) is used and the gaskets are always preindented (see section 3.5.3). All the drilling involved in gasket preparation is carried out in a miniature drill press fitted with a precision, micrometer drive, X-Y stage.

3.6.1 Standard Gasket.

A blank of approximately correct dimensions is cut from 500μm stock material. Since guide pins are used on the piston, to assist positioning of the gasket on the diamond, holes for these are drilled in the blank. This is then trimmed so that it fits cleanly within the cylinder bore and the gasket is marked so that it is always fitted in the same orientation. The gasket is then preindented to the required thickness. A simple indenting rig has been made so that the cell doesn't have to be assembled in the drive each time. As a precaution against diamond breakage preindentation is carried out in a series of steps of increasing force with a return to zero between each. A ball-end micrometer is used to measure the gasket thickness and when the correct thickness is obtained the gasket is removed for drilling. The best method for drilling the gasket hole at the exact centre of the indentation is largely a matter of personal preference. The procedure outlined below is the one the author has found the simplest and most reliable. The gasket is fixed to the X-Y stage on the drill press using double sided sticky tape and viewed obliquely from above with a binocular microscope. The exact centre is then located by repeated viewing from two perpendicular directions, always with the light source directly opposite the viewing direction so that the drill and its shadow form a straight line. The gasket can then be positioned so that this line exactly bisects the

indentation. Accurate centring of the gasket hole is easier with a smaller drill, so a 100μm guide-hole is drilled first and then opened out to the correct diameter (typically 250-300μm). Once drilled, excess burr is removed by hand using an oversize drill. Finally the gasket is cleaned with acetone in an ultrasonic bath.

3.6.2 Absorption Gasket.

The special requirement of gaskets used in absorption experiments is that they must also provide a mask to stop stray light from passing around the sample. This is achieved using laminated gaskets (see figure 3.7) prepared in the following way. A preform blank of 50μm stainless-steel foil is stuck face-to-face with a similar blank of 500μm thickness using cyanoacralate glue (the surfaces to be glued are first cleaned and roughened with medium grade emery paper). It has been found that a single ply of tissue paper between the layers of steel, combined with gentle pressure for about one minute after gluing, helps adhesion. Once the glue is set, guide-pin holes are drilled and the blank is trimmed and indented in the usual way. A 100μm hole is drilled at the centre of the indentation, after which the layers of steel are separated using acetone in an ultrasonic bath. The 100μm hole in the thicker layer is then drilled out to the usual diameter (250-300μm). The thinner layer, with the 100μm hole, acts as the mask. Excess burr is removed and the two gasket sections cleaned. It should be noted that the use of this type of gasket requires a slightly modified loading procedure (see section 3.8).

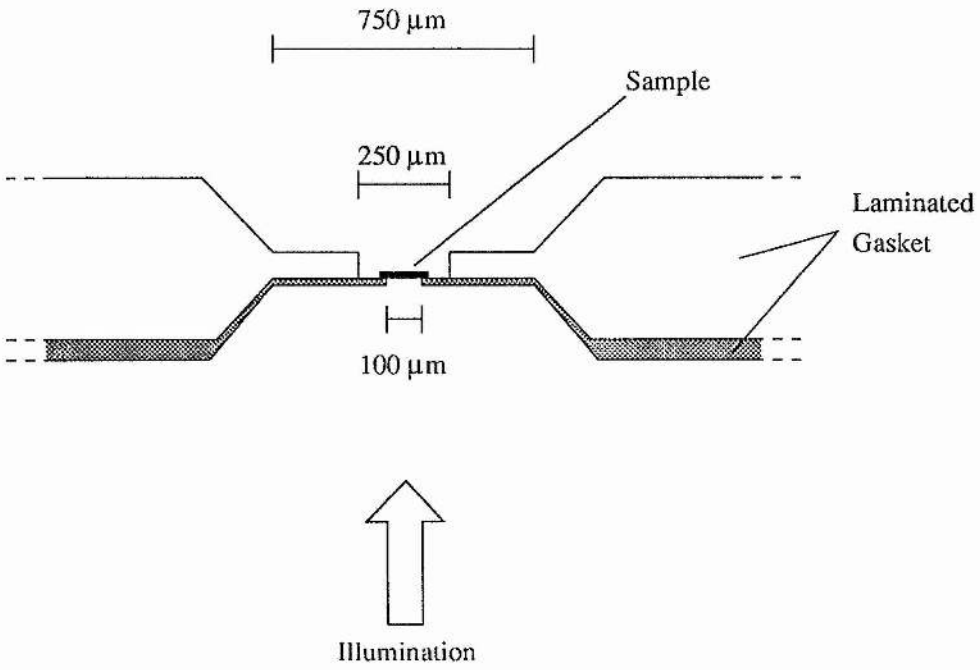

Figure 3.7 A schematic diagram of a laminated gasket, used for optical absorption experiments.

3.7 The Absorption Diamond.

The 'absorption diamond' has been developed as an alternative to the laminated gasket technique, described above, for providing a mask around a DAC sample. Whilst the laminated gasket technique has proved a viable way to perform absorption experiments in the DAC, the modifications it requires to standard gasket preparation and sample loading procedures present added complications and, inevitably, lead to a reduction in success rates.

The absorption diamond consists of a standard diamond anvil which, in addition to the usual metallisation and gold-plating for mounting purposes (see section 3.5.5), has also had its culet and upper facets metallised and gold-plated. In the centre of the culet a 100μm diameter hole is formed in the opaque coating. This is done by fixing the diamond to the X–Y stage of the miniature drill press and, after accurate centring, using a blunt 100μm drill and fine carborundum grinding paste to remove the gold-plating and metallised layer. This diamond can now be mounted on a DAC piston in the usual way. With the sample placed over the 100μm hole the gold-plating thus acts as a mask and prevents light from passing around the sample.

The main advantage with this technique is that gasket preparation and sample loading procedures are identical to those for standard DAC photoluminescence experiments. A certain amount of deterioration of the gold-plating can be expected after a large number of pressure cycles. However, since the metallised layer remains intact, a fresh layer of gold can easily be evaporated onto the diamond when necessary.

3.8 Sample Preparation and Loading.

The sample chamber in the DAC is typically 250μm in diameter and 80μm deep, so samples must be prepared accordingly. The first stage is to thin the sample; a simple jig is used, consisting of a steel cylinder with a groove 30μm deep machined in one end. The sample, cleaved to fit within this groove, is fixed face down using a hard thermosetting wax and the substrate is polished away on lapping film (using successively finer grades down to 1μm) until a 30μm flake remains. This is carefully removed from the jig using solvent (trichloroethylene) and tweezers and cleaned (with trichloroethylene and acetone) to remove wax and grease.

The sample is then cleaved to approximately 50x100μm using a scalpel or razor blade. Cleaving is carried out under a binocular microscope and with the sample constrained within a drop of 50:50 methanol/water to prevent it being lost. Ruby (for pressure calibration) is prepared in exactly the same way since grinding and cleaving makes the ruby samples easier to identify as ruby than ruby-chips prepared in pestle and mortar, which can easily be confused with dust.

The samples can now be manoeuvred onto the piston-mounted diamond. The piston, cleaned and lightly dusted with a solid lubricant (MoS_2), is held under the microscope in a suitable jig. The diamond culet should be clean and free from grease (a cotton bud dipped in acetone is used). A variety of tools may be used to transport the samples to the diamond, the choice is largely a matter of personal preference. The main problems is with samples being flicked out of the field of view and lost. The author uses a short length of fine malleable wire attached to a matchstick for easy manipulation.

There is unfortunately no simple substitute for patience and practice. Samples are picked up by electrostatic attraction and positioned on the diamond culet. Once this is done the gasket is lowered over the guide pins and onto the diamond. This operation is viewed under a microscope to check that the samples lie cleanly within the gasket hole. After checking that the second diamond culet is clean the cell is assembled.

When loading samples for an absorption experiment in which a laminated gasket is used the procedure is modified slightly. In this case the two gasket sections are positioned on the piston-mounted diamond, with the thinner section at the bottom. The indentation and guide pins are sufficient to align the two pieces; no further gluing is necessary. The sample, cleaved to approximately 150x150μm, is then placed in the gasket hole and manoeuvred so as to completely cover the small hole in the masking section. If necessary a small piece of ruby (or some other semiconductor) can be placed alongside the absorption sample for pressure calibration.

3.9 Pressure Media.

Choice of pressure media is discussed by Jayaraman[10] and Burnett *et al*[11]. The principle requirement of the pressure medium is that it must retain its hydrostaticity over the pressure and temperature range of interest. Furthermore, it is preferable if pressure changes can be made at low temperature without inducing non-hydrostatic stresses. The most commonly used pressure medium is a methanol/ethanol mixture. However, at cryogenic temperatures there is evidence of non-hydrostatic behaviour, particularly when pressure changes are made at low temperature[11]. The procedure for loading

methanol/ethanol also tends to be somewhat haphazard. Until recently all our DAC experiments were performed using argon as the pressure medium. As well as showing almost no evidence of non-hydrostaticity, the argon loading procedure is simple and reliable. However, it is generally reckoned that helium is the optimal cryogenic pressure medium[11] and this is what is now used. A bath cryostat has been installed which not only provides the ideal means for helium loading but also the capability of carrying out experiments at 2K. The procedures for argon and helium loading are described below.

3.9.1 Argon Loading.

Figure 3.8 shows the argon loading apparatus, the procedure is as follows. The cell is closed with light, finger-force; just enough to seat the gasket between the diamonds and prevent the possibility of the samples being washed out of the gasket hole. The cell, installed in its drive mechanism, is then placed in the loading tube and the system evacuated and flushed with high purity argon gas. This process is repeated and the system filled with argon gas (an overpressure of ~2bar is maintained) which is then cooled below its boiling point (87.3K) by immersing the loading tube in liquid nitrogen. The argon condenses in the loading tube thereby filling the gasket hole. After the initial rapid condensation ceases the system is left for a further ten minutes before the cell is closed with sufficient force being applied to seal the gasket. The degree of force required, and the pressure that will result, has to be established by trial for any particular set-up. The system is then allowed to warm up gradually (during which time resultant gas must be safely vented). PL is then carried out to check that the samples are under pressure.

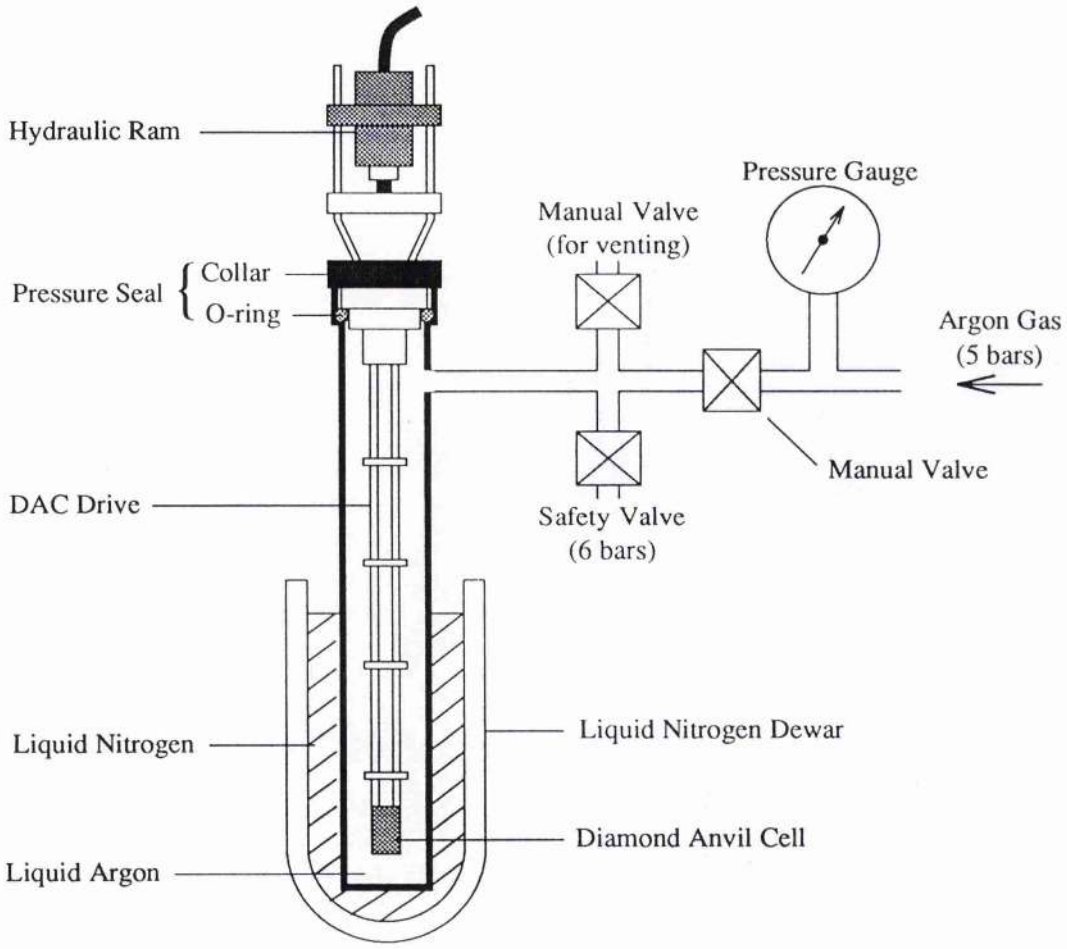

Figure 3.8 The argon loading apparatus for the miniature cryogenic diamond anvil cell.

It should be noted that the pressure in an argon loaded cell drops on cooling from room temperature. This effect is greater for small initial pressures; for example, a cell at 8kbar at 300K typically drops to ~3kbar at 10K, whereas a cell at 15kbar at 300K will drop to ~12kbar at 10K.

3.9.2 Helium Loading.

Helium loading in a bath cryostat simply requires an extra step in the standard cryostat filling procedure. The design of the cryostat may dictate the precise method used but the following procedure has been found to be very reliable.

The cryostat is first precooled by filling the sample chamber with liquid nitrogen. After several hours this is blown out with an over-pressure of nitrogen gas. The sample chamber is evacuated, backfilled with cold helium gas and then liquid helium is transferred into the cryostat in the usual way. The cell and drive assembly is then lowered slowly into the bath cryostat whilst monitoring the resulting helium boil-off. By keeping the boil-off rate slow and constant (typically taking 15-20 minutes to insert the drive) the amount of helium wasted is insignificant. With the cell in place the cryostat chamber is gradually pumped to below 37torr to bring the helium through the superfluid transition temperature. The cell is then left for ~30 minutes to ensure that all components reach thermal equilibrium and the gasket hole fills with helium. Once any ambient pressure measurements have been made then force can be applied to close and pressurise the cell.

3.10 Pressure Calibration.

Throughout this work the approach adopted towards pressure calibration has been to choose what we consider the most appropriate method for each particular experiment. Outlined below are some of the considerations that must be made in choosing a suitable pressure gauge.

The photoluminescence of the R1/R2 ruby lines, shown in figure 3.9, is known to move linearly with pressure (at 0.365Å/kbar) up to approximately 200kbar[12]. The luminescence is bright and visible, even at room temperature, which helps in alignment of the PL optics. Ruby is considered the primary pressure calibrant and is still regarded by many as the best. Under ideal conditions this is probably true; however, ideal conditions rarely exist in any laboratory and there are several reasons why ruby may not be the most suitable choice of pressure gauge for a semiconductor experiment (an example of the limitations of ruby as a pressure calibrant can be found in chapter 4). With a 1–metre spectrometer the very small shift in wavelength with pressure means that is difficult to achieve an accuracy better than ± 1kbar. In addition, temperature fluctuations can give rise to additional inaccuracies. Consequently, when ruby is used as a pressure gauge a second ruby chip is placed in the cryostat (stuck to the bottom of the cell) to act as an ambient pressure reference. It is also necessary to consider the PL emission of the sample and how it will change with pressure since ruby luminescence will swamp weaker emissions in the 650-750nm range. A final consideration is that there may be differences in pressure across the gasket hole which, with any pressure gauge separate from the sample, will introduce further errors. An alternative approach to pressure calibration

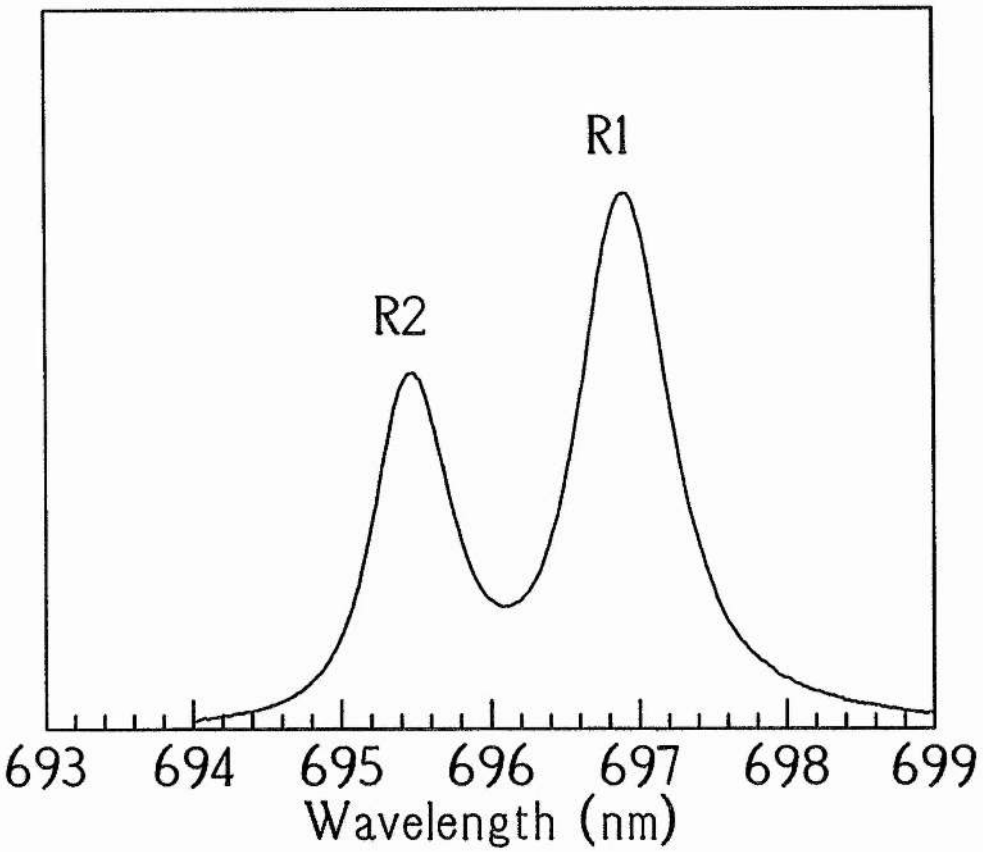

Figure 3.9 A room temperature photoluminescence spectrum of ruby, showing the R1 and R2 lines.

is to use a direct gap semiconductor, such as GaAs or InP, whose behaviour with pressure is known. This method has several advantages. Firstly the pressure coefficient of these materials is much greater than that of ruby, making them more sensitive to small changes in pressure. Furthermore, these materials are often incorporated into the design of the sample or are used as the substrate on which the sample is grown. This means that errors due to pressure differences across the gasket hole are largely eliminated. Having a pressure gauge that is part of the same single crystal as the sample also greatly reduces the amount of optical realignment necessary during the experiment. When using a semiconductor pressure gauge it is particularly important to consider the likely pressure range of the experiment and whether the chosen pressure gauge goes indirect or undergoes a phase transition within this range. The final method, employed whenever possible, is to use the position of the absorption edge of the sample, or its substrate (generally GaAs or InP), as a pressure gauge. This method eliminates one further possible source of error, namely that low temperature PL can originate from a variety of states lying close to the band edge and, as the pressure is raised, it may switch between these states.

As a final note it should be pointed out that for much of this work the design of the experiment is such that accurate pressure determination is not necessary. It will be seen that pressure is frequently no more than a dummy variable, or the results of interest may be found by extrapolating back to ambient pressure. For example, where a reference layer exists within the sample itself, energy differences can usefully be studied without the need to convert to pressure.

3.11 Precautions During the Experiment.

It is essential to plot a graph of applied force (actually hydraulic pressure; the ram is $0.85in^2$) versus pressure during the experiment. This plot, in addition to visual observation of the gasket hole, may provide the only indication of when a DAC run is about to fail (possibly with diamond breakage). Figure 3.10 shows some typical force pressure plots along with the conditions under which they were produced. The graph in figure 3.10(a) comes from a 'normal' high pressure run. Figure 3.10(b) is from an experiment that was terminated prematurely. At ~40kbar the force-pressure plot began to flatten out and observation of the gasket hole showed that it was getting larger, so the experiment was abandoned and repeated using a thinner gasket. Figure 3.10(c) is also from an unsuccessful experiment. In this case application of the maximum working force produced only a 7kbar rise in pressure and yet it could be seen that the gasket hole wasn't enlarging. The conclusion was therefore that the drive mechanism was jammed or frozen (an air-leak allowing ice to form in the compression tubes) so the drive was dismantled, cleaned, fitted with new O-rings and the experiment successfully repeated. Figure 3.10(d) is the force-pressure plot from an experiment in which the pressure was cycled. It can be seen that the cell shows a large hysteresis when the force is reduced. For this reason it is preferable to take measurements in a single run, increasing the pressure after each measurement. Force-pressure plots, along with initial and final gasket dimensions, are also useful references when preparing gaskets for future experiments.

Pressure changes should always be made whilst monitoring the strength of the PL feature of interest. Force is applied until the intensity, shown on the lock-in amplifier,

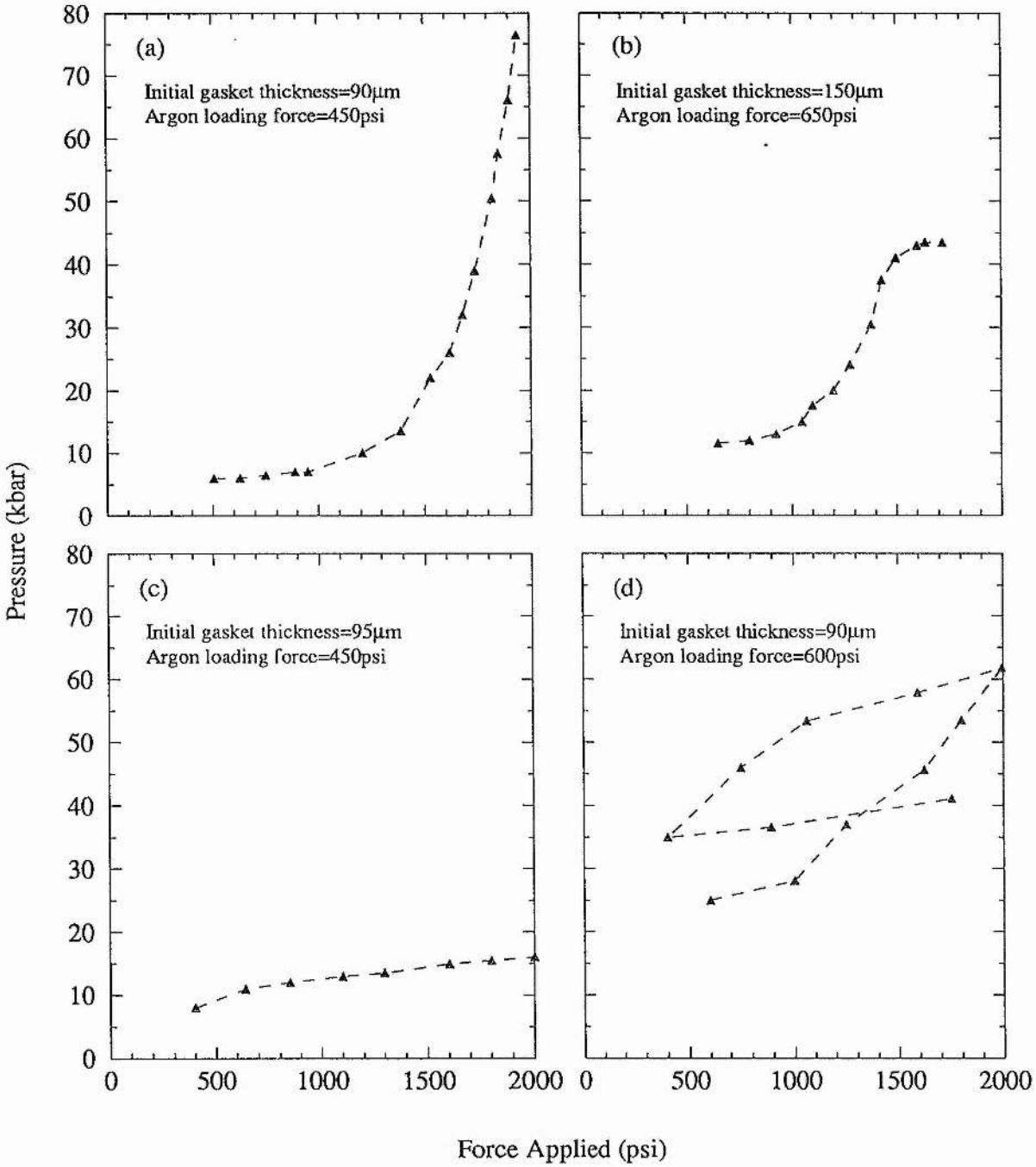

Figure 3.10 A selection of force-pressure plots from DAC experiments carried out at 2K. In all cases the initial gasket hole diameter was 250μm. The shape of the various curves is discussed in the text.

is halved. If this loss in intensity cannot be recovered by realignment of the optics then the PL peak has moved in energy (or quenched) with pressure. Very precise pressure changes can be made in this way and it also minimises the risk of missing sudden changes in the photoluminescence.

A final precautionary note; whenever a low temperature DAC run is finished, or for some reason the cell must be warmed up, the force should be backed off to a safe level (≤1000psi). As the cell warms up the pressure will increase and there is a risk of breaking a diamond if it is left under a high load.

3.12 References.

1. D.J.Dunstan, J. Phys. E: Sci. Instrum., **20**, 577 (1987)
2. J.E.Dmochowski, R.A.Stradling, J.L.Sly, D.J.Dunstan, A.D.Prins and A.R.Adams, Acta Physica Polonica A, **87**, 457 (1995)
3. D.J.Dunstan and W.Scherrer, Rev. Sci. Instrum., **59**, 627 (1988)
4. A.Jayaraman, Rev. Sci. Instrum., **57**, 1013 (1986)
5. D.J.Dunstan and I.L.Spain, J. Phys. E: Sci. Instrum., **22**, 913 (1989)
6. M.Seal, High Temps.-High Press., **16**, 573 (1984)
7. J.Gonzalez, J.M.Besson and G.Weill, Rev. Sci. Instrum. **57**, 106 (1986)
8. H.K.Mao, P.M.Bell, K.J.Dunn, R.M.Chrenko and R.C.DeVries, Rev. Sci. Instrum., **50**, 1002 (1979)
9. D.J.Dunstan, Rev. Sci. Instrum., **60**, 378 (1989)
10. A.Jayaraman, Rev. Mod. Phys., **55**, 65 (1983)
11. J.H.Burnett, H.M.Cheong and W.Paul, Rev. Sci. Instrum., **61**, 3904 (1990)
12. J.D.Barnett, S.Block, G.Piermarini, Rev. Sci. Instrum., **44**, 1 (1973)

CHAPTER 4.

High Pressure Study of the Indirect Band-Gaps of GaSb and InGaSb.

4.1 Introduction.

High pressure photoluminescence techniques have been applied to a series of $In_xGa_{1-x}Sb/GaSb$ quantum-well structures in order to investigate their indirect band-gaps. By studying several quantum-wells with different indium contents we have been able to extrapolate the results to zero indium and thus determine the indirect band-gaps of the binary compound, GaSb. We obtain results which are consistent, within experimental error, with accepted theoretical values. It is found that a major limiting factor on the precision of our determinations is the accuracy of the pressure calibration. Suggestions are made for improvements to the experiment which should allow this method to provide accurate determinations of indirect band-gaps in this and other direct band-gap systems.

4.2 Background.

In the field of optoelectronics there has been a rapid growth of interest in semiconductor heterostructure systems. Advances in epitaxial growth techniques mean that there is an increasingly large number of alloy systems from which heterostructure devices, such as laser diodes and detectors, can be fabricated (the specific device application will determine principally the choice of materials system). The properties of these heterostructure systems are usually defined largely in terms of the well-known bulk

properties of the binary compounds upon which they are based. However, there are cases in which certain parameters are not well known, or easily measurable, in the bulk binary compounds but which can be measured accurately in the heterostructures. The $In_xGa_{1-x}Sb$/GaSb system provides an example.

It is well known that, at low temperature, GaSb has a direct band-gap of 0.81eV[1,2]. However, the positions of the indirect conduction band minima (which can influence device performance considerably) are less well established. Values given in the literature range from 0.87–1.10eV for the L_c–Γ_v band-gap[3,4] and 1.16–1.24eV for the X_c–Γ_v band-gap[5,4]. Using high-pressure photoluminescence techniques, Warburton *et al*[6] were able to induce Γ_c–L_c and L_c–X_c crossovers in a strained $In_{0.15}Ga_{0.85}Sb$ quantum-well structure. Furthermore, because indirect PL transitions could be observed and followed beyond these crossovers, they were able to extrapolate back to ambient pressure and thus determine both the L_c–Γ_v and the X_c–Γ_v indirect band-gaps in quantum-confined, strained $In_{0.15}Ga_{0.85}Sb$. In contrast, when the same techniques had been applied to a bulk GaSb sample the PL had quenched at ~10kbar (probably due to Γ_c–L_c crossover) and no luminescence had been observed above this pressure. Consequently, no determination of the indirect band-gaps could be made for the bulk material. The reason is that in bulk samples the observation of indirect PL above crossover requires excellent crystal quality; greater than that currently achieved in most materials systems. In heterostructures, however, the reduced symmetry in the growth direction weakens the selection rule forbidding indirect transitions. This means that indirect PL is observed above crossover in many heterostructure systems[7,8].

So, by applying high-pressure PL techniques to an $In_xGa_{1-x}Sb$/GaSb quantum-well

structure, Warburton *et al*[6] determined the indirect band-gaps in quantum-confined, strained $In_{0.15}Ga_{0.85}Sb$. They found that their results were described reasonably well by a model of the $In_{0.15}Ga_{0.85}Sb/GaSb$ heterostructure constructed using material and electronic parameters taken from the literature. However, this calculation required some twelve parameters such as band-gaps, deformation potentials and elastic constants, for both the InGaSb quantum-well and the GaSb barrier material. Unfortunately, even for the binary compounds GaSb and InSb, many of these parameters are not well established. This means that, despite reasonable agreement between the observed and the 'expected' results, this single measurement of an $In_xGa_{1-x}Sb/GaSb$ quantum-well cannot confirm with any certainty the accuracy of the GaSb indirect band-gaps (or any of the other parameters) given in the literature.

The work described in this chapter is a development of the original experiment of reference 6. We show how high-pressure measurements can be used to determine the indirect band-gaps of GaSb without relying on the uncertain parameters quoted in the literature. This is done by finding the indirect band-gaps of several quantum-confined, strained $In_xGa_{1-x}Sb$ quantum-wells, each of which has a slightly different indium content, x. As the indium content is reduced towards zero, the quantum-well Γ, L and X band-gaps go continuously towards bulk GaSb values. Extrapolation to zero indium content thus gives the indirect band-gaps in bulk GaSb. Since most of the materials and electronic parameters vary almost linearly over the ternary alloy range between GaSb and InSb, this extrapolation is expected to be close to linear for the moderate indium contents ($x \approx 0.12$-0.24) used here.

4.3 Experimental Details.

Three $In_xGa_{1-x}Sb$/GaSb heterostructure samples were studied under hydrostatic pressure; all were grown by MOVPE at the Clarendon Laboratory, Oxford. They were grown along the [001] crystal orientation on semi-insulating GaAs substrates under conditions optimized for bulk GaSb growth[9]. Due to the large lattice mismatch between GaAs and GaSb all of the samples contained buffer layers, of ~4μm of GaSb, to minimise the effects of dislocations nucleated at the substrate interface. Two of the samples consisted of single $In_xGa_{1-x}Sb$ quantum-wells, each 40Å wide, grown on the buffer layer and capped with 400Å of GaSb. The indium contents of these quantum-wells were nominally x=0.24 and x=0.17. The third sample was a multi quantum-well structure, comprising of a stack of ten $In_{0.12}Ga_{0.88}Sb$ quantum-wells, each 40Å wide, between 100Å GaSb barriers. This sample was capped with a 1720Å thick layer of GaSb.

It is important to note that the indium contents (x) of the quantum-wells, given above, are nominal values and may be subject to uncertainty. However, any inaccuracies in these values are eliminated from our analysis (see below) by plotting the results as functions of the 0kbar, Γ_c–Γ_v, emission energy rather than indium content. Well-widths were determined from growth rates (calibrated by TEM of bulk $In_xGa_{1-x}Sb$ layers grown under identical conditions).

The high pressure measurements were all carried out at 2K with helium used as the pressure transmitting medium (full details of the DAC techniques are given in chapter 3). Pressure was measured using standard ruby fluorescence.

4.4 Results and Discussion.

Figure 4.1 shows typical 2K photoluminescence spectra at several pressures for the $In_{0.24}Ga_{0.76}Sb$/GaSb sample. Figure 4.2 shows the PL peak position from this sample, plotted as a function of pressure. Initially, on applying hydrostatic pressure, the PL peak was seen to move up in energy at a rate of +14.0±1meV/kbar. This value for the pressure dependence of the direct band gap is in good agreement with that of reference 6 which gives a pressure coefficient of +13.8±0.4meV/kbar for both bulk GaSb and a 90Å $In_{0.15}Ga_{0.85}Sb$/GaSb quantum-well. It also compares reasonably well with the figure of +14.5±0.3meV/kbar quoted by Noack *et al*[10] for bulk GaSb. As can be seen from figure 4.1, beyond a pressure of ~10kbar the intensity of the PL from the $In_{0.24}Ga_{0.76}Sb$ quantum-well was reduced by more than two orders of magnitude. Figure 4.2 shows that this drop in intensity coincides with a change in the pressure coefficient of the PL peak to a value of +4.0±0.5meV/kbar. Then at ~43kbar the pressure coefficient changes again to −1.3±0.8meV/kbar. These pressure coefficients are typical of L_c–Γ_v and X_c–Γ_v band-gaps respectively and compare well with the values of +3.9±0.5meV/kbar and −1.4±0.4meV/kbar obtained from an $In_{0.15}Ga_{0.85}Sb$/GaSb quantum-well[6]. We therefore conclude that our $In_{0.24}Ga_{0.76}Sb$ quantum-well sample undergoes L_c–Γ_c crossover at ~10kbar, followed by X_c–L_c crossover at ~43kbar. PL from the sample was followed up to ~57kbar; on increasing the pressure further the luminescence quenched rapidly and could no longer be observed. This is probably due to the onset of a structural phase-change in the bulk GaSb (GaSb undergoes a phase transition to a β–Sn structure at high pressure and measurements by Yu *et al*[11] have determined this transition pressure to be

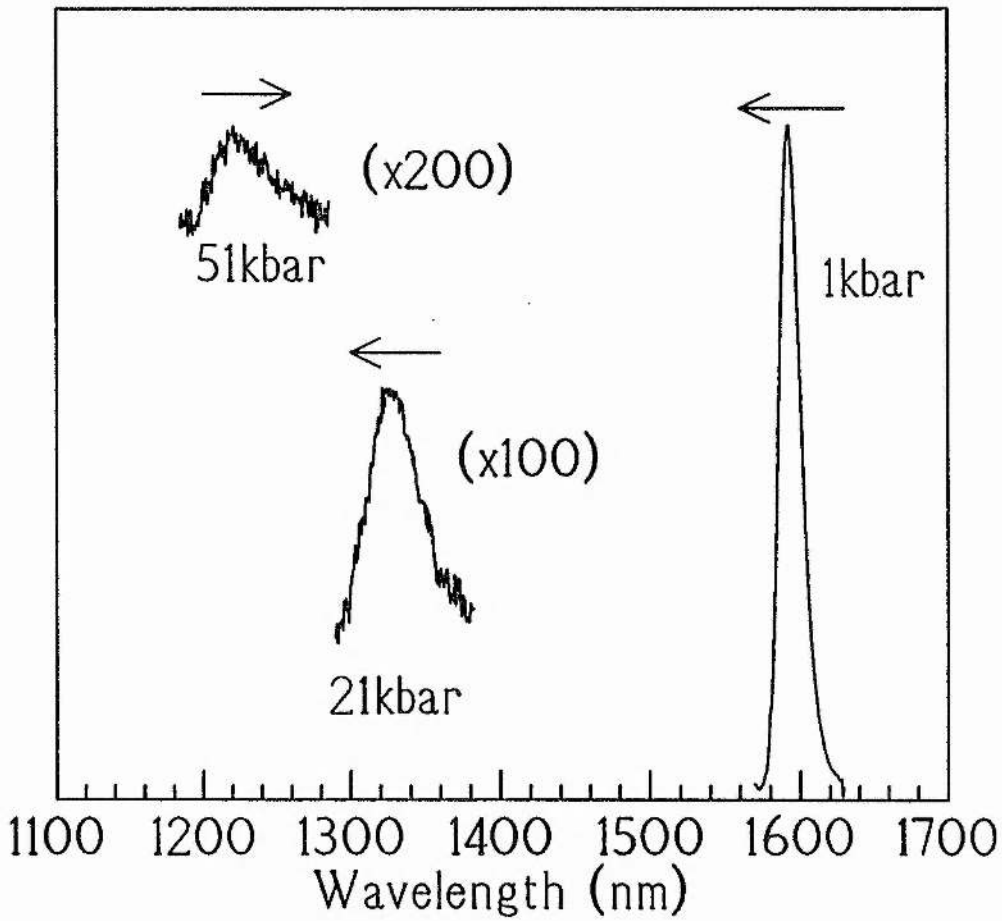

Figure 4.1 Typical PL spectra, at various pressures, from an $In_{0.24}Ga_{0.76}Sb/GaSb$ quantum-well. The spectra were all recorded at 2K.

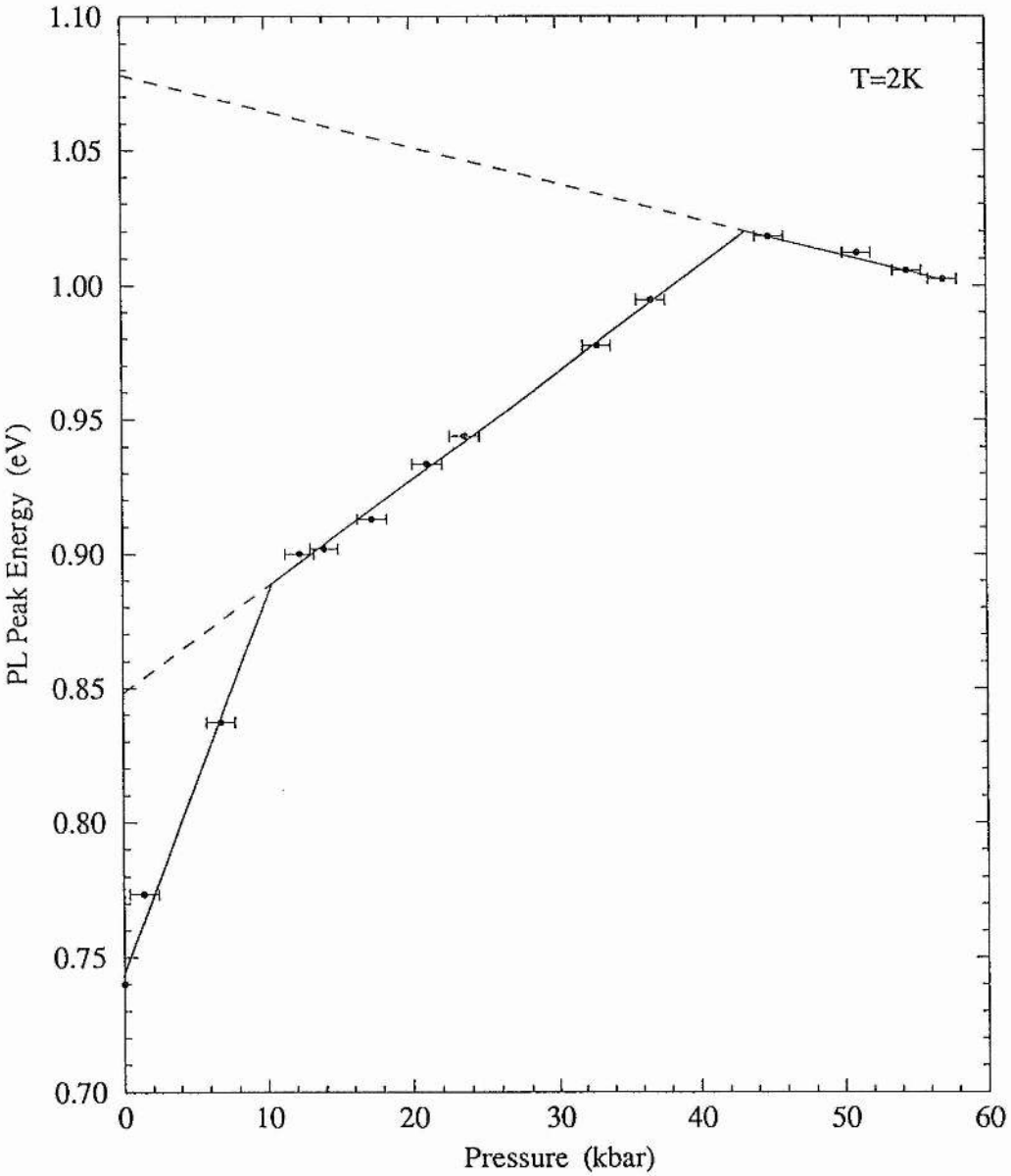

Figure 4.2 The PL peak energy, plotted as a function of pressure, for an $In_{0.24}Ga_{0.76}Sb/GaSb$ quantum-well.

62±3kbar).

So, by extrapolating the data shown in figure 4.2 back to ambient pressure (as indicated by the dashed lines in the figure) we can determine the low-temperature indirect band-gaps in quantum-confined, strained $In_{0.24}Ga_{0.76}Sb$. We thus obtain a value of 0.848±0.012eV for the L_c–Γ_v band-gap and 1.078±0.025eV for the X_c–Γ_v band-gap.

The same techniques were applied to the remaining $In_xGa_{1-x}Sb$/GaSb quantum-well samples. Figure 4.3 shows the PL peak positions plotted against pressure for these samples. It can be seen that clear Γ_c–Γ_v emission was observed from both samples, followed by L_c–Γ_c crossover and L_c–Γ_v emission. It is therefore possible in both cases to extrapolate back to ambient pressure and so determine the L_c–Γ_v band-gap. The x=0.17 sample (figure 4.3(a)) also displayed X_c–L_c crossover followed by X_c–Γ_v emission, thus enabling us to obtain the X_c–Γ_v band-gap. However, the PL from the x=0.12 sample (figure 4.3(b)) quenched before reaching X_c–L_c crossover and so no such determination could be made in this case.

Table 4.1 contains the measured Γ, L and X band-gaps (at 2K) and pressure coefficients from all the $In_xGa_{1-x}Sb$/GaSb samples studied. In figure 4.4 our values for the indirect band-gaps are plotted against the quantum-wells' 0kbar emission energy. As mentioned earlier, this is chosen as the ordinate, rather than indium content, so as to eliminate any error due to uncertainty in the exact composition. Clearly, given the large experimental errors (see below), we cannot extrapolate these data with any certainty to bulk GaSb values (i.e. to E_g^{Γ}=0.811eV); linear extrapolations of our data give L_c–Γ_v and X_c–Γ_v band-gaps of 0.94±0.035eV and 1.15±0.17eV respectively. However, the data are reasonably consistent with the dashed lines in figure 4.4 which show the theoretically

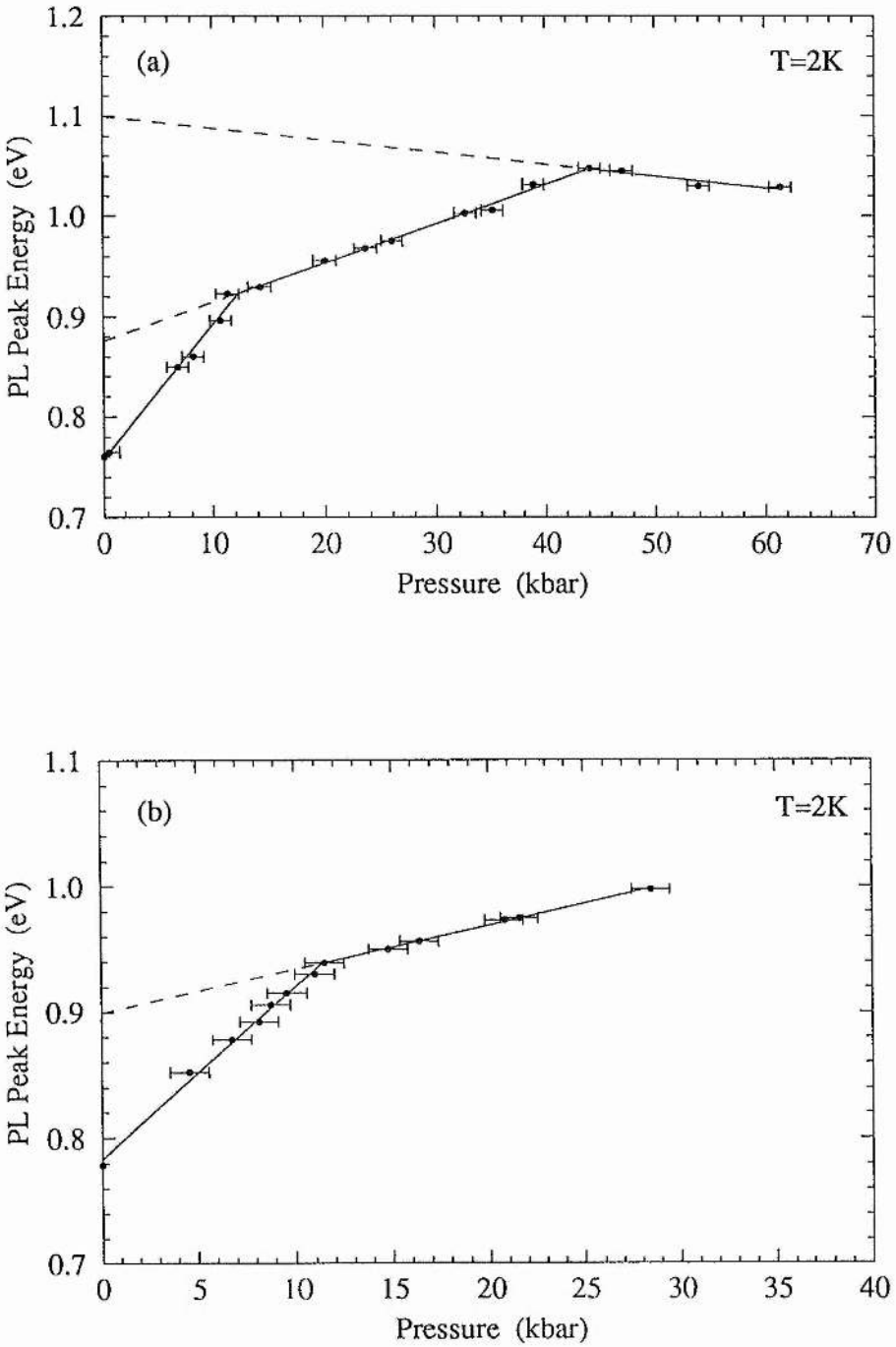

Figure 4.3 The PL peak energy, plotted as a function of pressure, for (a) an $In_{0.17}Ga_{0.83}Sb/GaSb$ quantum-well and (b) an $In_{0.12}Ga_{0.88}Sb/GaSb$ multi quantum-well structure.

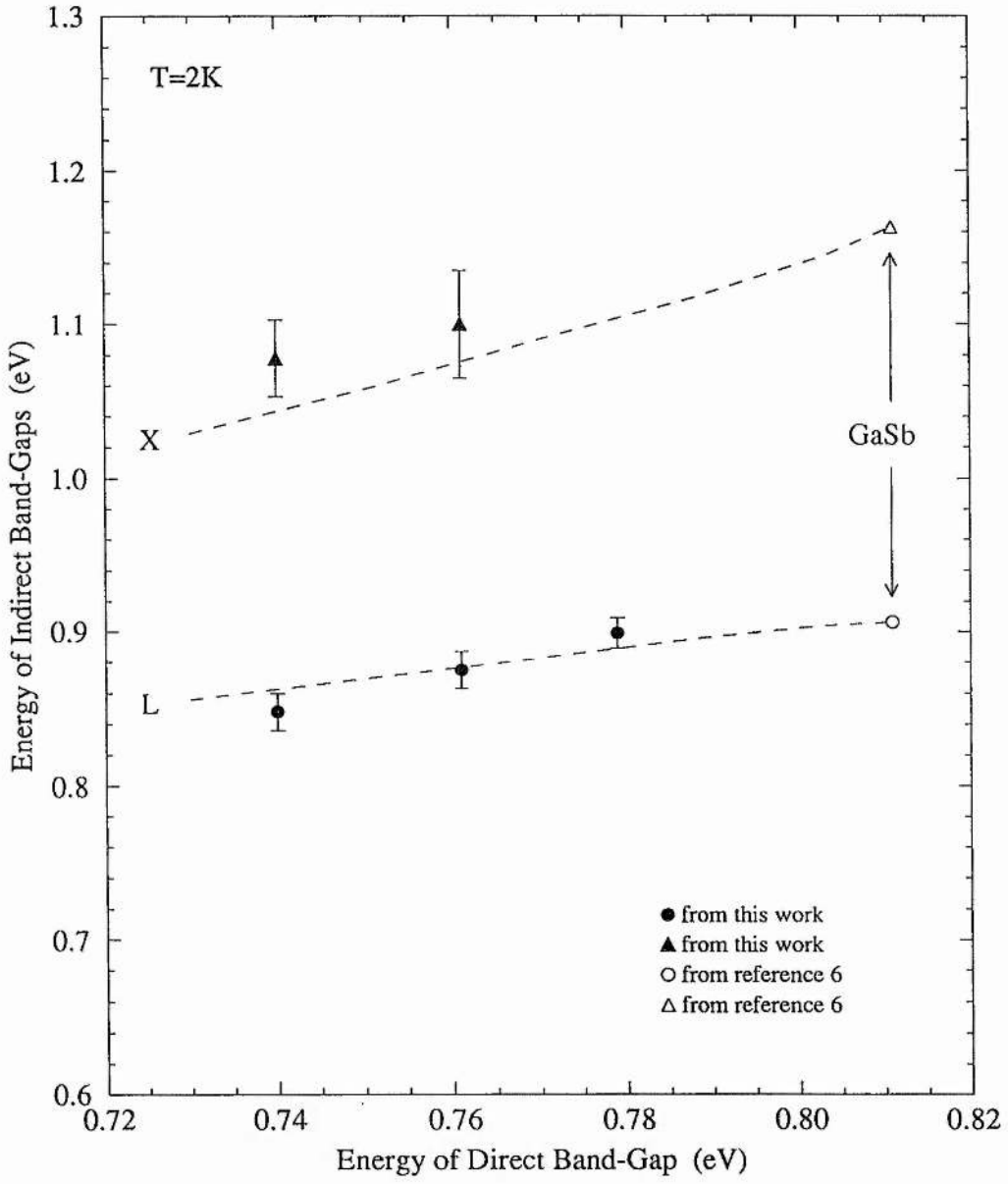

Figure 4.4 The indirect, excitonic band-gaps of a series of $In_xGa_{1-x}Sb/GaSb$ quantum-well samples, plotted as a function of indium content, x. Also shown (open symbols) are values for bulk GaSb, taken from reference 6.

expected variation of the indirect band-gaps of quantum-confined, strained InGaSb starting from the values for bulk GaSb. These theoretical calculations were made using an eight-band k.p Hamiltonian (strain effects are included via the Pikus-Bir strain Hamiltonian). The calculations were based on the $In_xGa_{1-x}Sb/GaSb$ quantum-well model suggested in reference 6, using the same material and electronic parameters taken from the literature[1,5,10,12-14].

So, although our experimental data is consistent with the accepted values of the indirect band-gaps in bulk GaSb, it is clear that a large reduction in the experimental error is necessary before this method can be used to confirm or refine these values. However, if this can be achieved then this experimental technique will be capable of yielding the bulk indirect band-gaps without relying on uncertain material and electronic parameters. The results of our calculations (see figure 4.4) confirm that, over the range of indium contents considered here, linear extrapolations of the indirect band-gaps to bulk GaSb values are valid. The only correction needed in order to obtain the true indirect band-gaps from the extrapolated values is the addition of the L and X exciton binding energies (see section 2.3) which are of the order of 10meV and 40meV respectively[12].

4.5 Suggestions for Further Work.

The most significant source of error in our data arises from the uncertainty in the pressure measurement. Using ruby fluorescence, which is still widely considered to be the established standard for pressure calibration, we are achieving an accuracy no better than ±1kbar (this can be estimated from the scatter of the Γ points in figure 4.2 around

COMPOSITION (nominal)	$In_{0.24}Ga_{0.76}Sb$	$In_{0.17}Ga_{0.83}Sb$	$In_{0.12}Ga_{0.88}Sb$
E_{Γ}^{Γ} (eV)	0.740±0.001	0.761±0.001	0.779±0.001
E_{Γ}^{L} (eV)	0.848±0.012	0.875±0.012	0.899±0.010
E_{Γ}^{X} (eV)	1.078±0.025	1.100±0.040	/
$dE/dP(\Gamma)$ (meV/kbar)	+14.0±1	+13.5±1	+13.6±1
$dE/dP(L)$ (meV/kbar)	+4.0±0.5	+3.9±0.5	+3.5±0.6
$dE/dP(X)$ (meV/kbar)	-1.3±0.8	-1.2±1	/

Table 4.1 The 2K band-gap energies and their pressure coefficients for a series of $In_xGa_{1-x}Sb$/GaSb quantum-well samples.

the fitted line). The limitations of ruby as a pressure calibrant are discussed in section 3.10 along with alternative methods of pressure calibration. It should be emphasized that in these experiments pressure is only a dummy variable. If, in addition to the high pressure PL measurements of the quantum-well, absorption techniques were used to measure the direct band-gap of the sample itself this would provide a suitable ordinate, in figures 4.2 and 4.3, for extrapolation of the indirect band-gaps back to their ambient-pressure values. This would eliminate the problems associated with pressure calibration and reduce the experimental errors considerably. Although these combined PL/absorption experiments are possible in the DAC, some further development of experimental techniques is required before this can reliably be performed at 2K and with helium as the pressure medium.

4.6 Conclusions.

Using a series of $In_xGa_{1-x}Sb$ quantum-wells grown in GaSb barriers we have demonstrated a method whereby high pressure techniques can be used to determine the indirect band-gaps in bulk GaSb. We obtain results which are consistent with accepted values but are prevented from improving on the accuracy or precision of these values by experimental uncertainties arising principally from using ruby as a pressure gauge. Suggestions are made for developments of the experimental technique which will eliminate the errors associated with pressure calibration. This method, which provides an example of how heterostructures may be used to measure bulk parameters, should then be capable of yielding accurate determinations of the indirect band-gaps in GaSb and

other bulk, direct band-gap materials.

4.7 References.

1. A.P.Roth and E.Fortin, Can. J. Phys., **56**, 1468 (1978)
2. W.Ruhle, W.Jakowetz, C.Wölk, R.Linnebach and M.Pilkuhn, Phys. Status. Solidi B, **73**, 225 (1973)
3. C.Alibert, A.Joullié, A.M.Joullié and C.Ance, Phys. Rev. B, **27**, 4946 (1983)
4. D.E.Aspnes, C.G.Olson and D.W.Lynch, Phys. Rev. B, **14**, 4450 (1976)
5. W.M.Coderre and J.C.Woolley, Can. J. Phys., **47**, 2553 (1969)
6. R.J.Warburton, R.J.Nicholas, N.J.Mason, P.J.Walker, A.D.Prins and D.J.Dunstan, Phys. Rev. B, **43**, 4994 (1991)
7. D.J.Wolford, T.F.Kuech, J.A.Bradley, M.A.Gell, D.Ninno and M.Jaros, J. Vac. Sci. Technol. B, **4**, 1043 (1986)
8. H.Q.Hou, L.J.Wang, R.M.Tang and J.M.Zhou, Phys. Rev. B, **42**, 2926 (1990)
9. S.K.Haywood, A.B.Henriques, N.J.Mason, R.J.Nicholas and P.J.Walker, Semicond. Sci. Technol., **3**, 315 (1988)
10. R.A.Noack and W.B.Holzapfel, Solid State Commun., **28**, 177 (1978)
11. S.C.Yu, I.L.Spain and E.F.Skelton, Solid State Commun., **25**, 49 (1978)
12. Landolt-Börnstein, *Numerical Data and Functional Relationships in Science and Technology*, Group III, Vol. 17a, ed. O.Madelung (Springer-Verlag, Berlin, 1982).
13. C.G.Van De Walle, Phys. Rev. B, **39**, 1871 (1989)
14. R.A.Noack, Phys. Status Solidi B, **90**, 615 (1978)

CHAPTER 5.

High Pressure Determination of the Band Structure of AlGaInP Bulk Crystals and Heterostructures.

5.1 Introduction.

This chapter contains the results from a systematic program of work in which low temperature photoluminescence techniques have been carried out at hydrostatic pressures up to 80kbar in order to determine the band structure of AlGaInP bulk crystals and measure band offsets in GaInP/AlGaInP heterostructures.

Using a series of specially designed samples it has been possible to determine how the energies of the Γ_c and X_c minima vary as a function of aluminium content in $(Al_xGa_{1-x})_{0.5}In_{0.5}P$. Lower limits have been put on the position of the L_c minima in this system and also in 1% compressively strained $Ga_{0.38}In_{0.62}P$. Band offsets have been measured in the unstrained $Ga_{0.5}In_{0.5}P/(Al_xGa_{1-x})_{0.5}In_{0.5}P$ system and the 1% compressively strained $Ga_{0.38}In_{0.62}P/(Al_xGa_{1-x})_{0.5}In_{0.5}P$ system as functions of aluminium content. The effects of ordering on pressure coefficients and the Γ_c–X_c energy separation in $Ga_{0.5}In_{0.5}P$ have also been measured.

5.2 Motivation.

There is currently considerable interest in the design and optimization of optoelectronic devices operating in the visible wavelength range. The development of

short-wavelength laser diodes, for example, will increase the information density available on optical data storage systems. It could also provide a cheap and reliable alternative to the He–Ne gas laser in various applications such as bar-code scanners and optical printers. In this context the AlGaInP materials system is an important one. By varying the alloy composition and using the effects of strain it is possible to produce devices emitting in the 620-690nm wavelength range[1].

Successful design and analysis of such devices requires an accurate knowledge of various material parameters, such as the relative positions of the Γ_c, L_c and X_c minima. In heterostructure devices an accurate knowledge of the band offsets is also essential. However, despite its technological importance, there is only limited and sometimes controversial data available on the band structure of AlGaInP and its compositional dependence. For example, it is known that GaInP is a direct band-gap material whereas AlInP is indirect, with the lowest lying conduction band state occurring at the X point[2]. However, literature values for the composition at which $(Al_xGa_{1-x})_{0.5}In_{0.5}P$ goes from direct to indirect vary from x=0.5[3] to x=0.7[4]. Furthermore, whilst theoretical calculations have suggested that the L_c minima in $Ga_{0.5}In_{0.5}P$ may lie approximately 135meV above the Γ_c minimum[5], its position in this and other alloys is essentially unknown.

Several measurements have been reported of band offsets in unstrained $Ga_{0.5}In_{0.5}P/(Al_xGa_{1-x})_{0.5}In_{0.5}P$ with values quoted for the band offset ratio, $\Delta E_c/\Delta E_g$, ranging from 0.39[6] to 0.67[7]. Unfortunately, most of these experiments have been carried out at different, single, points in the alloy range. Since experimental conditions and sample characteristics vary considerably, comparing data across the entire alloy range is difficult and inconclusive. In the case of strained $GaInP/(Al_xGa_{1-x})_{0.5}In_{0.5}P$ heterostructures, only

limited data exist regarding band offsets[8,9].

Finally, it is now well known that under certain conditions long range ordering of the group III atoms occurs during the growth of $Ga_{0.5}In_{0.5}P$[10]. The resulting alloys exhibit properties significantly different to those of their disordered equivalents; most notably a reduction in the direct band-gap[11]. However, many of the effects of ordering, including its influence on the position of the indirect conduction band minima, have not yet been accurately quantified or are the subject of debate.

5.3 Band Structure of Bulk AlGaInP Crystals.

5.3.1 Experimental Details.

All of the samples described in this section were grown by MOVPE on [001] oriented GaAs substrates under conditions optimized for high quality disordered growth[12]. Four bulk $(Al_xGa_{1-x})_{0.5}In_{0.5}P$ samples were grown with aluminium contents of x=0, x=0.3, x=0.4 and x=0.7. In all cases the AlGaInP layer was approximately 1μm thick. The $Ga_{0.5}In_{0.5}P$ (x=0) sample was grown by Optronics, Ireland while the x=0.3, x=0.4 and x=0.7 samples were grown at the Philips Optoelectronics Centre, Eindhoven. Double crystal X–ray diffraction measurements on these layers showed them to be lattice matched to their substrates to within ±0.1%. These samples were used to determine the compositional dependence of the Γ_c–Γ_v and X_c–Γ_v band-gaps and to put lower limits on the position of the L_c minima. Two further samples were grown, each consisting of a single 1% compressively strained $Ga_{0.38}In_{0.62}P$ quantum-well in unstrained $Ga_{0.5}In_{0.5}P$

barriers. The well widths were 23Å and 100Å respectively. Well widths were determined from growth rates, calibrated by TEM on test samples, with an estimated accuracy of ±5%. These samples were both grown at Philips Optoelectronics Centre and were used to put lower limits on the position of the L_c minima in strained $Ga_{0.38}In_{0.62}P$. Rapid thermal annealing experiments[13] confirmed that these bulk layers and quantum-well structures were highly disordered.

All of the high pressure measurements on these samples were carried out at 2K, as described in chapter 3, in a DAC in which helium was used as the pressure transmitting medium. In all cases pressure was measured using a ruby pressure gauge in addition to the GaAs emission from the sample's substrate.

5.3.2 Position of the Γ_c and X_c Minima in Bulk $(Al_xGa_{1-x})_{0.5}In_{0.5}P$.

Figure 5.1 shows typical 2K PL spectra for the $Ga_{0.5}In_{0.5}P$ sample at several pressures up to 32kbar. At ambient pressure a strong emission peak was observed at an energy of 1.974eV with a FWHM of 6meV. The nature and position of this peak are as we would expect from the direct Γ_c–Γ_v excitonic emission of high quality disordered $Ga_{0.5}In_{0.5}P$[3,12]. Figure 5.2 shows the hydrostatic pressure dependence of the luminescence peak energy. Initially the PL peak moves at a rate of +8.4±0.1meV/kbar. This is in good agreement with values reported by Chen *et al*[14] and Patel *et al*[15], for nominally identical material, of +8.4meV/kbar and +8.6meV/kbar respectively. At 28kbar the PL intensity dropped by two orders of magnitude and an additional emission peak was observed (shown in figure 5.1) approximately 30meV below the main PL peak. As the pressure

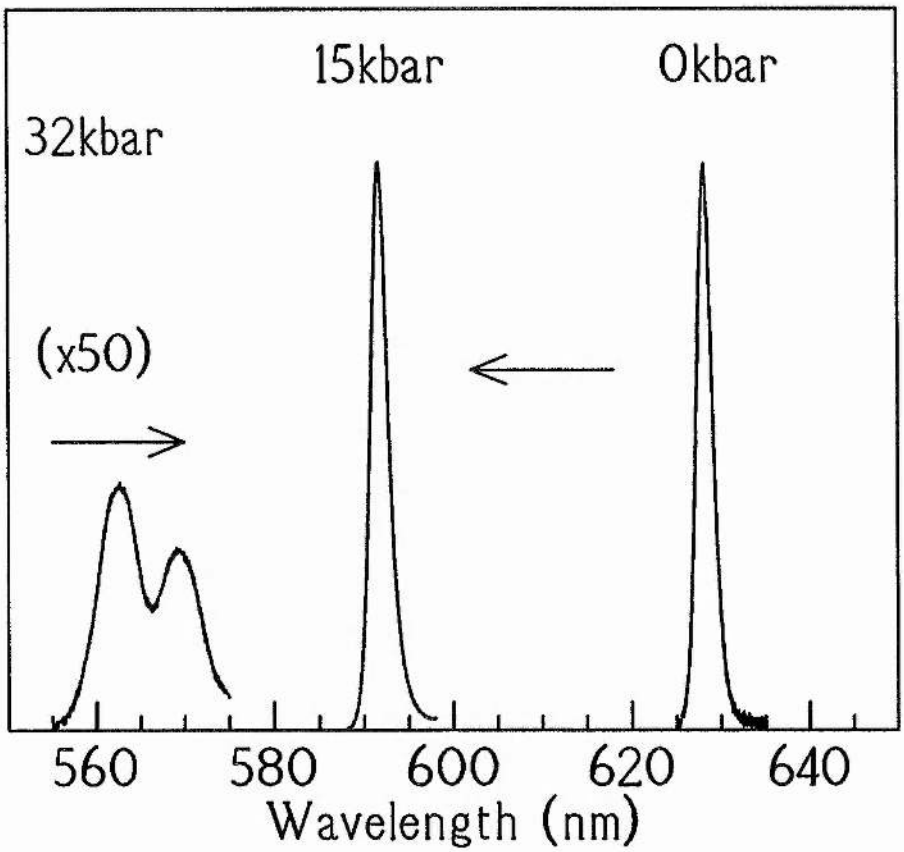

Figure 5.1 Typical PL spectra, at various pressures, from a $Ga_{0.5}In_{0.5}P$ sample at 2K. The arrows indicate the direction of movement of the peaks with pressure.

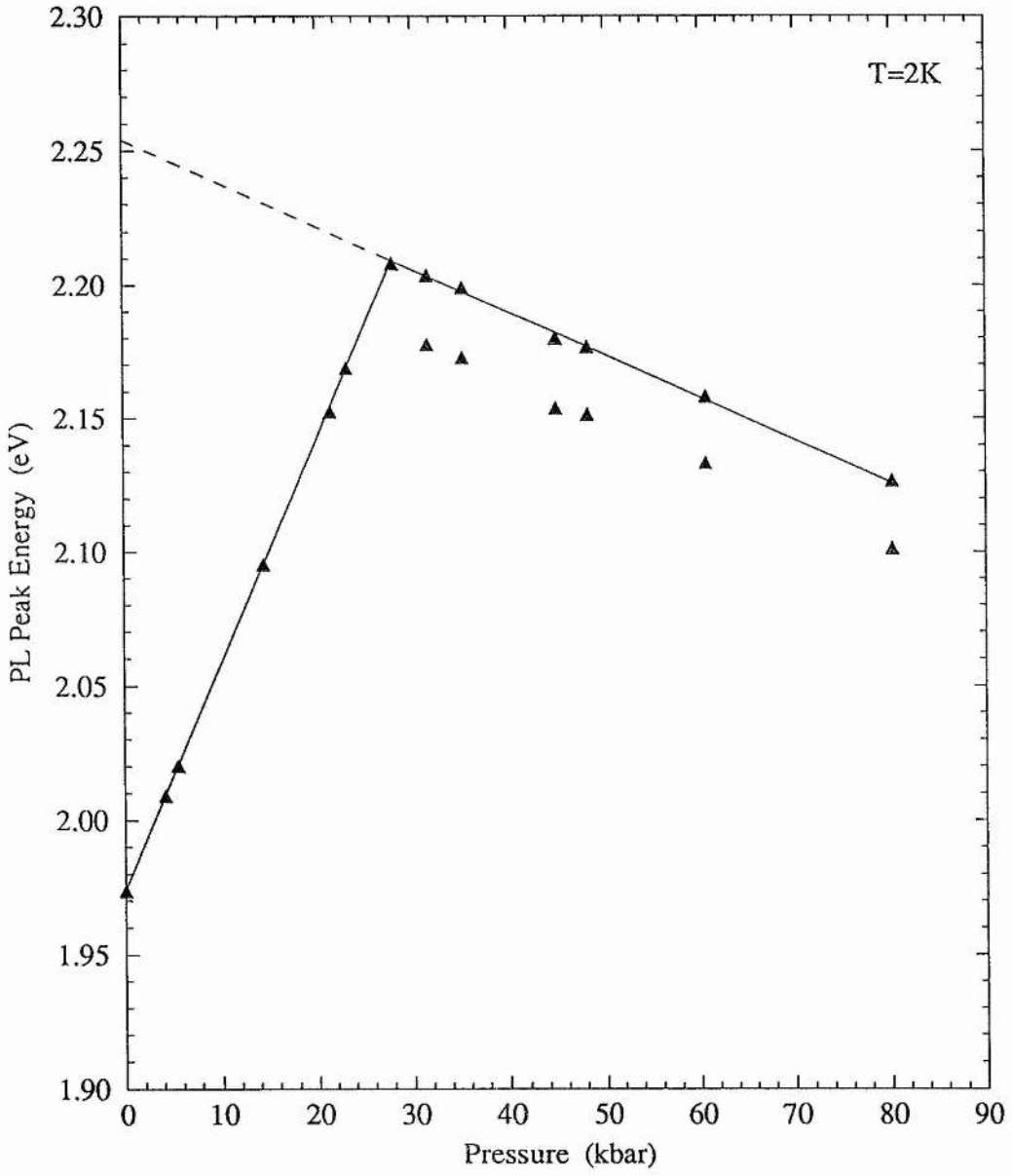

Figure 5.2 The PL peak energy, plotted as a function of pressure, for the $Ga_{0.5}In_{0.5}P$ sample.

was increased further, both peaks moved down in energy at a rate of −1.6±0.1meV/kbar. The intensity continued to decrease with pressure but it was possible to follow the PL peaks up to 80kbar. We interpret this as evidence that the X_c minimum crosses in energy with the Γ_c minimum at 28kbar, thus becoming the lowest-lying conduction band minimum. The observed pressure coefficient of −1.6±0.1meV/kbar is typical of that of an indirect X_c–Γ_v band-gap and compares reasonably well with the figure of −2.0±0.2meV/kbar given in reference 15. The presence of the satellite peak is attributed to LA–X phonon-assisted transitions (the observed phonon spacing of 30meV compares to a value of 31meV for the LA–X phonon in GaP[16] and 24meV in InP[16]). From figure 5.2 it is clearly possible to extrapolate the energy of the indirect transition back to ambient pressure. This gives a value of 2.254±0.005eV for the X_c–Γ_v excitonic band-gap at 2K.

The same analysis can be applied to the $(Al_xGa_{1-x})_{0.5}In_{0.5}P$ samples with x=0.3 and x=0.4. At ambient pressure the observed Γ_c–Γ_v excitonic band-gaps were 2.167eV and 2.223eV respectively. The results of the high pressure experiments are shown in figure 5.3. It can be seen that the X_c–Γ_c crossover occurred at ~12kbar in the x=0.3 sample and ~7kbar in the x=0.4 sample. Extrapolating back to ambient pressure gives X_c–Γ_v excitonic band-gaps of 2.29±0.01eV and 2.296±0.005eV respectively.

Ambient pressure PL from the x=0.7 sample was weak compared to that from the other samples. The spectra showed an emission peak at an energy of 2.313±0.005eV with two satellite peaks, 33meV and 47meV below the main peak. On applying hydrostatic pressure these peaks moved down in energy at a rate of −2.2±0.2meV/kbar. We therefore conclude that the x=0.7 sample is indirect at ambient pressure, with an X_c–Γ_v excitonic band-gap of 2.313±0.005eV. The satellite peaks are again attributed to phonon-assisted

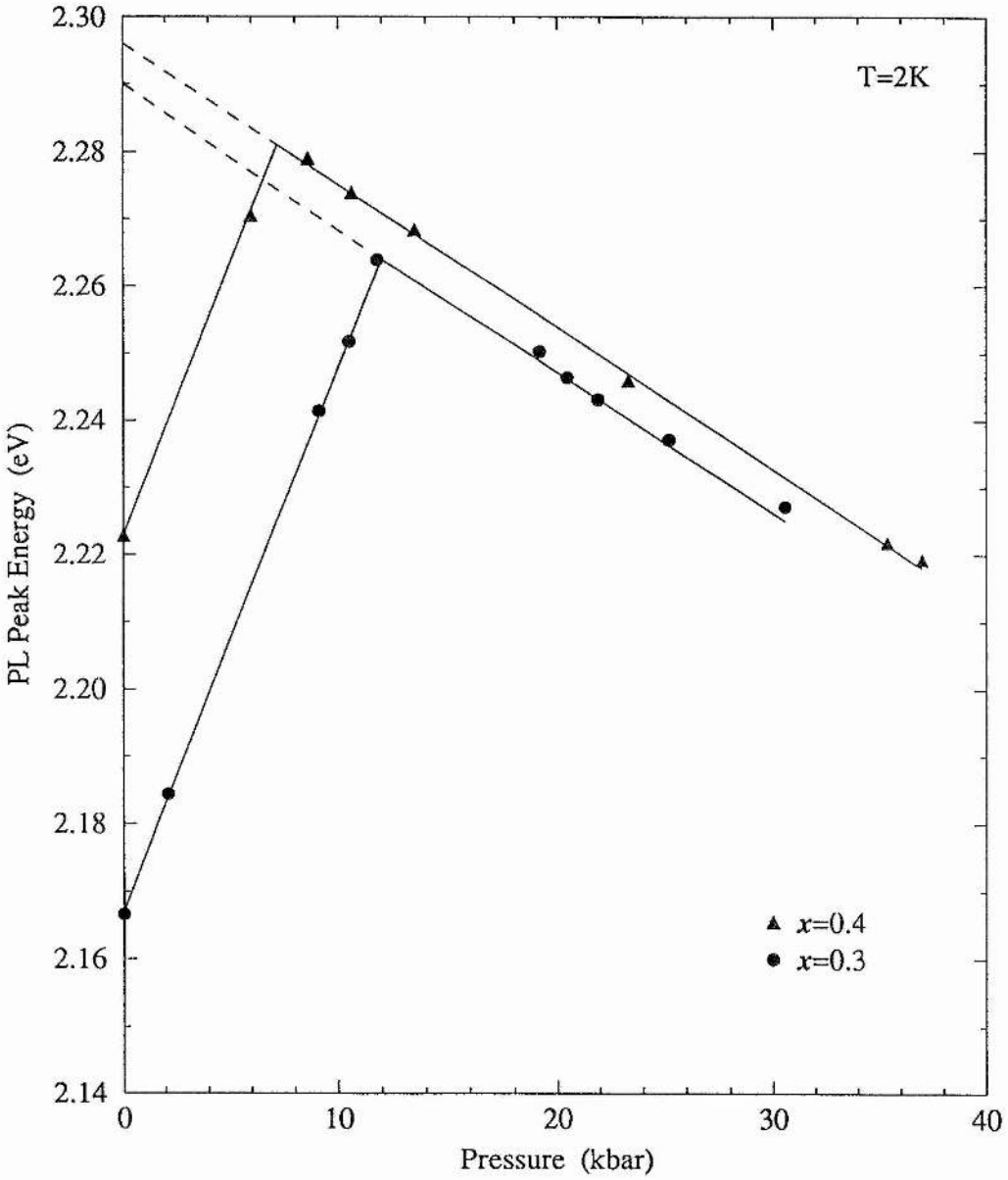

Figure 5.3 PL peak energies, plotted as functions of pressure, for the $(Al_xGa_{1-x})_{0.5}In_{0.5}P$ samples with x=0.3 and x=0.4.

transitions.

The Γ and X excitonic band-gaps in $(Al_xGa_{1-x})_{0.5}In_{0.5}P$ have thus been determined, at 2K, for compositions of x=0, x=0.3, x=0.4 and x=0.7. Least-squares fits to the data give us compositional dependencies of:

$$E_{PL}^{2K}(\Gamma) = (1.980 + 0.61x)\text{eV} \quad (5.1)$$

and

$$E_{PL}^{2K}(X) = (2.260 + 0.085x)\text{eV} \quad (5.2)$$

It should be noted that in order to obtain the true Γ and X band-gaps, $E_g(\Gamma)$ and $E_g(X)$, it is necessary to adjust the values of $E_{PL}(\Gamma)$ and $E_{PL}(X)$ by adding the exciton binding energies. In the absence of experimentally determined exciton binding energies we estimate values from those available in the literature. Interpolation between values given for GaP[16] and InP[16] gives 5meV for the direct exciton binding energy and 22meV for the indirect exciton binding energy. Equations 5.1 and 5.2 can now be modified to give the compositional dependencies of the Γ and X band-gaps in $(Al_xGa_{1-x})_{0.5}In_{0.5}P$:

$$E_g^{2K}(\Gamma) = (1.985 + 0.61x)\text{eV} \quad (5.3)$$

and

$$E_g^{2K}(X) = (2.282 + 0.085x)\text{eV} \quad (5.4)$$

Figure 5.4 shows the determined Γ and X band-gaps, corrected for exciton binding energies and plotted as a function of aluminium composition (x). The fits represented by equations 5.3 and 5.4 are shown as solid lines. Also included, for comparison, are data taken from a recent study by Lambkin *et al* on AlInP[17].

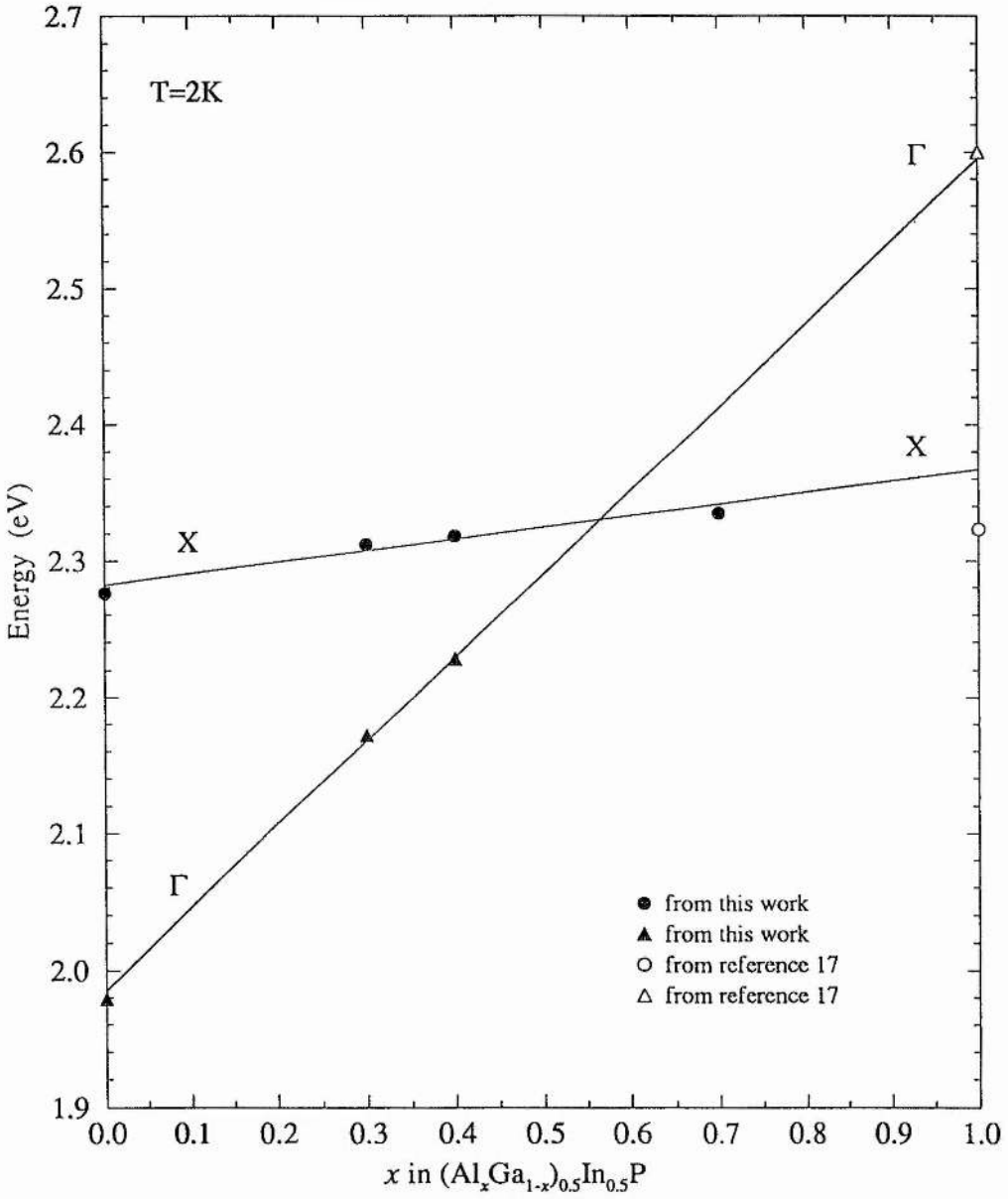

Figure 5.4 The Γ and X band-gap energies of $(Al_xGa_{1-x})_{0.5}In_{0.5}P$ as functions of aluminium content, x. The lines represent fits to our data, given by equations 5.3 and 5.4. Also shown are AlInP data from reference 17.

5.3.3 Position of the L_c Minima in $(Al_xGa_{1-x})_{0.5}In_{0.5}P$.

Applying hydrostatic pressure to a semiconductor in which the L_c minima start closer to the Γ_c than to the X_c may lead to L_c–Γ_c crossover and a range of pressure in which the L_c minima are lowest[18]. If the L_c–Γ_v emission can be followed over this pressure range then it is possible to extrapolate its energy back to ambient pressure in the way described in the previous section for X levels. However, no such L_c–Γ_c crossover was observed in the high pressure data from any of the $(Al_xGa_{1-x})_{0.5}In_{0.5}P$ samples. Despite this, in the case of the x=0, x=0.3 and x=0.4 samples, it is still possible to put lower limits on the positions of the L_c minima. In the x=0 sample the X_c–Γ_c crossover occurred at 28kbar and at an energy of 2.209eV; below this no evidence was seen of L_c–Γ_v transitions. So, by extrapolating back from this point at a rate of +4meV/kbar, which is taken as typical for the pressure dependence of L_c minima (see section 2.2), we conclude that the L_c minima must be at least ~125meV above the Γ_c minimum. Doing the same for the x=0.3 and x=0.4 samples gives lower limits for the L_c–Γ_c separation of approximately 2.216meV and 2.252meV respectively.

5.3.4 Position of the L_c Minima in Compressively Strained $Ga_{0.38}In_{0.62}P$.

A similar method to that described in the previous section can be applied to the problem of finding the position of L_c minima in strained GaInP. However, the growth of strained material requires the use of thin layers, most commonly in the form of quantum-wells. This means that quantum confinement energies have to be included in the analysis.

We use electron and heavy-hole confinement energies which have been calculated by solving a single-band envelope-function Schrodinger equation, using effective masses taken from the literature[16,19]. The zone-centre effective masses in the conduction band are corrected using standard k.p theory. The reliability of the confinement energies is tested by comparing the band-gap required to give the observed PL energies in quantum-wells of different thicknesses. In the case of the compressively strained $Ga_{0.38}In_{0.62}P$ samples, described in section 5.3.1, we find that the PL from both the 23Å and 100Å wells is consistent with a low-temperature band-gap of 1.84eV. For the 23Å quantum-well we get values of 65meV for the electron confinement energy and 35meV for the heavy-hole confinement. In fact, quantum confinement raises the Γ_c electron towards the L_c thus making a Γ–L–X sequence of crossovers more probable. It is for this reason that we chose the narrower quantum-well for this attempt to try and locate the L_c minima. Figure 5.5 shows the results of a high pressure experiment, carried out at 2K, on the 23Å, 1% compressively-strained $Ga_{0.38}In_{0.62}P$ quantum-well. At ambient pressure PL was observed from the quantum-well at an energy of 1.940eV. Applying pressure caused this peak to move up in energy but no L_c–Γ_c was observed below ~29kbar, at which point the luminescence intensity quenched rapidly. The PL energy at this point represents a lower limit on the energy of the L_c–Γ_v transition at this pressure. Extrapolating back at 4meV/kbar (as indicated by the dashed line in figure 5.5) shows this limit to be 2.05eV at ambient pressure. This places the L_c minimum at least 110meV above the quantum-confined Γ_c state. Adding the electron confinement of 65meV therefore gives a minimum L_c–Γ_c separation of 175meV in bulk, 1% strained $Ga_{0.38}In_{0.62}P$ at ambient pressure. In arriving at this figure we have ignored the effects of L confinement (any L confinement

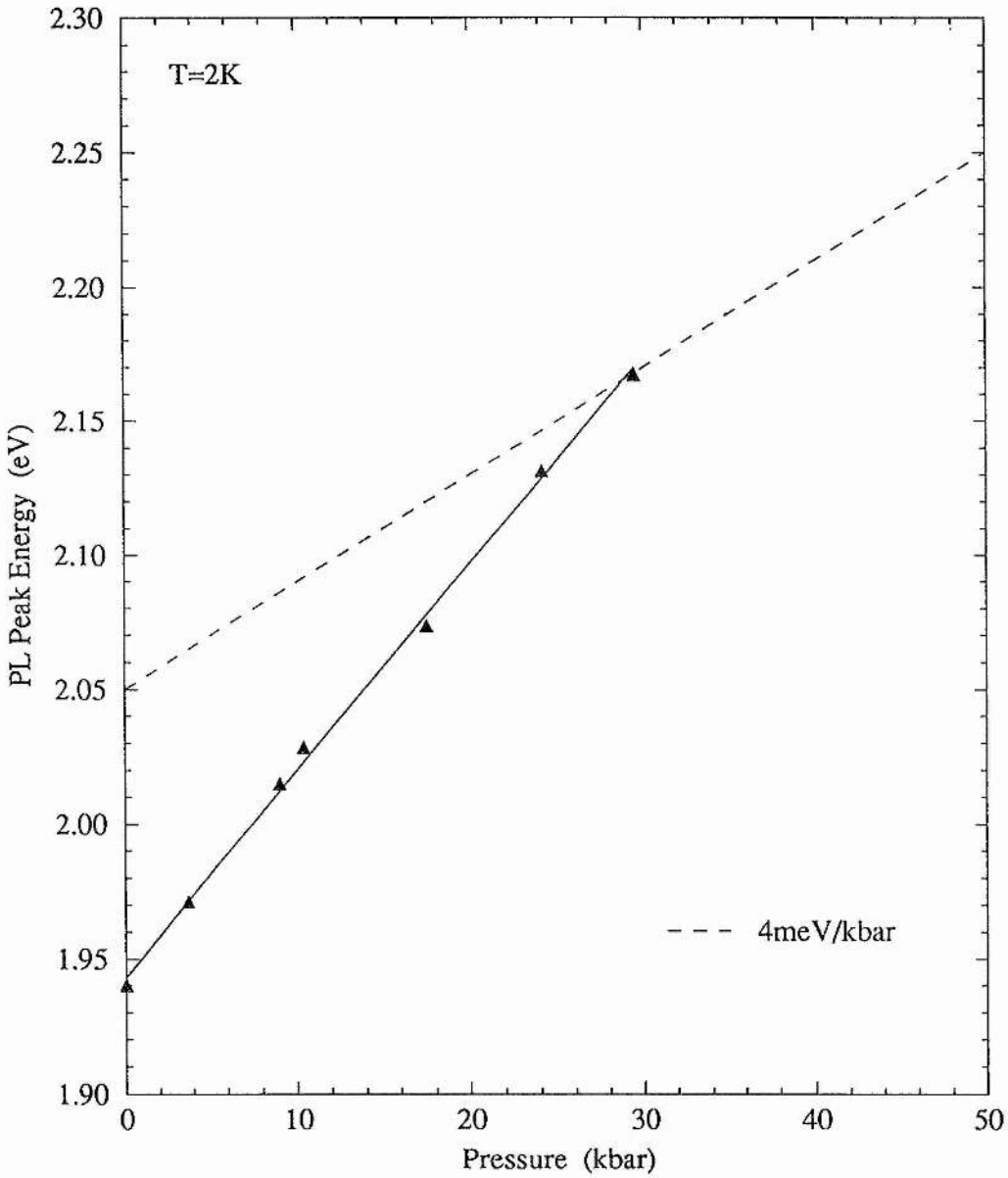

Figure 5.5 The PL peak energy plotted against pressure for a 23Å, 1% compressively-strained $Ga_{0.38}In_{0.62}P/Ga_{0.5}In_{0.5}P$ quantum-well.

energy would have to be subtracted from our determined value for the minimum L_c–Γ_c separation). Due to the lack of data on the L minima in GaInP we cannot say whether the quantum-well L states will be confined or not. If we assume the maximum possible confinement for L_c electrons in a 23Å well we would have to reduce our minimum L_c–Γ_c separation, by approximately 35meV, to ~140meV.

5.3.5 Discussion of Bulk Band Structure Results.

Figure 5.4 shows the results of our band structure measurements. The solid lines are the fits to our data, given by equations 5.3 and 5.4. From this it can be seen that, in $(Al_xGa_{1-x})_{0.5}In_{0.5}P$ alloys where $x \geq 0.57$, the indirect X_c–Γ_v band-gap will be lower in energy than the direct band-gap. This is significantly lower than the figure of x=0.7 given by Bour *et al*[4] for $(Al_xGa_{1-x})_{0.5}In_{0.5}P$ at room temperature. Since our determinations were made at 2K, we should consider how temperature will affect these results. Room temperature PL measurements were made of the x=0, x=0.3 and x=0.4 samples. A least-squares fit to the 300K data gives the compositional dependence of the direct band-gap in $(Al_xGa_{1-x})_{0.5}In_{0.5}P$ at 300K to be:

$$E_g^{300K}(\Gamma) = (1.900 + 0.61x)\text{eV} \qquad (5.5)$$

For x=1 this gives $E_g(\Gamma)$=2.510 which agrees well with the value given by Lambkin *et al*[17] of $E_g(\Gamma)$=2.515. Comparing equations 5.3 and 5.4 it is clear that the increase in $E_g(\Gamma)$ in going from 300K to 2K is 85meV. This is consistent with the equivalent increases in InP

and GaP of 80meV and 90meV respectively[16]. As far as the temperature dependence of $E_g(X)$ is concerned, the only data available which is relevant to this system is for GaP and AlP. This gives the increase in $E_g(X)$, in going from 300K to 2K, to be 78meV for GaP[16] and 80meV for AlP[16]. So, if we assume that in $(Al_xGa_{1-x})_{0.5}In_{0.5}P$ this increase is approximately 78meV then, from equation 5.4, we get:

$$E_g^{300K}(X) = (2.204 + 0.085x)eV \qquad (5.6)$$

Now, equating equations 5.5 and 5.6 shows that, at room temperature, the aluminium content above which $(Al_xGa_{1-x})_{0.5}In_{0.5}P$ will be indirect is $x\sim0.58$; still considerably less than the figure quoted in reference 4. However, our low-temperature results are in good agreement with recent work by Mowbray *et al*[3]. For $(Al_xGa_{1-x})_{0.5}In_{0.5}P$ at 2K they conclude that the direct and indirect (X) excitonic band-gaps coincide in energy when $x=0.5\pm0.02$. From our determination of the excitonic band-gaps (equations 5.1 and 5.2) we find the corresponding value to be $x=0.53$.

As for the position of the L_c minima; little data is available for comparison with our experimentally determined limits. However, the work of Bugajski *et al*[5] suggests that, at 300K, the L_c–Γ_c separation is ~135meV in $Ga_{0.5}In_{0.5}P$ and ~180meV in $Ga_{0.38}In_{0.62}P$. If we assume that the temperature dependencies of the L_c and Γ_c minima are similar, then Bugajski's results are at least consistent with our determined lower limits of ~125meV and ~140meV respectively.

5.4 Band Offsets in GaInP/$(Al_xGa_{1-x})_{0.5}In_{0.5}P$ Heterostructures.

5.4.1 Experimental Details.

The four samples described below were grown by MOVPE at Philips Optoelectronics Centre, Eindhoven, under the same conditions as the samples described in section 5.3.1.

The first, unstrained, sample consisted of two 100Å-wide $Ga_{0.5}In_{0.5}P$ quantum-wells in 500Å $(Al_{0.7}Ga_{0.3})_{0.5}In_{0.5}P$ barriers and two 40Å-wide $Ga_{0.5}In_{0.5}P$ quantum-wells in 500Å $(Al_{0.3}Ga_{0.7})_{0.5}In_{0.5}P$ barriers. Three 1% compressively-strained single-quantum-well samples were also grown. Each consisted of a $Ga_{0.38}In_{0.62}P$ quantum-well in unstrained $(Al_xGa_{1-x})_{0.5}In_{0.5}P$ barriers; aluminium contents were x=0, x=0.3 and x=0.4. The well widths for these samples were 100Å, 80Å and 100Å respectively (determined by growth rates, see section 5.3.1).

High pressure measurements were all made at 2K, as described in chapter 3, with helium used as the pressure transmitting medium. Pressure was measured using both ruby fluorescence and PL from the sample's substrate.

5.4.2 Band Offsets in Unstrained $Ga_{0.5}In_{0.5}P/(Al_xGa_{1-x})_{0.5}In_{0.5}P$ Heterostructures.

Section 5.3.2 contains several examples of pressure-induced X_c–Γ_c crossover in bulk $(Al_xGa_{1-x})_{0.5}In_{0.5}P$ alloys. Similarly, the application of hydrostatic pressure to quantum-well structures can cause X_c–Γ_c crossing; though now the Γ_c levels in the wells

and barriers can cross in energy with the X_c levels in either the wells or the barriers (depending on their initial positions). If crossover occurs with the barrier X_c then a direct determination of the band offsets may be possible, as described in section 2.4. However, if the Γ_c of the quantum-well crosses with its own X_c level then no such determination can be made. So, if we want to measure band offsets in a new system, the first problem to address is whether the Γ_c of the well will cross with the barrier X_c or its own. The sample represented in figure 5.6 was grown in order to solve this problem for the unstrained $Ga_{0.5}In_{0.5}P/(Al_xGa_{1-x})_{0.5}In_{0.5}P$ system. Figures 5.6(a) and 5.6(b) both represent the band structure of a sample containing two types of quantum-well; one in barriers with a low aluminium content (x=0.3), the other in barriers with a high aluminium content (x=0.7). On an absolute scale we would expect the energy of the X_c level either to decrease with aluminium content (as shown in figure 5.6(a)), or to increase with aluminium content (as in figure 5.6(b)). Consequently we would expect that applying high hydrostatic pressure to such a sample should give rise to one of the following two types of behaviour;

i) in the case illustrated by figure 5.6(a), the quantum-well Γ_c levels will cross with the barrier X_c levels and we would expect the well in the high aluminium content barriers to cross first; i.e. at a lower pressure and lower energy.

ii) in the case illustrated by figure 5.6(b), the quantum-well Γ_c levels will cross with their own X_c levels and so we would expect both wells to cross at the same pressure and the same energy.

In fact, the actual sample contained two of each type of quantum-well (to enhance PL

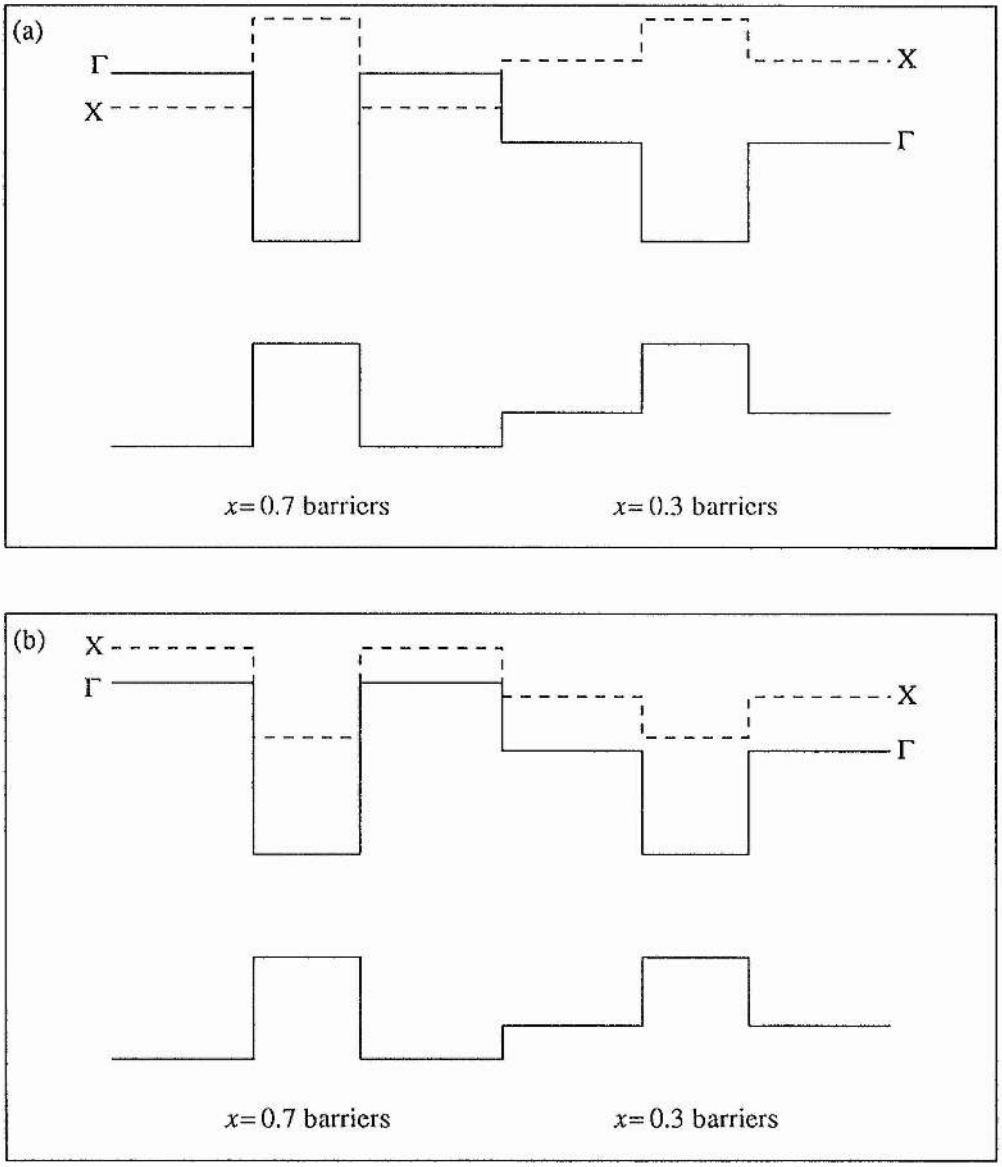

Figure 5.6 A schematic representation of a sample containing two quantum-wells, one grown in high aluminium content barriers (x=0.7), the other in low aluminium content barriers (x=0.3); (a) shows the case where hydrostatic pressure will cause crossing between the barrier X_c and the well Γ_c (the well in x=0.7 barriers will cross at a lower pressure) and (b) shows the case where the well Γ_c will cross with its own X_c level (both wells cross at the same pressure).

intensities) and in order to make the two types of well distinguishable by PL the wells in the x=0.3 barriers were made slightly narrower, thus increasing their confinement energy slightly. Pushing the confined Γ_c state in this well up, towards the lowest X_c level, also lowers its crossover pressure slightly.

The results of a high pressure experiment on this sample are shown in figure 5.7. Figure 5.7(a) shows the PL energy plotted as a function of pressure for both pairs of quantum-wells. The corresponding PL intensities are shown in figure 5.7(b). The PL from the 40Å wells in x=0.3 barriers increased in energy, at a rate of +8.1±0.1meV/kbar, until a pressure of 23kbar was reached. Above this pressure the PL energy decreased at approximately −1.9meV/kbar and the intensity of the PL dropped rapidly. PL could not be observed above 27kbar. Similarly, the PL energy of the 100Å wells in x=0.7 barriers initially increased, however, beyond 19kbar the PL moved down in energy and the luminescence intensity quenched rapidly. Although in neither case could the indirect emission be followed over a large pressure range, it is clear, particularly from the intensity data of figure 5.7(b), that the well in x=0.7 barriers crosses first. In fact, by comparing the pressures at which the PL intensity from each sample drops by given factors we determine that the well in x=0.7 barriers crosses over 4±0.5kbar before the well in the x=0.3 barriers. As explained above, the fact that the well in the x=0.7 barriers crosses first indicates that the quantum-well Γ_c states are crossing with the X_c states of the barrier, and not their own. Furthermore, having shown this, it is now possible to use the data from this sample to determine the band offsets in the $Ga_{0.5}In_{0.5}P/(Al_xGa_{1-x})_{0.5}In_{0.5}P$ system for compositions of x=0.3 and x=0.7.

First we consider the 40Å quantum-wells in the x=0.3 barriers. The pressure

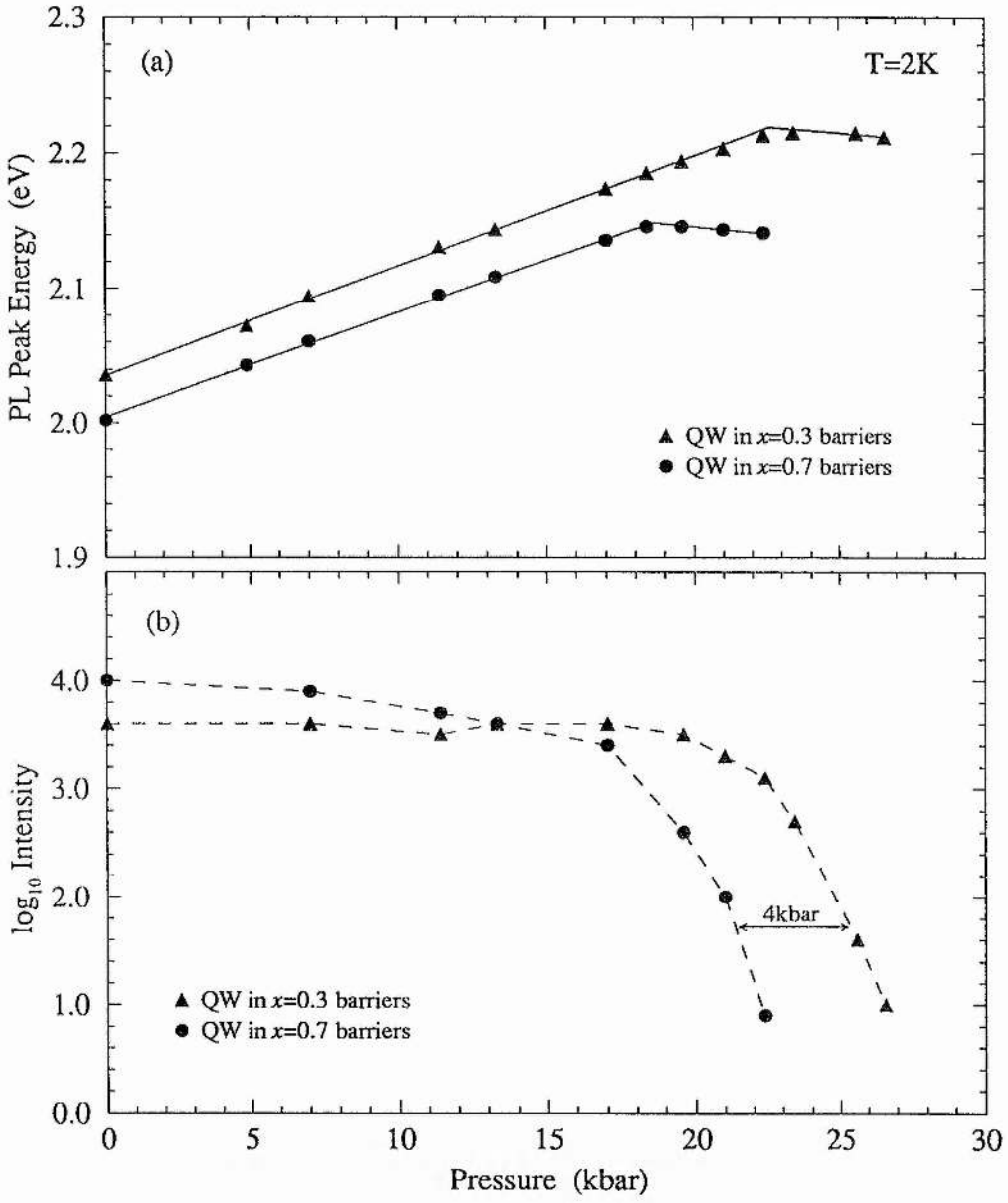

Figure 5.7 High pressure PL data from unstrained $Ga_{0.5}In_{0.5}P/(Al_xGa_{1-x})_{0.5}In_{0.5}P$ quantum-wells; showing (a) PL peak energies plotted as a function of pressure for a 40Å well in x=0.3 barriers and a 100Å well in x=0.7 barriers (barrier emissions are omitted for the sake of clarity), and (b) the PL intensity from the quantum-wells as a function of pressure.

dependence of the PL from the wells and barriers is shown in figure 5.8. At ambient pressure the PL peaks are separated by an energy difference, shown as ΔE_1 in figure 5.8, of 117meV. In order to obtain from this the difference between the well and barrier band-gaps, ΔE_g, we have to add the conduction and valence band confinement-energies. The confinement energies used in this, and subsequent, analysis have been calculated by the method described in section 5.3.4. Adding the confinement energies (42meV and 15meV respectively) we thus obtain a value of ΔE_g=174±10meV at ambient pressure. At ~13kbar a clear Γ_c–X_c crossover was observed from the barrier emission. The indirect barrier emission moved at a rate of ~1.9±0.3meV/kbar and was followed up to 26kbar. As described earlier, crossover in the wells occurred at 23kbar with the emission quenching rapidly over the next 5kbar. Since the indirect emission from the wells could not be followed over a large range of pressure, we assume that its pressure dependence is the same as that of the barrier (in effect we are assuming that the valence band offset is independent of pressure). This therefore gives a value for ΔE_2, which represents the difference in energy between the valence band states in the barriers and the wells, of ΔE_2=18meV. Adding the valence band confinement gives a valence band offset of ΔE_v=33±5meV. Since $\Delta E_g=\Delta E_v+\Delta E_c$ (see figure 2.3), we get ΔE_c=141±15meV. So, for $Ga_{0.5}In_{0.5}P/(Al_xGa_{1-x})_{0.5}In_{0.5}P$ in which x=0.3, we determine that $\Delta E_v=(0.19\pm0.05)\Delta E_g$.

The same analysis can be applied to the 100Å quantum-wells in x=0.7 barriers. The only difference is that, as expected from our band structure results, the barrier emission is already indirect at ambient pressure. In order to find ΔE_g we therefore use our previous determinations (see section 5.3.2) to obtain a value for the direct band-gap of $(Al_{0.7}Ga_{0.3})_{0.5}In_{0.5}P$ of 2.407eV. Correcting for quantum-confinement of the well states,

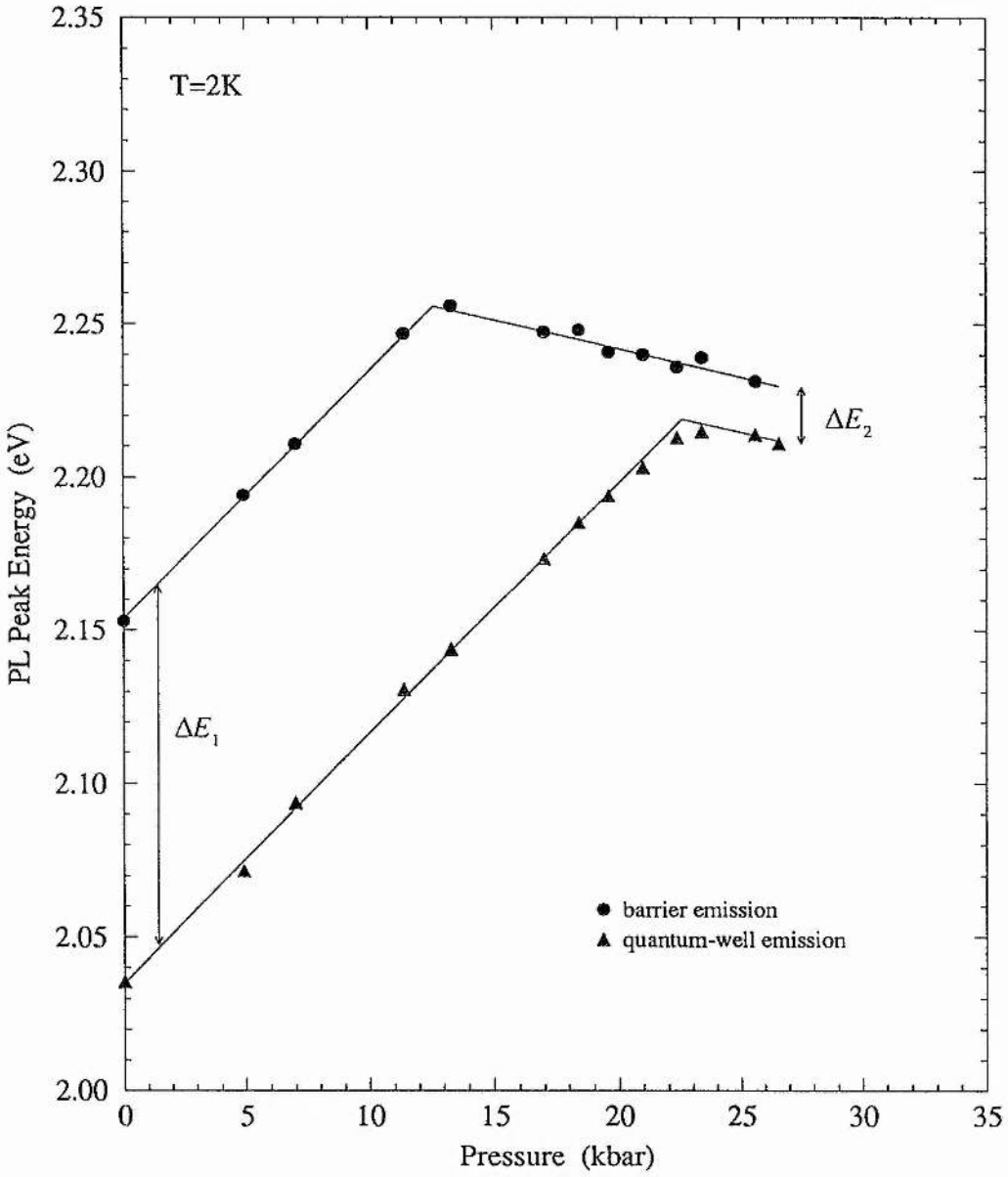

Figure 5.8 High pressure PL data from the 40Å $Ga_{0.5}In_{0.5}P/(Al_{0.3}Ga_{0.7})_{0.5}In_{0.5}P$ sample. PL emission is shown from the quantum-well and the barriers. The values ΔE_1 and ΔE_2 are defined in the text.

this leads to a value of ΔE_g=427±15meV. Once again we assume that the well and barriers have the same pressure coefficient after crossover. Correcting for the quantum-well valence-band confinement gives a value of ΔE_v=121±7meV. This leads to a value of ΔE_c=306±22meV. So, for $Ga_{0.5}In_{0.5}P/(Al_xGa_{1-x})_{0.5}In_{0.5}P$ in which x=0.7, we find that $\Delta E_v=(0.28\pm0.03)\Delta E_g$.

5.4.3 Band Offsets in Strained $Ga_{0.38}In_{0.62}P/(Al_xGa_{1-x})_{0.5}In_{0.5}P$ Heterostructures.

In the previous section it was shown that, in the case of unstrained $Ga_{0.5}In_{0.5}P$ quantum-wells in $(Al_xGa_{1-x})_{0.5}In_{0.5}P$ barriers, hydrostatic pressure can cause crossing of the quantum-well Γ_c minima with the barrier X_c minima. This enabled a determination of the band offsets to be made. In order to use the same high pressure techniques to measure band offsets in a strained $Ga_{0.38}In_{0.62}P/(Al_xGa_{1-x})_{0.5}In_{0.5}P$ system it must similarly be shown that any observed Γ_c–X_c crossovers are with the barrier X_c states and not those of the quantum-well. Applying the same principle as was applied to the unstrained system, one might expect to be able to show this by comparing the crossover points of the x=0 and x=0.4 samples. However, as it turns out, the energy separation between the barrier X_c and the well Γ_c (shown as $\Delta E_c(X^b-\Gamma^w)$ in figure 5.10) is almost constant over the range x=0 to x=0.4. Consequently, the x=0, x=0.3 and x=0.4 samples will all cross at roughly the same point. So, in the case of the strained system we do not have the same direct experimental evidence as there was for the unstrained system. However, calculations show that the increased indium content in the well has little affect on the X_c^{well}–Γ_v^{well} band-gap except that the resultant strain-splitting lowers the $X_{x,y}$ minima by ~38meV.

Now, we have established that the total change in band-gap between strained and unstrained GaInP is 145meV (see sections 5.3.2 and 5.3.4) and, assuming a 50:50 band offset ratio (shown below), this means that the valence band moves up by ~72meV. As a result the position of the well X_c above that of the barrier X_c increases by ~34meV. This self-consistent argument suggests that, as in the unstrained system, the quantum-well Γ_c levels will cross with the barrier X_c levels rather than their own. We can therefore determine band offsets in the strained $Ga_{0.38}In_{0.62}P/(Al_xGa_{1-x})_{0.5}In_{0.5}P$ system.

The results of high pressure PL on the sample containing the strained $Ga_{0.38}In_{0.62}P$ quantum-well in x=0.3 barriers are shown in figure 5.9. At ambient pressure PL-peaks are seen from the barrier and the quantum-well with an energy separation, ΔE_1, of 293meV. Correcting for confinement we obtain a value for the difference in band-gaps of ΔE_g=330±5meV. The barrier X_c was seen to cross with its own Γ_c at ~12kbar (as we would expect from the results of section 5.3.2) and emission resulting from the indirect transitions, moving at a rate of −1.9±0.2meV/kbar, was observed and followed up to 40kbar. The quantum-well Γ_c crossed with the barrier X_c at 33kbar. Once again, the indirect emission was followed up to 40kbar. Since the X_c^{barrier}–$\Gamma_v^{\text{barrier}}$ and X_c^{barrier}–Γ_v^{well} transitions were followed over a reasonable range of pressure we can extrapolate accurately their energy difference, ΔE_2, back to ambient pressure and so, after adding the valence band confinement-energy, determine the valence band offset at ambient pressure. This determination, therefore, does not rely on an assumption of the pressure-independence of the valence band offset. In this way we obtain values of ΔE_v=100±15meV and ΔE_c=230±20meV. So, in the case of $Ga_{0.38}In_{0.62}P/(Al_xGa_{1-x})_{0.5}In_{0.5}P$, when x=0.3 we obtain $\Delta E_v=(0.30\pm0.05)\Delta E_g$.

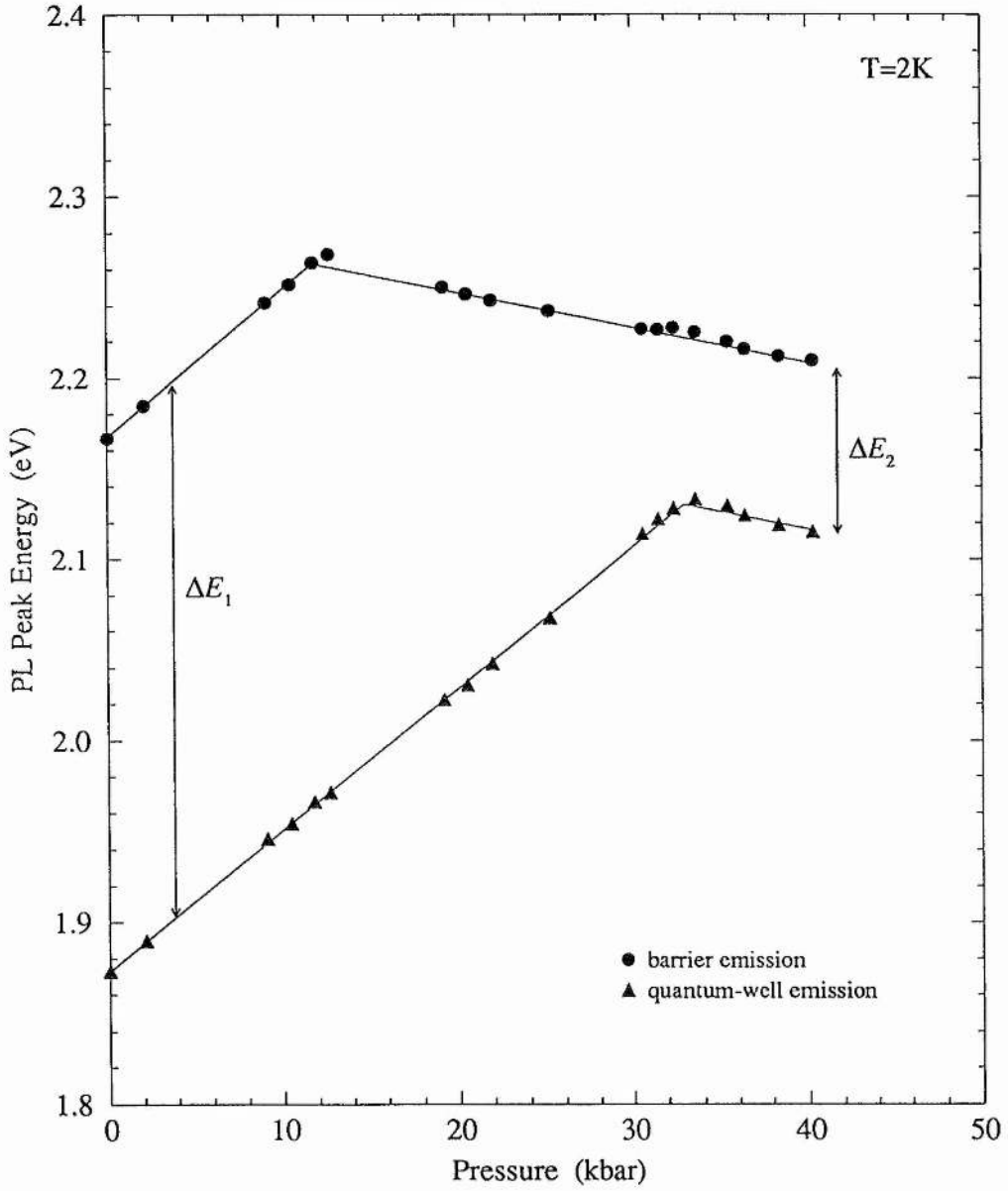

Figure 5.9 High pressure PL data from the 1% compressively strained $Ga_{0.38}In_{0.62}P/(Al_{0.3}Ga_{0.7})_{0.5}In_{0.5}P$ sample, showing the PL from the quantum-well and the barriers. ΔE_1 and ΔE_2 are defined in the text.

The exact same techniques and analysis were applied to the strained $Ga_{0.38}In_{0.62}P$ quantum-wells in x=0 and x=0.4 barriers. When x=0 we obtain values of ΔE_v=72±8meV and ΔE_c=68±16meV (ΔE_v=(0.5±0.1)ΔE_g) and when x=0.4 we get ΔE_v=113±10meV and ΔE_c=270±20meV (ΔE_v=(0.30±0.04)ΔE_g).

5.4.4 Discussion of Band Offset Results.

The band offsets determined in sections 5.4.2 and 5.4.3 for the unstrained and 1% compressively strained GaInP/$(Al_xGa_{1-x})_{0.5}In_{0.5}P$ systems are plotted, as functions of barrier composition (x), in figure 5.10. There is clearly evidence of bowing and our data for the unstrained system can be fitted within experimental error by the following equations:

$$\Delta E_v(\text{meV}) = 63x + 157x^2 \qquad (5.7)$$

and

$$\Delta E_c(\text{meV}) = 547x - 157x^2 \qquad (5.8)$$

Also shown in figure 5.11(a) (though not included in the fits given above) are data for x=1 taken from reference 17.

The data for the 1% compressively strained system can be fitted well by simply adding an offset of 72meV (which corresponds to half the difference between the unstrained and 1% strained GaInP band-gaps) to equations 5.7 and 5.8. So, for the strained system we get:

$$\Delta E_v(\text{meV}) = 72 + 63x + 157x^2 \qquad (5.9)$$

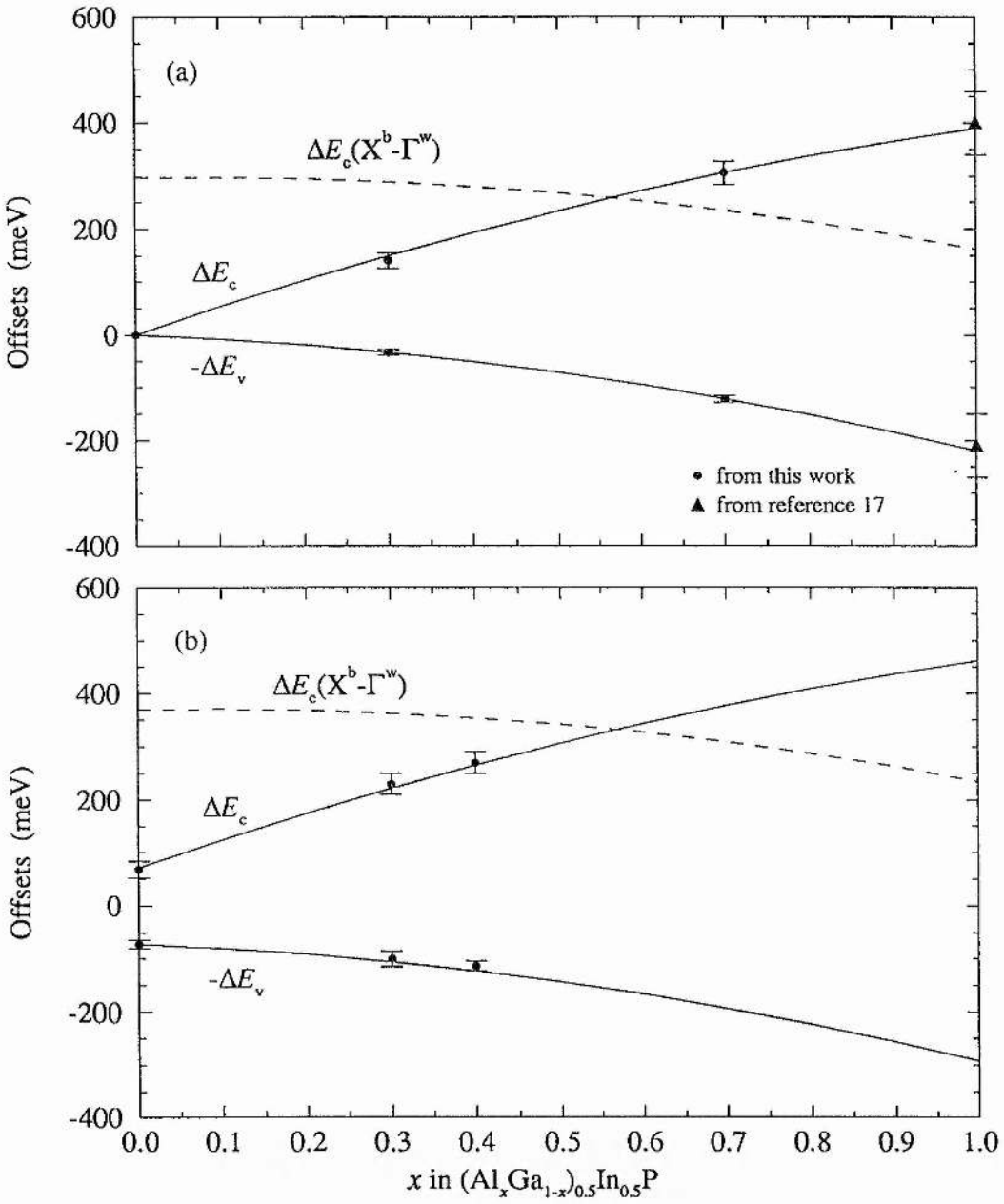

Figure 5.10 The compositional dependencies of the band offsets in (a) unstrained GaInP/$(Al_xGa_{1-x})_{0.5}In_{0.5}P$ and (b) 1% compressively strained GaInP/$(Al_xGa_{1-x})_{0.5}In_{0.5}P$. The solid lines represent the fits given by equations 5.7-5.10. The dashed lines give the energy separation between the barrier X_c and quantum-well Γ_c levels (referred to in section 5.4.3).

and $$\Delta E_c(\text{meV}) = 72 + 547x - 157x^2 \qquad (5.10)$$

It should be noted that in our determination of the valence band offsets for the unstrained system we have assumed a pressure-independent valence band discontinuity. Based on the work of Lambkin *et al* in the InGaAs/InP[20] system, in which the valence band discontinuity is shown to be almost constant with pressure, this would seem to be a reasonable assumption and is in agreement with the model solid theory of Van de Walle and Martin[21]. However, Patel *et al*[22] suggest that in GaInP/AlInP heterostructures the valence band offset increases with pressure. If this is the case then we estimate that our values of ΔE_v for the x=0.3 and x=0.7 samples would be ~12meV and ~23meV too large respectively.

5.5 Comparison of Ordered and Disordered $Ga_{0.5}In_{0.5}P$.

5.5.1 Ordering in $Ga_{0.5}In_{0.5}P$.

It is now well established that under certain growth conditions $Ga_{0.5}In_{0.5}P$ grown by MOVPE on (001) GaAs can form a partially ordered alloy[10,23]. Furthermore, it has been shown that this long-range ordering reduces the direct band-gap of the ordered alloy by 50–100meV[10,24] compared to that of the disordered alloy. The generally accepted explanation of this phenomenon is that the group–III sublattice forms an ordered phase which has a Cu–Pt type structure with long-range ordering in the [111] direction. This causes folding of the Brillioun zone in which one of the L minima fold into the Γ and the

coupling between these bands causes the change in the direct band-gap[25]. However, there have also been reports suggesting that ordering occurs in the [110] direction[10] or the [001] direction[26]. Furthermore, whilst the effect of ordering on the direct band-gap has been widely reported, the effect on the indirect conduction band minima is not so well established. Recent work by Uchida *et al*[24] suggests that the Γ_c–X_c separation is unaffected by ordering; a result which is not expected if the ordering is in the [111] direction, but which they interpret as evidence of ordering in the [001] direction, as proposed by Kurtz[26].

We have previously determined (see section 5.3.2) the Γ_c–X_c separation in disordered $Ga_{0.5}In_{0.5}P$. Below, we present the results of a high pressure PL experiment in which we do the same for ordered $Ga_{0.5}In_{0.5}P$. The same experiment also reveals the influence of ordering on the direct Γ_c–Γ_c band-gap and its pressure dependence.

5.5.2 Experimental Details.

The ordered $Ga_{0.5}In_{0.5}P$ sample, like the disordered sample measured previously, was grown by Optronics, Ireland. It consisted of a $Ga_{0.5}In_{0.5}P$ layer, approximately 1μm thick, grown on an (001) oriented GaAs substrate. The growth temperature (700°C) and gas-flow ratio in the input group–III and group–V sources were chosen so as to favour ordered growth[12]. Double-crystal X–ray diffraction showed the sample to be lattice-matched to within ±0.1%. The experimental procedure was identical to that used for the disordered $Ga_{0.5}In_{0.5}P$ sample (see section 5.3.1).

5.5.3 Results and Discussion.

Figure 5.11 shows ambient pressure PL spectra from the ordered $Ga_{0.5}In_{0.5}P$ samples at 2K. A strong emission peak is observed at an energy of 1.888eV, which is assumed to result from excitonic Γ_c–Γ_v transitions. Extra peaks can be seen above and below the main peak in the spectrum from the ordered sample. Whilst such peaks are a common feature in the spectra of partially ordered alloys, their origin has not yet been explained (the most common suggestion is that they result from the recombination of spatially separated carriers from regions of ordered and disordered material). Figure 5.12 shows the pressure dependence of the PL from the ordered sample. On initial application of hydrostatic pressure the intensity of these extra PL peaks quenched rapidly while the main peak moved up in energy at a rate of +7.3±0.1meV/kbar. This figure, which agrees well with that given in reference 24, compares to a pressure coefficient of +8.4±0.1meV/kbar for the disordered sample. The drop in pressure coefficient with ordering is a commonly reported result[24,27]. Above 37kbar the PL emission reduced in intensity and the emission peak moved down in energy at a rate of −1.8meV±0.2/kbar, indicating that Γ_c–X_c crossover had occurred. Indirect transitions were observed up to ~66kbar at which point the emission became too weak to follow. Extrapolating the energy of the indirect transitions back to 0kbar gives an ambient pressure X_c–Γ_c separation of 337±15meV in partially ordered $Ga_{0.5}In_{0.5}P$. This compares to a value of 280meV in the disordered sample. Although this increase in the X_c–Γ_c separation in the ordered alloy is generally expected, it does contradict the results of reference 24 (see below).

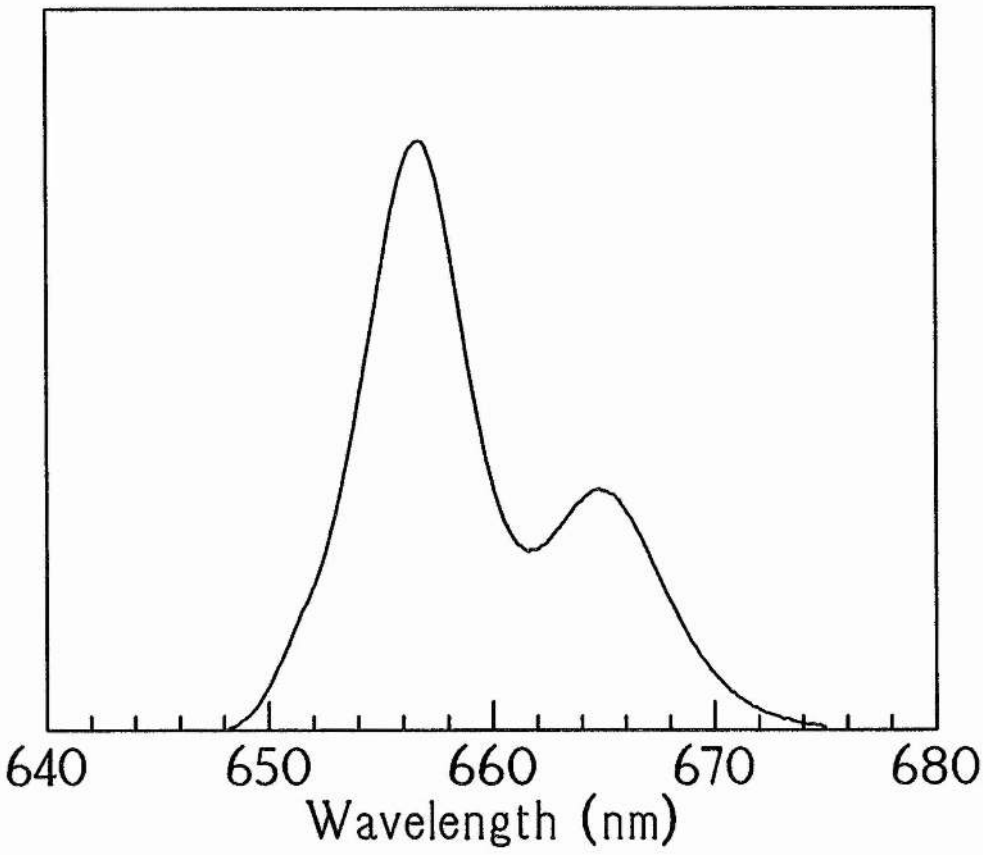

Figure 5.11 An ambient pressure photoluminescence spectrum from the ordered $Ga_{0.5}In_{0.5}P$ sample, recorded at 2K.

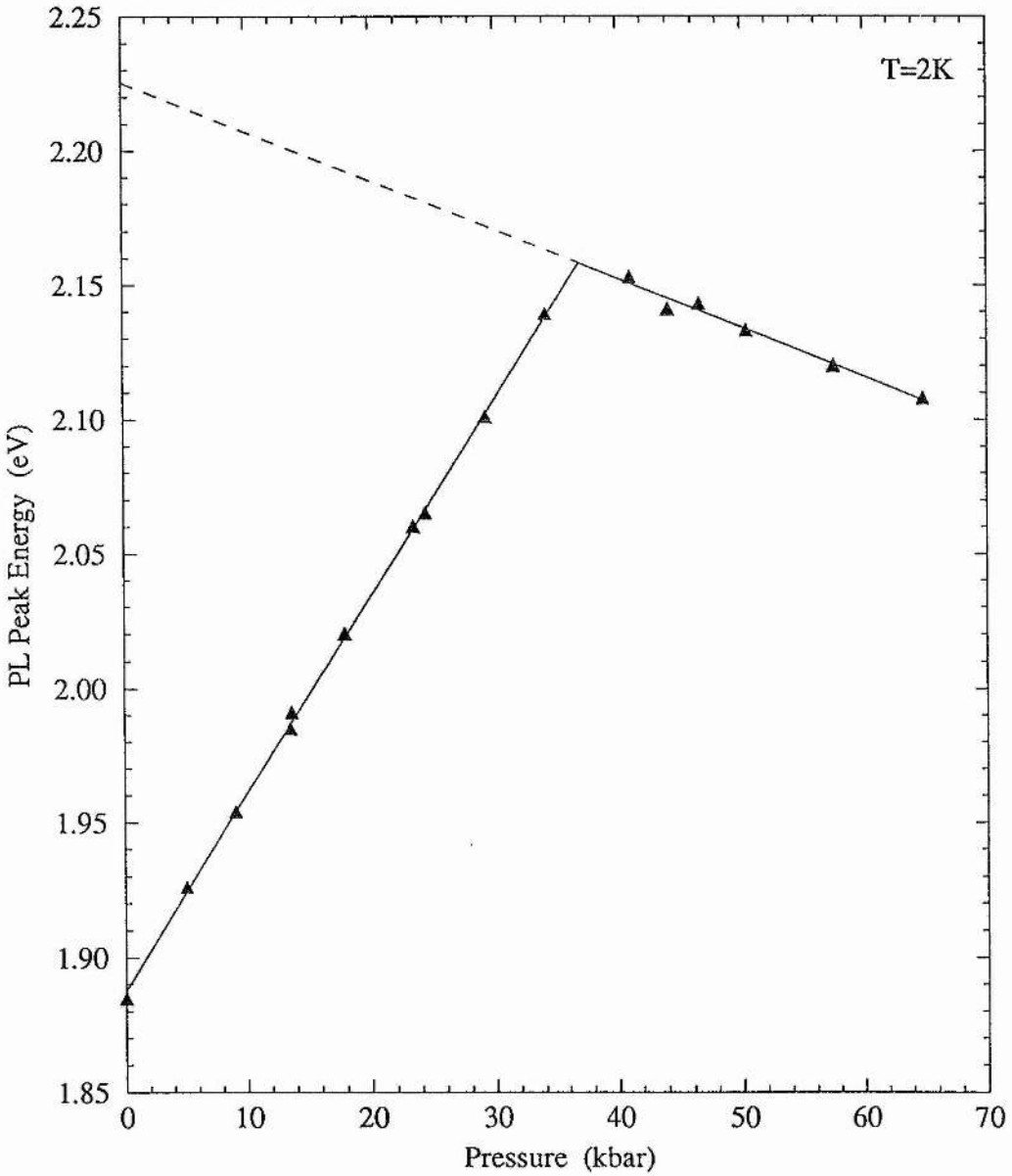

Figure 5.12 The PL peak energy, plotted as a function of pressure, for the ordered $Ga_{0.5}In_{0.5}P$ sample.

If, as is generally believed, the ordering in GaInP is along the [111] direction, then such ordering would lead to mixing between Γ_c and one of the four L_c states, causing a shift in the Γ_c energy. Each of the other L_c states will also mix with an X_c state, allowing a shift in each of the X_c energies, although there is no reason to expect the X_c shift to be the same as the Γ_c shift.

Uchida *et al*[24] give results of similar high pressure PL experiments, though carried out at room temperature, from which they conclude that the X_c–Γ_c separation remains almost constant regardless of ordering. In the light of the theory outlined above this seems surprising. They explain their results by suggesting a model in which ordering along the [001] direction (as proposed in reference 26) causes mixing, not only of the Γ_c and L_c but also the X_c levels. Whilst this could cause a change in the position of the X_c minima it doesn't adequately explain why the X_c–Γ_c separation should remain constant.

5.6 Summary and Suggestions for Further Work.

We have measured directly the Γ_c–Γ_v and X_c–Γ_v band-gaps in $(Al_xGa_{1-x})_{0.5}In_{0.5}P$ alloys at several points across the alloy range. Using these results we have obtained equations describing the compositional dependence of these direct and indirect band-gaps. We have also placed limits on the position of the L minima in unstrained and 1% compressively strained AlGaInP. Band offsets in unstrained and 1% compressively strained GaInP/$(Al_xGa_{1-x})_{0.5}In_{0.5}P$ have also been determined as functions of barrier

composition, x. Finally, we have begun to study the effects of ordering and, in particular, we have measured the effect that ordering has on the X_c–Γ_c separation in $Ga_{0.5}In_{0.5}P$.

There is obviously considerable scope for further work. Both the bulk band structure measurements and the determinations of the heterostructure band offsets (strained and unstrained) could be repeated over the alloy range, though this time with the degree of ordering as a variable. As well as providing us with the basic material parameters necessary for design and analysis of devices, the results may well shed some light on the precise nature and mechanisms of atomic ordering. The effects of a combination of strain and ordering are of particular interest since GaInP strained-layer lasers have been fabricated which show improved performance over their unstrained equivalents[29,30].

Finally, the precise position of the L minima in AlGaInP remains unknown. However, the work described here suggests that high pressure PL is not likely to solve this particular problem.

5.7 References.

1. D.P.Bour, D.W.Treat, R.L.Thornton, T.L.Paoli, R.D.Bringans, B.S.Kruser, R.S.Geels, D.F.Welch and T.Y.Wang, J. Cryst. Growth, **124**, 751 (1992)
2. A.Onton and R.J.Chicotka, J.Appl. Phys., **41**, 4205 (1970)
3. D.J.Mowbray, O.P.Kowalski, M.Hopkinson, M.S.Skolnick and J.P.R.David, Appl.Phys.Lett., **65**, 213 (1994)
4. D.P.Bour, *Quantum Well Lasers*, ed. P.S.Zory Jr (Academic Press, New York, 1993)
5. M.Bugajski, A.M.Kontkiewicz and H.Mariette, Phys. Rev. B, **28**, 7105 (1983)
6. T.Hayakawa, K.Takahashi, M.Hosoda, S.Yamamoto and T.Hijikata, Jpn. J. Appl. Phys., **27**, 1553 (1988)
7. M.D.Dawson and G.Duggan, Phys. Rev. B, **47**, 12598 (1993)
8. M.D.Dawson and G.Duggan, Appl. Phys. Lett., **64**, 892 (1994)
9. R.P.Schneider Jr, R.P.Bryan, E.D.Jones and J.A.Lott, Appl. Phys. Lett., **63**, 1240 (1993)
10. A.Gomyo, T.Suzuki, K.Koboyashi, S.Kawata and I.Hino, Appl. Phys. Lett., **50**, 673 (1987)
11. S-H.Wei and A.Zunger, Phys. Rev. B, **49**, 14337 (1994)
12. A.Valster, C.T.H.F.Liedenbaum, M.N.Finke, A.L.G.Severens, M.J.B.Boermans, D.E.W.Vandenhoudt and C.W.T.Bulle-Lieuwma, J. Cryst. Growth, **107**, 403 (1991)
13. Y.Hamisch, R.Steffen, A.Forchel and P.Rontgen, Appl. Phys. Lett., **62**, 3007 (1993)

14. J.Chen, J.R.Sites, I.L.Spain, M.J.Hafich and G.Y.Robinson, Appl. Phys. Lett., **58**, 744 (1991)

15. D.Patel, J.Chen, S.R.Kurtz, J.M.Olson, J.H.Quigley, M.J.Hafich and G.Y.Robinson, Phys. Rev. B., **39**, 10978 (1989)

16. Landolt-Börnstein, *Numerical Data and Functional Relationships in Science and Technology*, Group III, Vol. 17a, ed. O.Madelung (Springer-Verlag, Berlin, 1982)

17. J.D.Lambkin, A.Morrison, L.Considine, W.M.Kelly, G.M.O'Connor and C.McDonagh, *Proc. 22nd Int. Conf. Phys. Semicond.*, Vancouver, Canada, 15th–19th August (1994)

18. R.J.Warburton, R.J.Nicholas, N.J.Mason, P.J.Walker, A.D.Prins and D.J.Dunstan, Phys. Rev. B, **43**, 4994 (1991)

19. M.P.C.M.Krijn, Semicond. Sci. Technol., **6**, 27 (1991)

20. J.D.Lambkin, D.J.Dunstan, E.P.O'Reilly and B.R.Butler, J. Cryst. Growth, **93**, 323 (1988)

21. C.G.Van de Walle and R.M.Martin, Phys. Rev. B, **35**, 8154 (1987)

22. D.Patel, M.J.Hafich, G.Y.Robinson and C.S.Menoni, Phys. Rev. B, **48**, 18031 (1993)

23. S.McKernan, B.C.DeCooman, C.B.Carter, D.P.Bour and J.R.Shealy, J. Mater. Res., **3**, 406 (1988)

24. K.Uchida, P.Y.Yu, N.Noto and E.R.Weber, Appl. Phys. Lett., **64**, 2858 (1994)

25. S.-H.Wei and A.Zunger, Appl. Phys. Lett., **56**, 662 (1990)

26. S.R.Kurtz, J. Appl. Phys., **74**, 4130 (1993)

27. M.Shoji, T.Kobayashi, R.Deol and J.Nakahar, Jpn. J. Appl. Phys., **32**, 276 (1993)

28. T.Kanata, M.Nishimoto, H.Nakayama and T.Nishino, Phys. Rev. B, **45**, 6637 (1992)

29. J.Hashimoto, Appl. Phys. Lett., **58**, 879 (1991)

30. A.Valster, C.J.Van der Poel, M.N.Finke and M.J.B.Boermans, *Conf. Digest 13th IEEE Intern. Semicond. Laser Conf.*, Takamatsu, Japan (1992)

CHAPTER 6.

Anomalous Band-Gap Pressure Coefficients in Strained InGaAs.

6.1 Introduction.

In a series of high pressure experiments the pressure dependence of the photoluminescence from a variety of strained $In_xGa_{1-x}As$ samples has been investigated. The PL from a 1% compressively strained $In_{0.67}Ga_{0.33}As$ quantum-well, grown on an [001] oriented InP substrate, is found to have an unexpectedly low pressure coefficient. It is shown that if this reduction in the pressure coefficient is a function of strain, rather than simply of composition, then it is consistent with the anomalous pressure coefficients reported previously for compressively strained $In_xGa_{1-x}As$ quantum-wells (with $x \leq 0.25$) grown on an [001] oriented GaAs substrate[1]. An $In_{0.15}Ga_{0.85}As$ quantum-well grown on [111] oriented GaAs has also been investigated but shows no such anomaly. The pressure dependence of the direct band-gap of several $In_xGa_{1-x}As$ quantum-wells grown under tensile strain has also been measured. Further work is required to produce a conclusive interpretation of these tensile results. However, preliminary indications suggest that the pressure coefficients of the material under tensile strain show an anomaly that is opposite in sign to that of compressively strained $In_xGa_{1-x}As$.

The possible causes of anomalous pressure coefficients are discussed and suggestions are made for further work which may help to explain the experimental results described above. One line of further work, namely an investigation of the elastic constants of strained InGaAs, has been instigated with some preliminary work carried out

at the Synchrotron Radiation Source at the Daresbury Laboratory. This has involved the development of a novel high-pressure X–ray diffraction technique capable of yielding the size and shape of the unit cell of epitaxial InGaAs, grown pseudomorphically on GaAs, as a function of pressure.

6.2 Background.

The use of strained-layer semiconductor heterostructures in the fabrication of optoelectronic devices is now commonplace. As well as providing the potential for improved device performance, departure from a strictly lattice-matched growth regime greatly increases the number of alloy compositions available and so increases the range of band-gaps that can be obtained[2–5]. The InGaAs/GaAs strained layer system has attracted considerable interest in the attempt to produce lasers with an operating wavelength of 980nm, for pumping erbium-doped fibre amplifiers. Consequently, the band structure of InGaAs/GaAs strained quantum-wells has been extensively studied by a variety of techniques, including the use of hydrostatic pressure[1,6]. In one such study Wilkinson *et al*[1] measured the pressure dependence of the PL from a series of $In_xGa_{1-x}As/GaAs$ quantum-wells, each 100Å wide, with a range of indium contents from x=0 to x=0.25. The pressure coefficients that they obtained were unexpectedly low. Furthermore, they could not be explained as artifacts of the heterostructure system under pressure, such as rapidly varying band offsets; they were associated with the InGaAs quantum-well material itself. Their data indicated that the pressure coefficient varies linearly according to the following expression:

$$dE/dP = (10.7 - 6.0x)\text{meV/kbar} \qquad (6.1)$$

This represents an unexpectedly strong dependence on composition. Using this expression to extrapolate to x=1 yields a value of +4.7meV/kbar for the pressure coefficient of InAs; this is very different from the measured value for bulk InAs of +10.2meV/kbar[7]. Indeed, given the overall similarity of direct band-gap pressure coefficients in III–V semiconductors[8], a 14% reduction in the pressure coefficient of $In_xGa_{1-x}As$ in going from x=0 to x=0.25 is both significant and surprising. It should be remembered, however, that in increasing the indium content we are also increasing the compressive strain in the quantum-well. So, the apparent compositional dependence of the pressure coefficients could actually be a strain dependence (this would account for the inconsistency between the results from strained InGaAs and those from bulk, unstrained, InAs). Indeed, unexpectedly low pressure coefficients have been observed in the compressively strained GaAsSb/GaAs system[9,10] as well as the InGaAs/GaAs system[1,6].

Based on the information outlined above the aims of this investigation were as follows: to verify the existence of anomalous pressure coefficients in strained $In_xGa_{1-x}As$; to establish whether they are caused by strain or are simply a function of composition; to carry out further experiments to isolate and identify the precise cause of this anomaly.

6.3 Experimental Details.

During the course of this work five samples were investigated using high pressure photoluminescence techniques. Sample parameters are given in table 6.1. Samples 1 and

SAMPLE NUMBER	DESCRIPTION OF SAMPLE	WELL-WIDTH (Å)	STRAIN ($\Delta a/a$)	SUBSTRATE
1	Compressively strained $In_{0.67}Ga_{0.33}As$ SQW in $In_{0.67}Ga_{0.33}As_{0.7}P_{0.3}$ barriers.	100Å	+1%	InP (100)
2	Unstrained $In_{0.53}Ga_{0.47}As$ SQW in $In_{0.67}Ga_{0.33}As_{0.7}P_{0.3}$ barriers.	100Å	0%	InP (100)
3	Compressively strained MQW containing: $In_{0.15}Ga_{0.85}As$ QW (×5) in GaAs barriers.	100Å	+1%	GaAs (111)B
4	Tensile MQW containing: $In_{0.39}Ga_{0.61}As$ QW $In_{0.43}Ga_{0.57}As$ QW $In_{0.46}Ga_{0.54}As$ QW $In_{0.50}Ga_{0.50}As$ QW $In_{0.53}Ga_{0.47}As$ QW in $In_{0.67}Ga_{0.33}As_{0.7}P_{0.3}$ barriers.	 40Å 60Å 80Å 100Å 100Å	 -1% -0.75% -0.5% -0.25% 0%	InP (100)
5	Tensile MQW containing: $In_{0.46}Ga_{0.54}As$ QW $In_{0.39}Ga_{0.61}As$ QW $In_{0.53}Ga_{0.47}As$ QW in $In_{0.67}Ga_{0.33}As_{0.7}P_{0.3}$ barriers.	 40Å 90Å 500Å	 -0.5% -1% 0%	InP (100)

Table 6.1 Sample details for the $In_xGa_{1-x}As$ samples investigated by high pressure photoluminescence.

2 were grown by MOVPE at BTL, Ipswich. Sample 3 was grown by MBE at the EPSRC III–V Central Facility at the University of Sheffield. Samples 4 and 5 were grown by MOVPE at BNR(Europe), Harlow. Layer thicknesses, alloy compositions and sample quality were confirmed by a variety of techniques including low temperature PL (all samples), double-crystal X–ray diffraction (samples 1, 2, 4 and 5) and transmission electron microscopy (samples 1 and 2). One further sample was used, for the X–ray diffraction measurements at the Daresbury Laboratory. This consisted of a 1000Å partially relaxed layer of $In_{0.20}Ga_{0.80}As$ grown on an [001] oriented GaAs substrate. This sample was grown by MBE at the RSRE (now the DRA), Malvern.

The high pressure photoluminescence measurements on samples 1, 2, 3 and 5 were carried out at 10K in a DAC in which argon was used as the hydrostatic pressure medium. In the case of sample 4, high pressure PL measurements were performed at 2K and helium was used as the pressure medium. Full details of DAC techniques are given in chapter 3. A piece of ruby, to act as a pressure gauge, was loaded along with the sample(s). However, wherever possible a semiconductor pressure gauge was also used (see section 3.10); usually either the sample's own substrate or some other layer within the sample itself.

6.4 Experimental Results From Compressively Strained InGaAs.

6.4.1 InGaAs/InGaAsP Quantum Well on [001] InP Substrate.

Figure 6.1 shows typical low temperature PL spectra from sample 1 at various

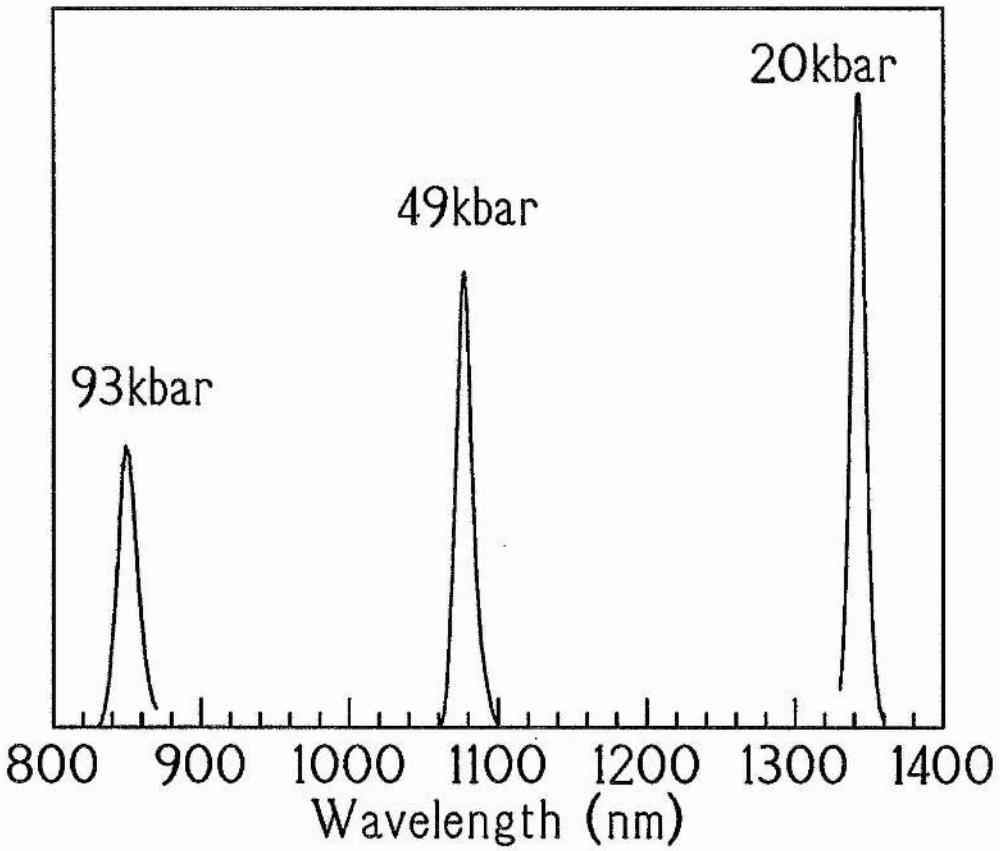

Figure 6.1 Typical low temperature (10K) PL spectra, shown at various pressures, for sample 1.

pressures. At ambient pressure a strong emission peak was observed with an energy of 0.744eV; this is consistent with what we expect for a 1% compressively strained, 100Å $In_{0.67}Ga_{0.33}As$ quantum-well. The FWHM of only 1.8meV confirms the high quality of this sample. Applying hydrostatic pressure caused this peak to move up in energy. Figure 6.2 shows the pressure dependence of the PL peak energy from sample 1. The intensity of the PL emission from the quantum-well remained reasonably constant up to a pressure of ~111kbar. Upon increasing the pressure further the intensity quenched rapidly. It should be noted that InP, which forms the substrate of this sample, undergoes a structural phase transition at approximately this pressure (unfortunately, values quoted in the literature for this transition pressure vary from 100–120kbar[11–14]).

It is clear from figure 6.2 that the dependence of the PL peak energy on pressure is sub-linear. This behaviour is not unexpected (see section 2.2) and has been reported previously for several materials including InGaAs[15], GaAs[16] and InP[11] (indeed, it is probably not observed more frequently simply because the pressure range of most experiments is not sufficient for the effect to be noticeable). In such cases the pressure dependence of the PL energy is normally expressed as a quadratic equation; a least-squares fit to the data from sample 1 gives:

$$E_{PL}(\text{eV}) = 0.747 + (9.44\pm0.2)\times10^{-3}P - (20\pm2)\times10^{-6}P^2 \qquad (6.2)$$

where P is pressure in kbar. The nonlinearity arises from nonlinearity in the relationship between pressure and lattice constant (lattice constant is, after all, the more fundamental variable of interest). We would, therefore, expect to obtain a linear

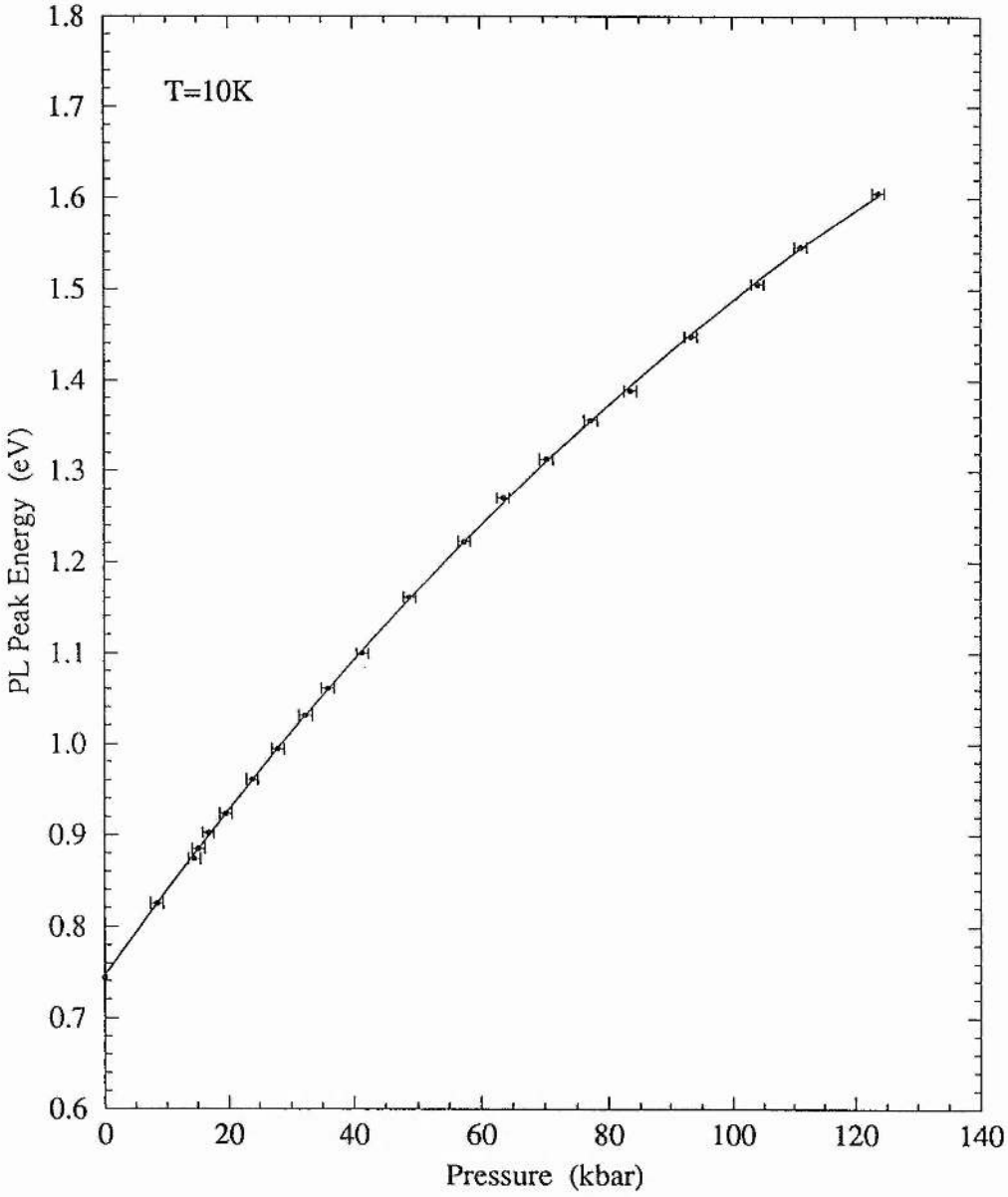

Figure 6.2 The PL peak energy, plotted as a function of pressure, for sample 1. The line represents the fit to the data given by equation 6.2.

relationship if the data from sample 1 were replotted against 'change in lattice constant', rather than pressure. Conversion from pressure to lattice constant is done by means of the Murnaghan empirical equation of state[17]:

$$-(\Delta a/a_0)_T = 1 - [(B'/B)P + 1]^{-1/(3B')} \qquad (6.3)$$

where B is the bulk modulus and B' the derivative of the bulk modulus with respect to pressure. Since the InGaAs quantum-well structure is constrained in two dimensions by the InP substrate we use the following expression[15]:

$$B^{QW} = {}^2/_3 B^{InP} + {}^1/_3 B^{InGaAs} \qquad (6.4)$$

The bulk moduli of InP and InGaAs have not been measured at low temperature. For InP we therefore take the value, derived in the literature[18], of B^{InP}=764kbar. For the bulk modulus of $In_{0.67}Ga_{0.33}As$ we interpolate between the measured low-temperature values[19] for InAs, GaAs and GaP; this gives a value of B^{InGaAs}=679kbar. So, from equation 6.4 we obtain B^{QW}=736kbar. For the pressure derivative of the bulk modulus we take the recommended[19] value of B'=4.5. Figure 6.3 shows the data from sample 1 replotted as a function of 'change in lattice constant' rather than pressure. The data can now be fitted, within experimental error, with a straight line:

$$E_{PL}(eV) = E_0 + 3\Xi(\Delta a/a_0) \qquad (6.5)$$

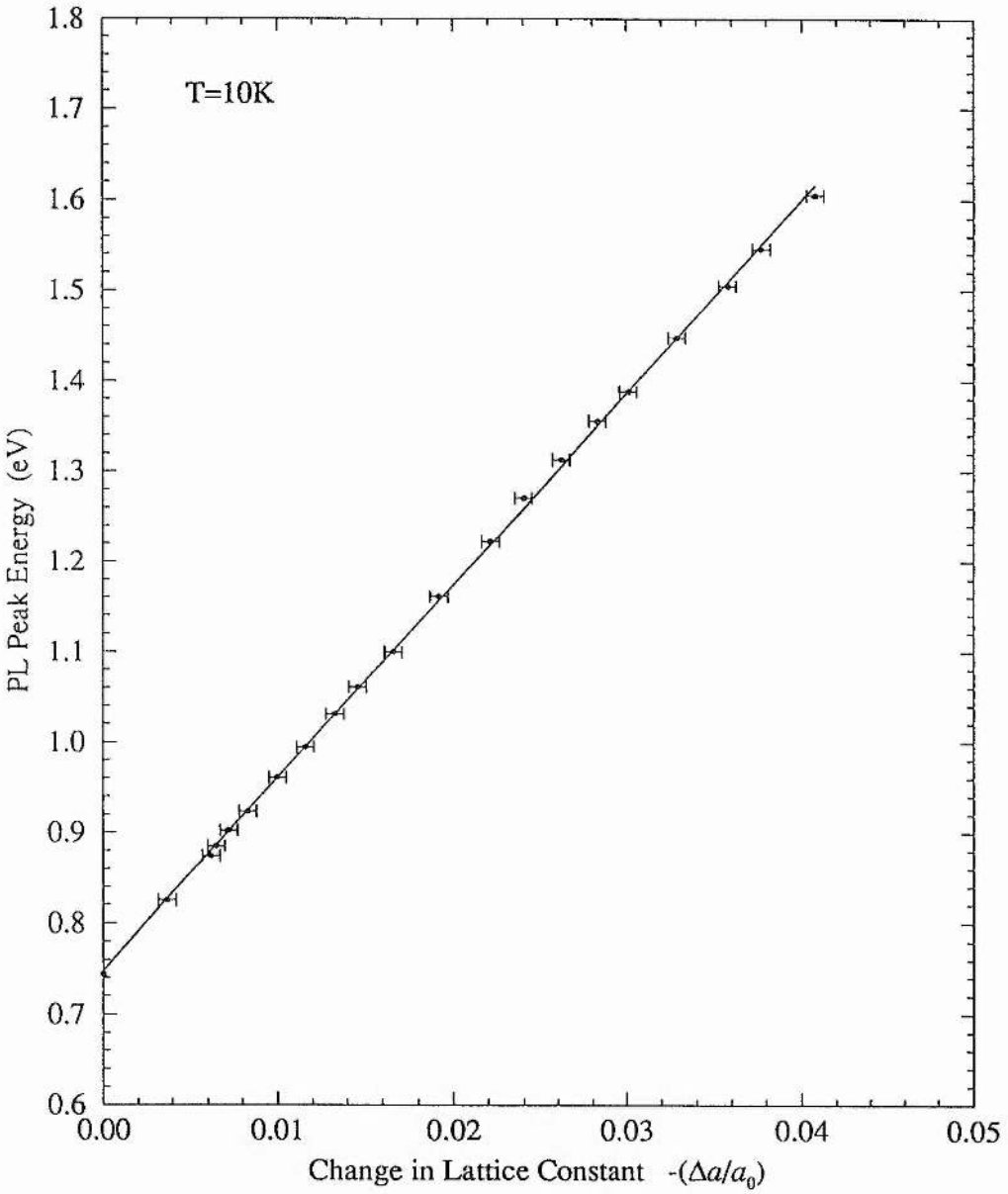

Figure 6.3 The high pressure PL data from sample 1, replotted as a function of change in lattice constant. The straight line is given by equation 6.5.

where Ξ is the deformation potential of the conduction band minimum with respect to the top of the valence band. So, if we assume that the values of B and B' given above are correct, we obtain a deformation potential of Ξ=−7.09±0.05eV for a 1% compressively strained $In_{0.67}Ga_{0.33}As$ quantum-well. Since the quantum-well is wide, we can take this to be a reasonable approximation for the deformation potential of bulk strained $In_{0.67}Ga_{0.33}As$. This value is significantly lower than the value for unstrained $In_{0.53}Ga_{0.47}As$, measured by Lambkin *et al*[15], of Ξ=−8.25±0.1eV. Whilst this analysis does help to explain the sub-linear dependence of PL energy on pressure, a note of caution must be expressed regarding the precise value of Ξ that we have determined. In addition to the errors quoted above there are systematic errors, due to uncertainties in the values of B and B', which have to be considered. As will be shown below, there may be reason to suspect that the elastic constants of strained material differ from those of the bulk material and this would clearly affect the value of the bulk modulus.

What is certain is that the linear pressure coefficient of +9.44±0.2meV/kbar (see equation 6.2) that we have determined for a 1% compressively strained $In_{0.67}Ga_{0.33}As$ quantum-well is significantly lower than the pressure coefficient of unstrained $In_{0.53}Ga_{0.47}As$, quoted in reference 15 as +10.95±0.1meV/kbar. However, nor does it agree with the compositional dependence (determined empirically for $x \leq 0.25$) given by equation 6.1. This supports the suggestion that strain, and not simply composition, gives rise to anomalous pressure coefficients in $In_xGa_{1-x}As$. In order to confirm this, and to get a more accurate quantitative measurement of the anomaly (which could be compared directly with the results of reference 1), an experiment was

performed to measure the difference between the pressure coefficients of a 100Å, 1% compressively strained, $In_{0.67}Ga_{0.33}As$ quantum-well (sample 1) and a 100Å, unstrained, $In_{0.53}Ga_{0.47}As$ quantum-well (sample 2).

At ambient pressure a PL peak was observed from the quantum-well of sample 2 at an energy of 0.829eV. The intensity and width of this peak (FWHM=2meV) were similar to those for sample 1. The results of two high pressure experiments in which sample 1 and sample 2 were loaded together into the DAC are shown in figure 6.4. The energy difference between the PL peaks from the two quantum-wells is plotted against the PL peak energy of sample 1. Plotting the results in this way gives an accurate measure of the difference between the pressure coefficients of the two samples, independent of any uncertainty in pressure measurement. In this type of plot a horizontal line would indicate identical pressure coefficients; the positive gradient in figure 6.4 indicates that the pressure coefficient of sample 2 is greater than that of sample 1 by a factor of 1.094±0.002. So, if we take the pressure coefficient of sample 1 to be +9.44meV/kbar then we obtain a value for sample 2 of +10.33±0.02meV/kbar. The good agreement between the data from the two separate pressure runs gives us confidence that errors due to pressure differences across the DAC sample-space are not influencing our results. Furthermore, in the second of these runs a ruby pressure gauge was included as an extra check; this yielded pressure coefficients of +9.39±0.3meV/kbar and +10.27±0.3meV/kbar for samples 1 and 2 respectively.

In figure 6.5 our determined pressure coefficients are plotted along with those of reference 1 for comparison. Also plotted is the pressure coefficient of bulk InAs as determined by Tsay *et al*[7]. It can be seen that the reduction in the pressure coefficient,

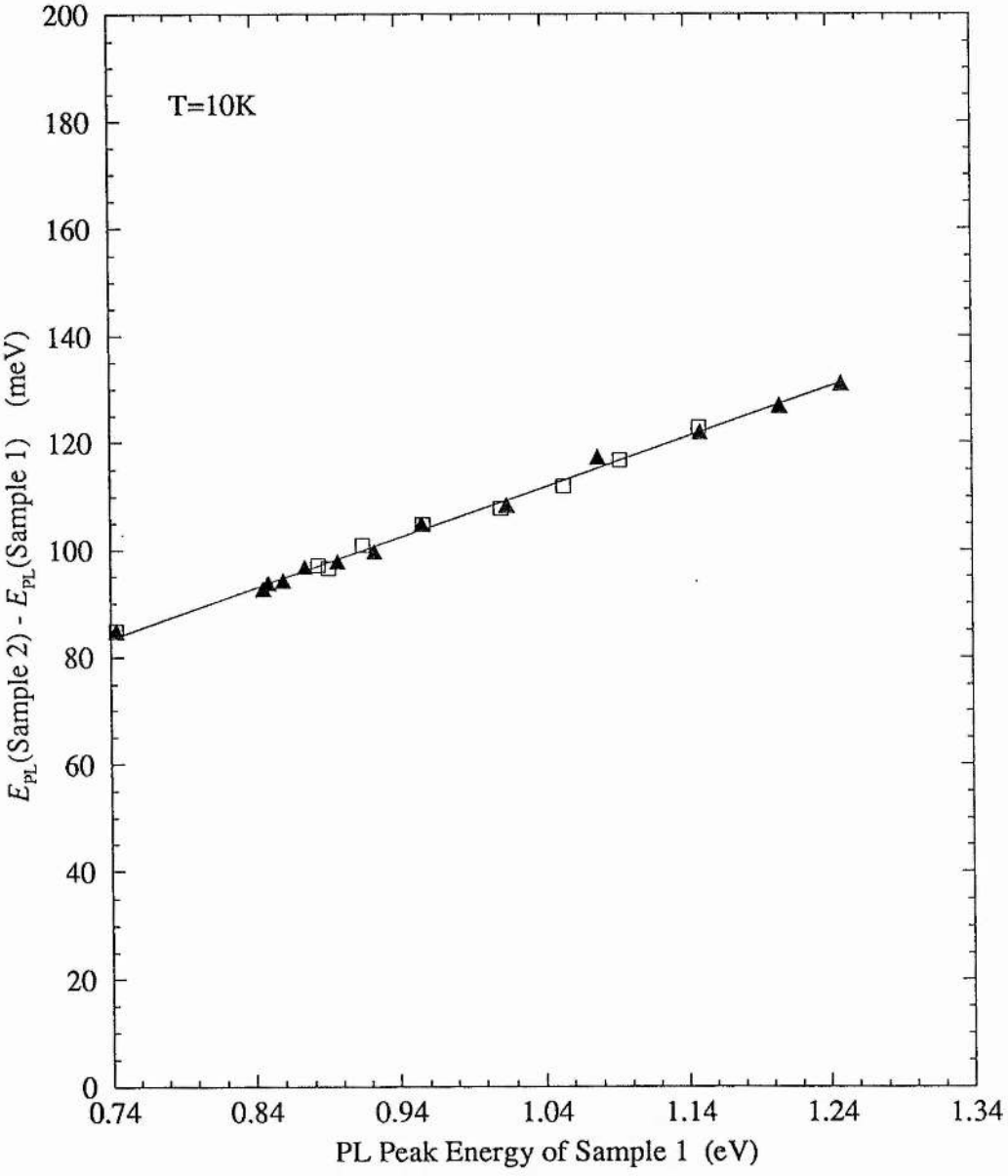

Figure 6.4 In this graph the energy difference between the PL peaks from samples 1 and 2 is plotted against the emission energy of sample 1. This type of plot gives an accurate measure of the difference in the pressure coefficients of sample 1 and sample 2.

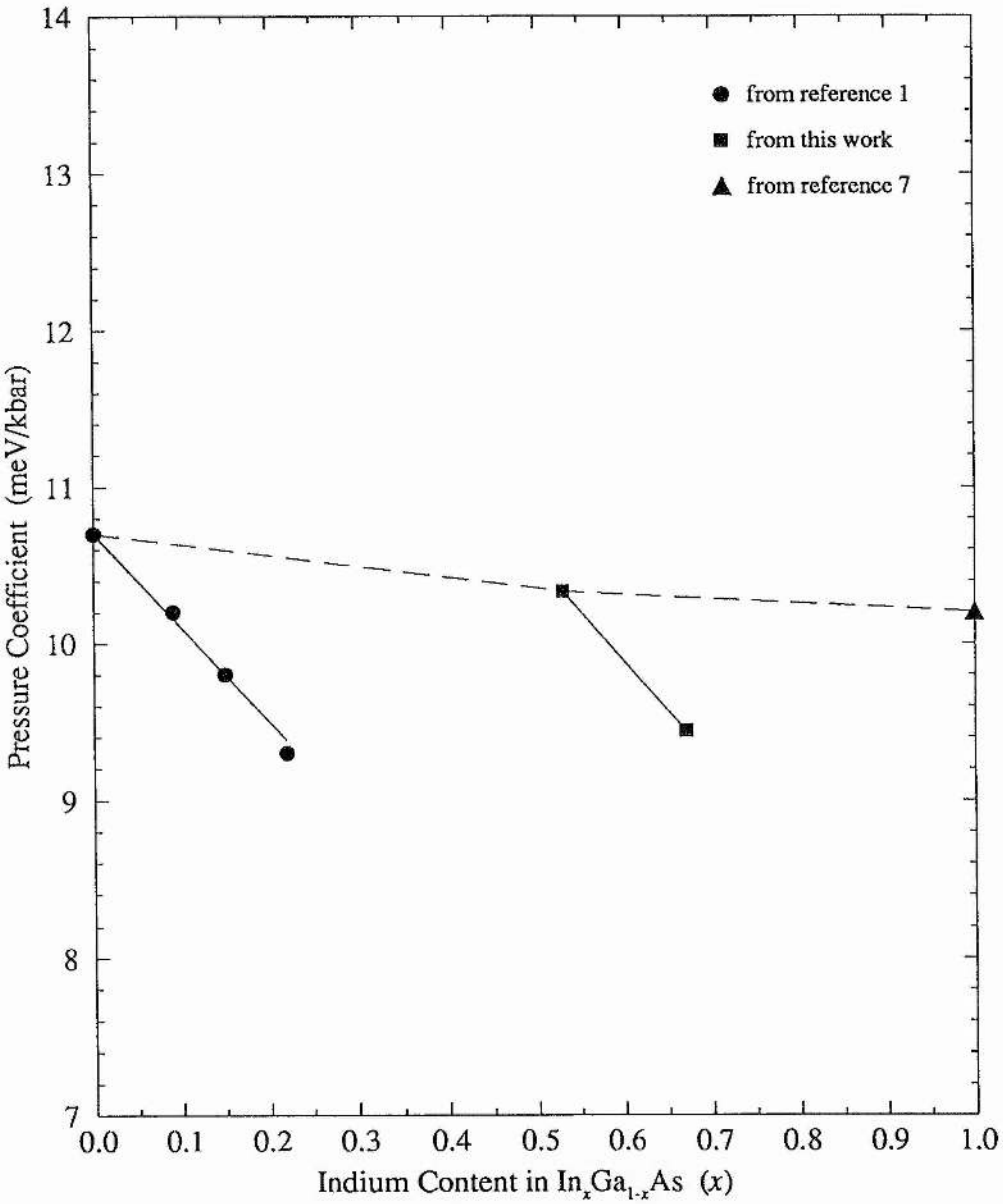

Figure 6.5 The pressure coefficients of $In_xGa_{1-x}As$ as a function of indium content, x. With the exception of the x=1 point, which is a bulk material value, these results all come from 100Å quantum-wells.

of 8.6±0.2%, in going from unstrained $In_{0.53}Ga_{0.47}As$ to 1% compressively strained $In_{0.67}Ga_{0.33}As$ corresponds very well to the 8.4% reduction, determined in reference 1, in going from unstrained GaAs to 1% strained $In_{0.15}Ga_{0.85}As$. These results therefore confirm the existence of anomalously low pressure coefficients in $In_xGa_{1-x}As$ quantum-wells grown on [001] oriented substrates. They also show that it is strain, rather than simply composition, which gives rise to the anomaly.

6.4.2 InGaAs/GaAs Quantum Well on [111] GaAs Substrate.

A high pressure PL experiment was carried out on sample 3, the 1% compressively strained $In_{0.15}Ga_{0.85}As$ quantum-well grown on a [111] oriented GaAs substrate. Figure 6.6(a) shows low temperature PL spectra from this sample at a pressure of 3kbar. A weak emission peak from the GaAs substrate can be seen; initially this was used to calibrate pressure (although a ruby pressure gauge was also loaded along with the sample). At a pressure of ~15kbar the intensity of the substrate emission became too weak to be followed and beyond this point pressure was measured using standard ruby fluorescence. Figure 6.6(b) shows the pressure dependence of the PL from sample 3. Upon initial application of hydrostatic pressure the PL peak was seen to move up in energy at a rate of +10.67±0.3meV/kbar. This value is very similar to the pressure coefficient of GaAs (+10.7meV/kbar)[20] and, within experimental error, agrees with the value that one obtains by linearly interpolating between the pressure coefficient of GaAs and that of InAs[7]. Above ~40kbar the PL intensity dropped by more than two orders of magnitude and the PL peak energy

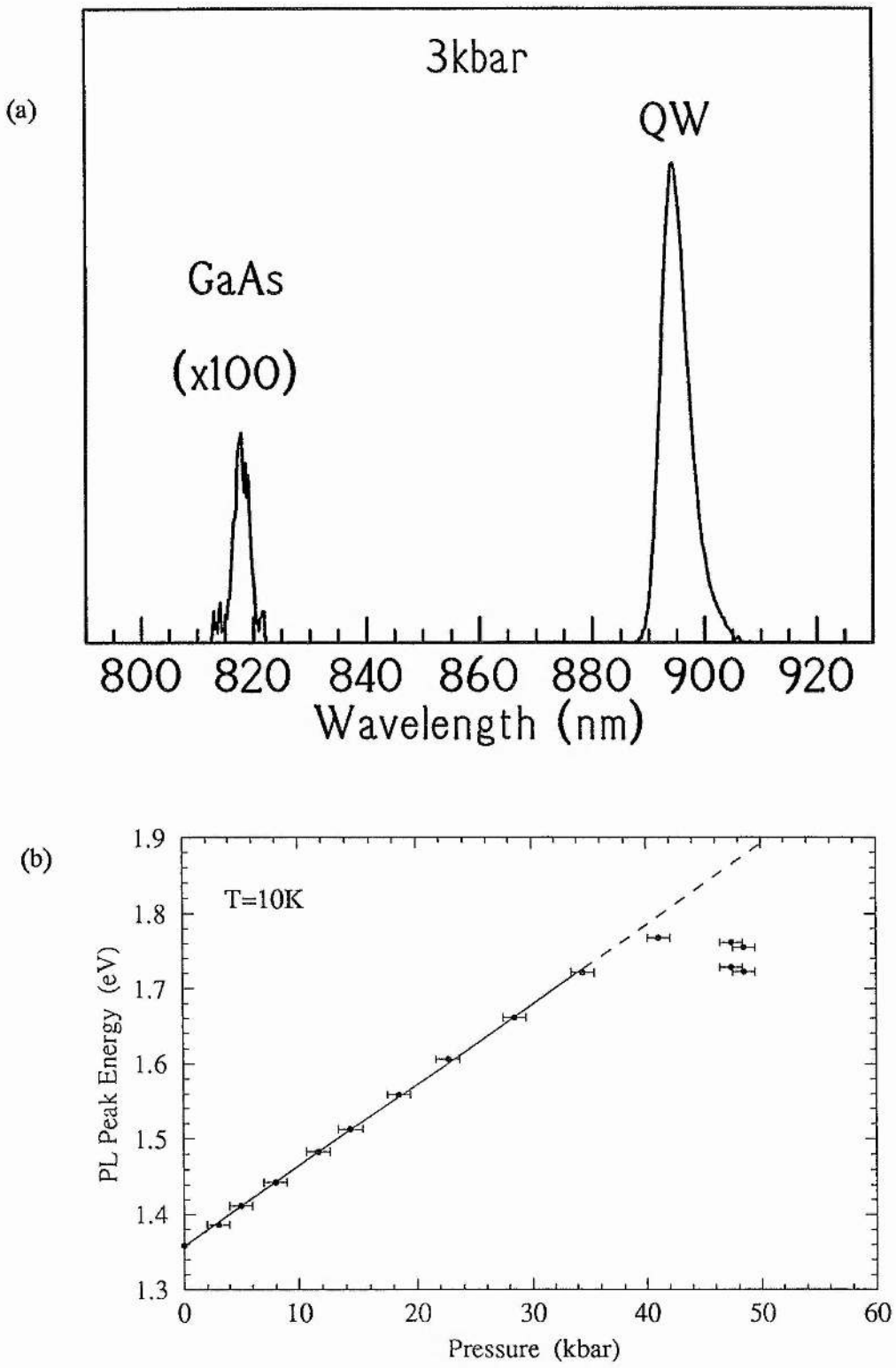

Figure 6.6 (a) The PL from sample 3 at 10K and 3kbar. A weak emission peak can be observed from the GaAs substrate, and (b) the PL peak energy as a function of pressure for sample 3.

began to decrease with pressure. A satellite peak was observed ~30meV below the main emission peak. This is all indicative of a Γ_c–X_c crossover having occurred (the position of satellite peak suggests that it results from an LO–X phonon-assisted transition[21]). However, the PL was very weak and could not be followed over a sufficient range of pressure to allow a determination of its pressure coefficient.

A more accurate measure of the difference between the direct band-gap pressure coefficient of sample 3 and that of GaAs can be obtained from figure 6.7. Here the energy difference between the quantum-well emission and the GaAs emission is plotted against the GaAs emission energy. A linear least-squares fit to the data gives a gradient of 0±0.01, which indicates that the pressure coefficient of sample 3 is the same as that of GaAs to within ±0.1 meV/kbar.

So, a 1% compressively strained $In_{0.15}Ga_{0.85}As$ quantum-well, grown on a [111] GaAs substrate, shows no sign of the anomalously low pressure coefficients found in compressively strained $In_xGa_{1-x}As$ quantum-wells grown on [001] substrates.

6.5 Experimental Results From InGaAs Under Tensile Strain.

Sample 4 was the first tensile sample to be studied under high pressure. This sample contained an unstrained $In_{0.53}Ga_{0.47}As$ quantum-well in addition to four $In_xGa_{1-x}As$ quantum-wells, each grown under a successively higher tensile strain. In order to separate their PL energies the widths of the strained quantum-wells were also varied, with the most highly strained well being the narrowest, and the least strained the widest. Full details of the sample design are contained in table 6.1. Low

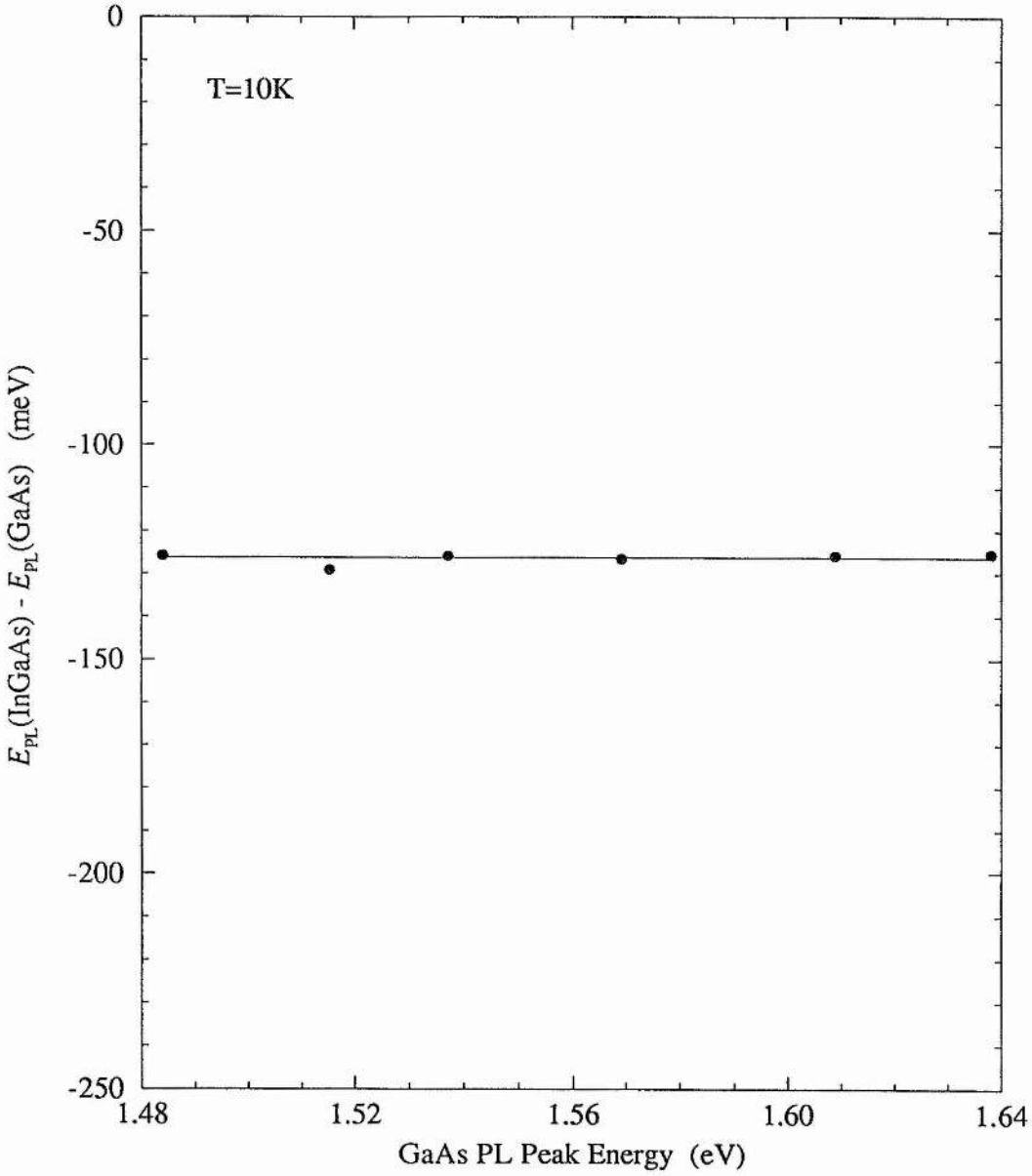

Figure 6.7 The difference in energy between the quantum-well PL and the GaAs substrate PL, plotted as a function of the GaAs emission energy, for sample 3.

temperature, ambient pressure PL from this sample is shown in figure 6.8 and the results of high pressure PL on this sample are shown in figure 6.9. In this graph the difference between the PL energy of the unstrained well and each of the strained wells is plotted as a function of the emission energy of the unstrained well. Clearly, from these results as they stand, it is not immediately possible to identify a simple trend in the behaviour of the pressure coefficients as a function of tensile strain. This is because, in addition to any possible anomalous strain effects, we also have to consider the effect of the different well-widths on the pressure coefficients.

The pressure coefficient of PL transitions between quantum-confined states is influenced by a number of factors (see section 2.3) including the difference in the pressure coefficients of the well and barrier materials, the pressure dependence of the band offsets and the variation of the effective mass of the electrons with pressure. In reference 1, by assuming a valence band offset which is independent of pressure and a linear increase in the effective mass of the electron with pressure, the high-pressure PL results from a series of compressively strained $In_{0.15}Ga_{0.85}As/GaAs$ quantum-wells of various widths were successfully modelled. It was found that it is the difference in the pressure coefficients of the well and barrier materials, and the proportion of the carrier wave function in each, that is the major cause of the variation of pressure coefficients with well-width.

So, before we can judge whether the pressure coefficients of the quantum-wells contained in sample 4 are anomalous we must first consider the expected behaviour, given their different well-widths. The dashed lines in figure 6.9 are the result of theoretical calculations (made using an eight-band Hamiltonian, with strain effects

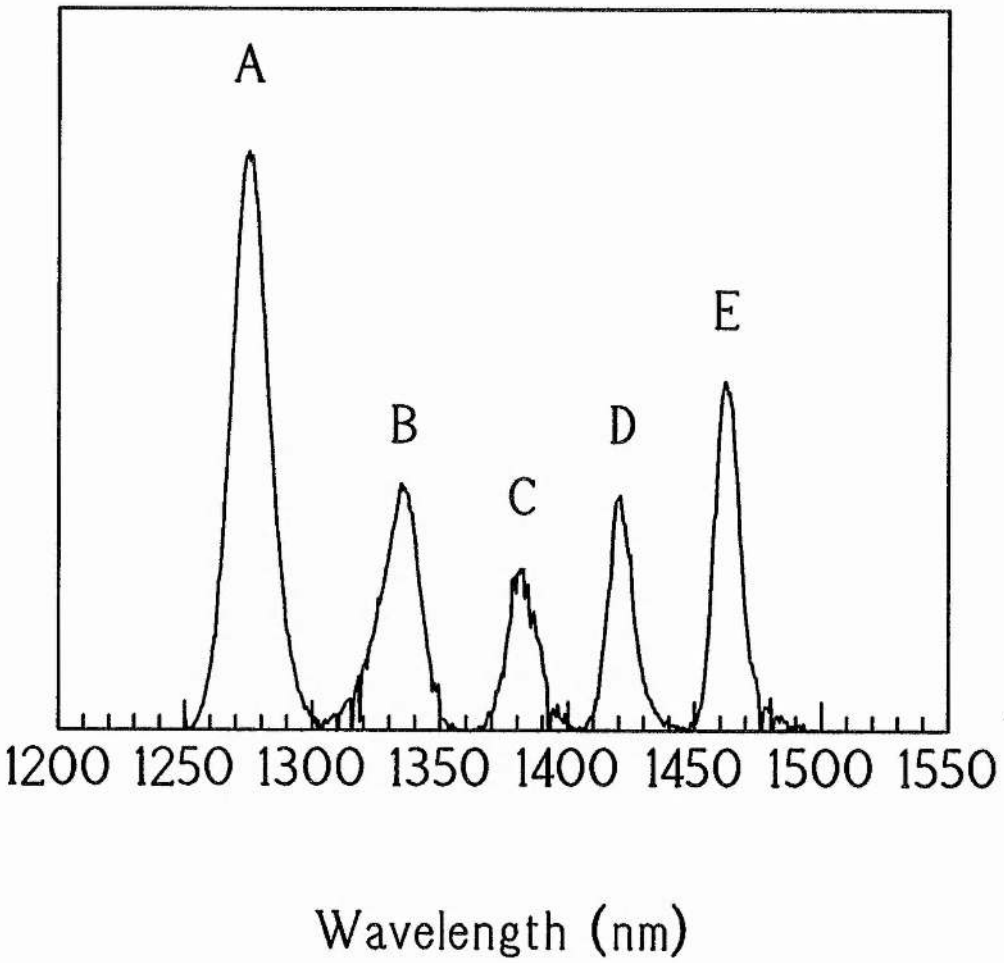

Figure 6.8 Ambient pressure PL from sample 4, recorded at 2K. The PL peaks correspond to the 40Å, −1% quantum-well (A); the 60Å, −0.75% well (B); the 80Å, −0.5% well (C); the 100Å, −0.25% well (D) and the 100Å, unstrained well (E).

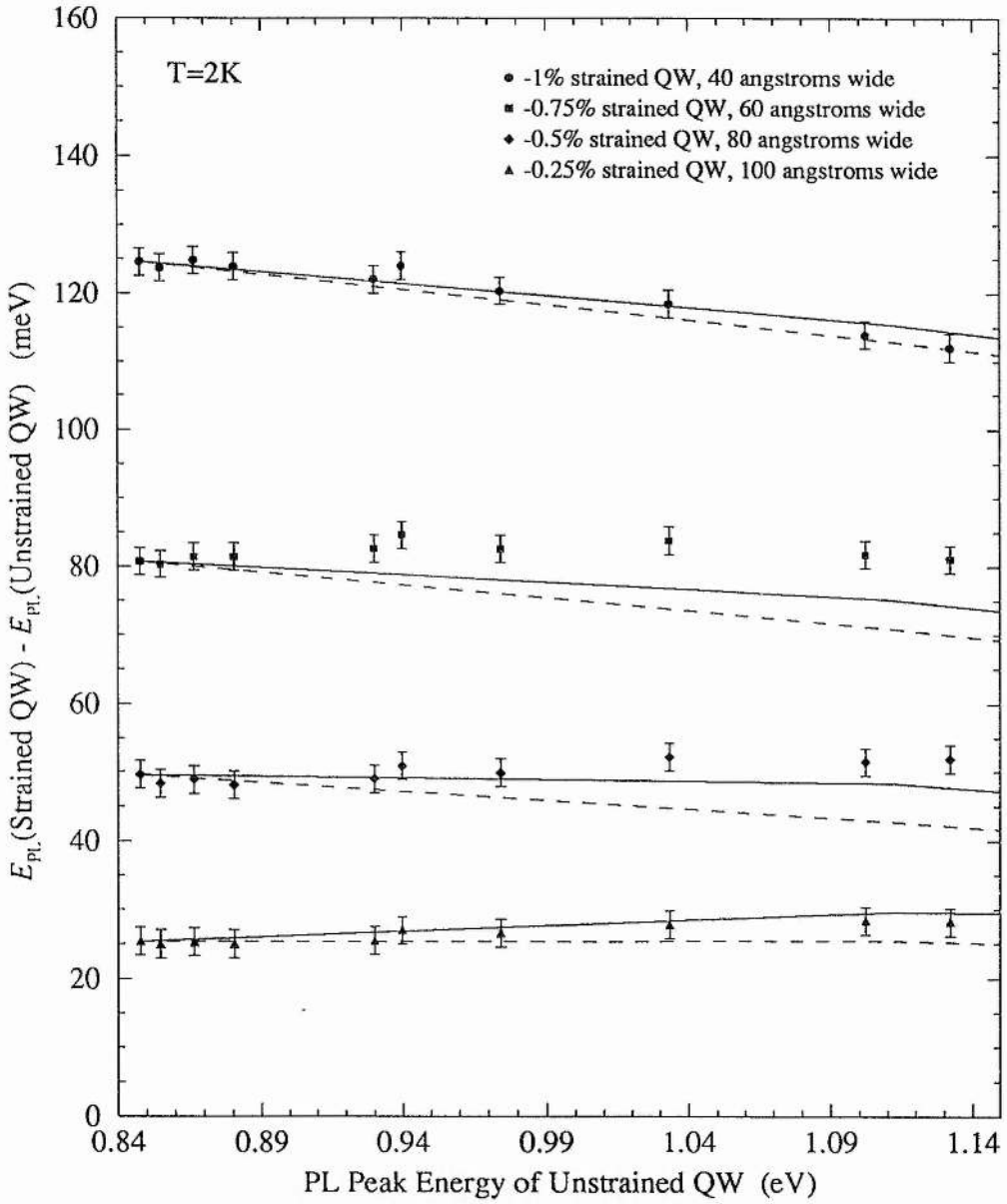

Figure 6.9 High pressure data from sample 4. For each of the strained quantum-wells the difference between its PL peak energy and that of the unstrained (reference) well is plotted against the emission energy of the unstrained quantum-well. The solid and dashed lines represent the expected behaviour, according to the different theoretical models discussed in the text.

included via the Pikus-Bir Hamiltonian) and show the expected variation of the pressure coefficients due to the different widths of the quantum-wells. It can be seen that, whilst this is in reasonable agreement with the experimental data from the 40Å and 100Å wells, it agrees poorly with the data from the 60Å and 80Å wells. So, does this indicate 'expected' or 'anomalous' behaviour? If a strain-dependent anomaly *is* present in these tensile wells it may, indeed, be least apparent in the 40Å and 100Å wells. In the 100Å well this is simply because the amount of tensile strain in this well is the smallest (-0.25%). In the 40Å well, however, this argument does not apply as the tensile strain is greater (-1%). Here, the apparent absence of an anomaly could be due to the narrowness of the quantum-well. In narrow quantum-wells the carrier wave function will penetrate the barrier material further and so the pressure coefficient of the quantum-well may be more influenced by the pressure coefficient of the barrier material than by the (possibly anomalous) pressure coefficient of the well material (see above). The solid lines in figure 6.9 result from theoretical calculations in which the same input parameters have been used as in the previous calculation, except that the pressure coefficient of the quantum-well material has been increased by +1meV/kbar per percent of tensile strain. This represents an anomaly equal in magnitude but opposite in sign (see below) to that found in the compressively strained material. It can be seen that there is now good agreement with the data from the 40Å and 100Å wells and, although still not a good fit, an improved fit to the data from the 60Å and 80Å wells. This currently represents the best theoretical fit to this data and further work is clearly required to explain the discrepancy between the experimental data and the theoretical calculations (see section 6.8).

One further tensile sample was investigated using high pressure PL. Sample 5 contained two tensile quantum-wells in addition to an unstrained $In_{0.53}Ga_{0.47}As$ well. However, with respect to sample 4, the trend of decreasing well-width with increasing tensile strain was reversed. The ambient pressure PL spectrum from sample 5 is shown in figure 6.10. It can be seen that the intensity of the PL peak from the 90Å, −1% strained quantum-well is less than that from the narrower strained well. As hydrostatic pressure was applied it became even less intense with respect to the other peak and eventually became lost in the low-energy tail of this peak. For this reason the PL from the -1% strained well could not be followed over the same range of pressure as the other strained well. In figure 6.11 the high pressure PL results from this sample are plotted in the same way as those from sample 4. The solid lines in this graph are the result of identical calculations to those carried out for sample 4 in which the pressure coefficient of the quantum-well material is assumed to have an 'anomaly' of +1meV/kbar per percent tensile strain. Once again, this currently represents the best theoretical fit to the data.

6.6 Discussion of High Pressure Photoluminescence Results.

The results from our high pressure PL investigation of strained InGaAs can be summarized as follows:

The pressure coefficients of compressively strained $In_xGa_{1-x}As$, grown on [001] oriented substrates, exhibit an anomalous strain-dependence of approximately −1meV/kbar per percent of strain. Compressively strained $In_{0.15}Ga_{0.85}As$ grown on a

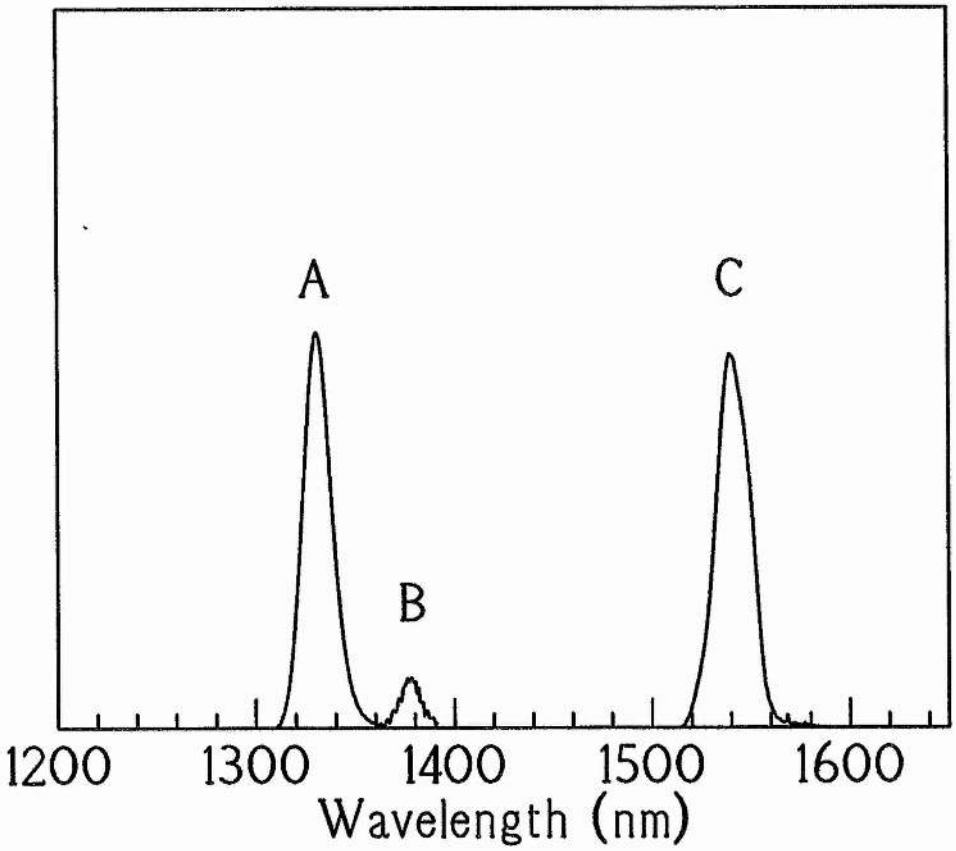

Figure 6.10 Ambient pressure PL from sample 5, recorded at 10K. The peak labelled A corresponds to the 40Å, -0.5% strained quantum-well. Peak B corresponds to the 90Å, -1% well and C is from the unstrained GaAs well.

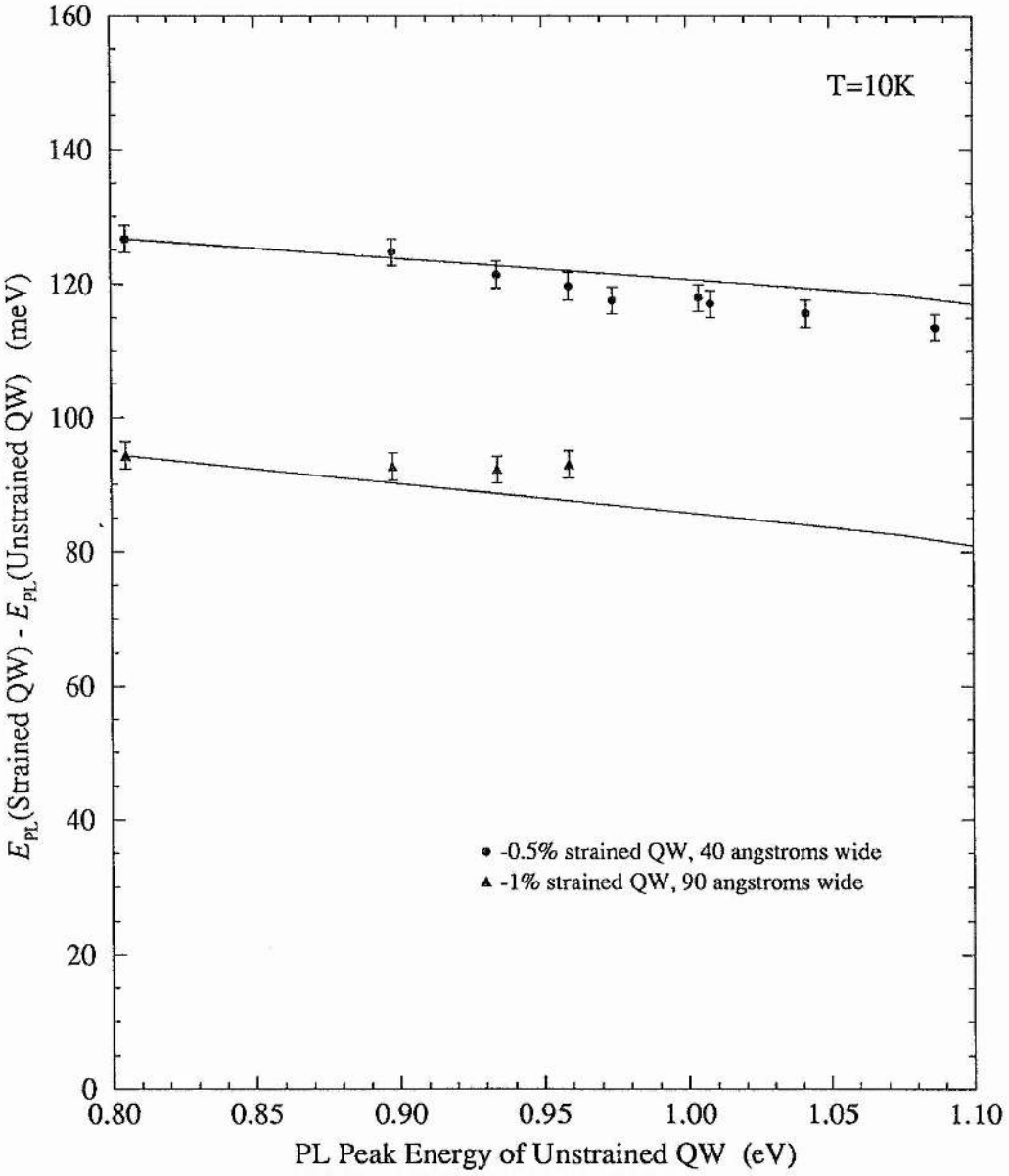

Figure 6.11 High pressure data from sample 5. For each of the strained wells the difference between its PL peak energy and that of the unstrained InGaAs well has been plotted against the emission energy of the unstrained InGaAs. The lines correspond to the expected behaviour, according to the model described in the text.

[111] oriented substrate, however, shows no such strain-dependence; the value of its pressure coefficient is equal to that one would expect from simple interpolation between the pressure coefficients of GaAs and InAs. Preliminary investigations of the pressure coefficients of $In_xGa_{1-x}As$ grown under tensile strain, on [001] substrates, are not conclusive but may indicate an anomaly similar in magnitude but opposite in sign to that found in the compressively strained system.

In addition to the PL data from the tensile samples there is further evidence, albeit indirect evidence, for suspecting that tensile strain will give rise to an increase, rather than a decrease, in pressure coefficients. This is illustrated in figure 6.12. It has been shown clearly that, on the compressive side, strain causes a reduction in pressure coefficients[1]. Furthermore, the dependence of pressure coefficient on compressive strain appears to be a linear one. Intuitively this suggests that if the anomaly continues on the tensile side the relationship will continue linearly, as illustrated by figure 6.12(a), and so have the effect of raising pressure coefficients. If the anomaly was the same on both the tensile and compressive sides then, based on the data from reference 1, we would have the situation illustrated by figure 6.12(b). This type of 'sawtooth' relationship is generally not expected from real physical situations; much more likely would be a curved relationship such as that illustrated in figure 6.12(c). However, as stated above, there is no evidence of such curvature in data from the compressively strained system.

Now, given the experimental data outlined above, we should consider the possible reasons for strain giving rise to unexpected pressure coefficients. Broadly speaking there are two distinct possibilities. The first is that the size and shape of the

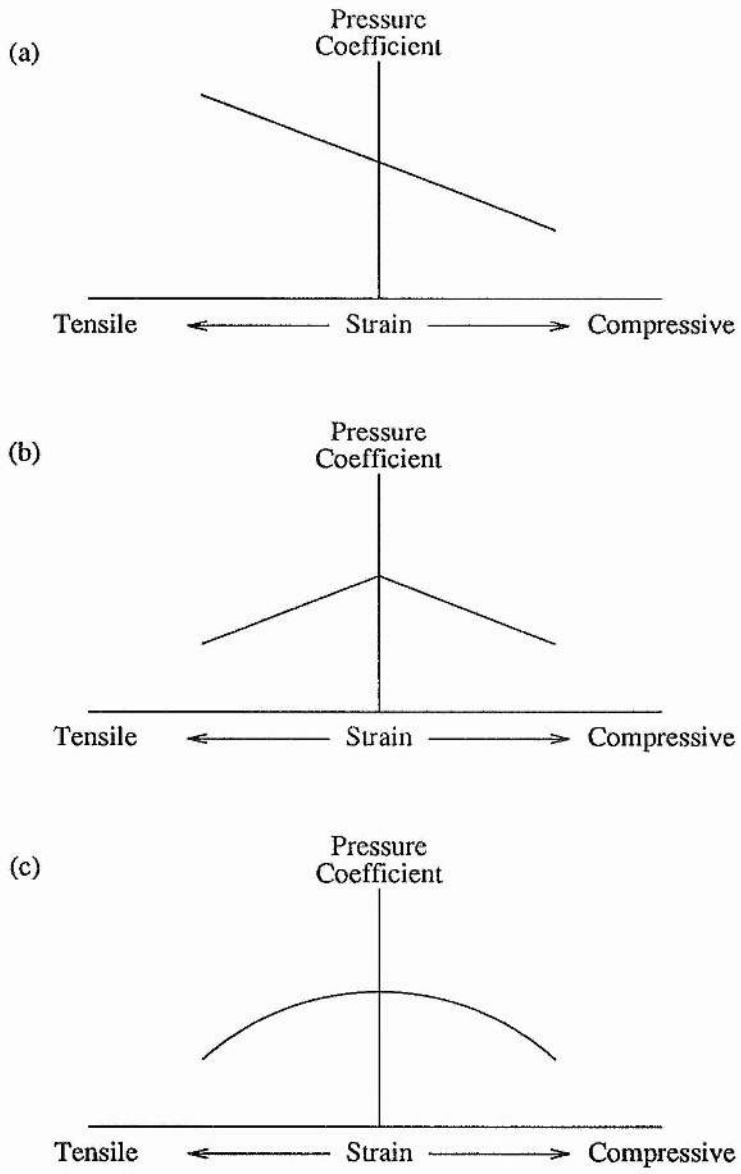

Figure 6.12 A schematic diagram showing possible trends in the relationship between pressure coefficient and strain. The different patterns of behaviour are discussed in the text.

unit cell of strained InGaAs, under hydrostatic pressure, is not as expected; in other words the elastic properties of the material are anomalous. The second possibility is that the electronic band-structure theory does not adequately describe the situation of combined hydrostatic and biaxial strains. So, we have to consider which of these options is best supported by the data. In this respect the most relevant finding is probably that the anomaly is found in the [001] oriented samples but not in the [111] oriented sample. If it is a band-structure problem giving rise to the anomalous pressure coefficients then why should it not do so regardless of substrate orientation? If, on the other hand, it is a problem related to the elastic properties of the material, which are not necessarily isotropic, then it is conceivable that there could be an elastic anomaly in the [001] orientation but not in the [111] orientation. In deciding whether we are dealing with a band-structure problem or an elasticity problem it is also interesting to consider the possible implications of each scenario when comparing behaviour of the tensile and compressively strained systems. First let us assume that the anomalous pressure coefficients are a result of the unexpected elastic behaviour of strained material. The fact that compressive strain causes a reduction in pressure coefficients implies that the volume of the InGaAs unit cell is reducing less than expected with pressure in the compressed layer. However, in pseudomorphic growth the strained layer is constrained in two dimensions by the substrate, so this means the reduced compressibility must be in the growth direction. In such a case it would seem reasonable that for a layer under tensile strain the opposite effect would apply; the layer would be more compressible in the growth direction and consequently the pressure coefficient would be increased. Now let us assume that the elastic properties

are completely normal and that anomalous pressure coefficients in strained material originate from unexpected behaviour in the electronic band-structure. Both tensile and compressive strain can be resolved into hydrostatic and shear components, the only difference being the sense of the shear component. In a bulk layer of cubic material the sense of the shear component shouldn't matter and so we would expect tensile strain to have the same effect as compressive strain, that is to lower the pressure coefficient.

Considering the arguments and the experimental data summarised above it would seem that the unexpected pressure coefficients measured in strained InGaAs are more likely to be the result of an elastic anomaly than an electronic anomaly. Further work is required, however, before this can be verified conclusively (see below).

6.7 Coarse Powder X-Ray Diffraction.

In order to try and establish whether the elastic properties of strained InGaAs are indeed anomalous, a programme of work has been started in which high-pressure X–ray powder-diffraction techniques will be used to measure directly the size and shape of the unit cell of strained InGaAs and the way in which it changes with hydrostatic pressure. The work has been carried out at the Daresbury Laboratory using the Synchrotron Radiation Source wiggler radiation and an Imaging Plate detector system. Initial measurements were carried out on a sample consisting of a 1000Å $In_{0.2}Ga_{0.8}As$ strained-layer, grown on a GaAs substrate (see section 6.3).

In conventional X–ray powder diffraction the sample is usually ground into a

powder sufficiently fine that continuous powder rings are obtained, without any bright spots resulting from individual crystallites. Integrating these powder rings around 2π gives intensity profiles from which lattice spacings can be obtained. However, the strained-layer samples that we wish to investigate present particular problems which require a modification of conventional techniques. The first problem is the very small volume of sample that can be utilised. As with all DAC experiments the available sample space is limited to approximately 250μm in diameter by 50μm deep. In addition, the strained $In_{0.2}Ga_{0.8}As$ material that we wish to study is in the form of an epilayer, only 1000Å thick, attached to a substrate of GaAs. So, even after thinning the sample to 10μm (by mechanical polishing of the substrate) the InGaAs represents only 1% of the total material. The second problem is that the powder rings from the InGaAs strained-layer and the GaAs substrate will be very close together since the lattice spacings of $In_{0.2}Ga_{0.8}As$ and GaAs differ only by about 1.4%. The width of the rings (which is determined by the instrument) therefore makes it difficult to distinguish between those originating from the InGaAs and those from the GaAs. These two problems combined to make it impossible to resolve the InGaAs data. It was found, however, that by making the powder relatively coarse the continuous rings were replaced by spotty rings in which bright spots, resulting from single crystallites, were randomly positioned around the diffraction rings. So, in a typical pattern there would be many bright spots originating from GaAs and a few bright spots originating from InGaAs. Crucially though, since they originate from different crystallites, the GaAs and InGaAs spots would rarely appear immediately adjacent to one another. So, by integrating only those segments of rings in which InGaAs spots were prevalent, it was

possible to produce intensity profiles in which the InGaAs peaks could be clearly distinguished from the GaAs peaks.

A certain amount of care has to be taken in preparing the coarse powder for such an experiment. Preparation by grinding is not suitable as this is likely to produce many crystallites consisting solely of GaAs and only a few which also contain the InGaAs layer. Also, if the powder is made too fine, InGaAs crystallites may even become separated from their substrate and so lose their misfit strain. Furthermore, grinding may give rise to dislocations in the material which could cause strain relaxation. Instead, samples were prepared by first polishing away the back of the substrate until a thickness of ~10μm was reached. The sample was then cleaved, using a razor blade under a microscope, into roughly 10μm cubes.

Composition and strain values deduced from 0kbar data, obtained using this technique, agree well with those from previous DXRD measurements of this sample. However, since most of our initial SRS beamtime was spent developing the technique we have not yet obtained high pressure X-ray data of sufficient quality for useful analysis.

6.8 Suggestions for Further Work.

A considerable amount of work remains to be done in this field. The importance of this work has less to do with the anomalous pressure coefficients themselves than with establishing the root cause of the anomaly and the further implications which it might have.

In terms of high pressure PL, work should be continued on the tensile InGaAs/GaAs system. Initially this means further work to explain the data already obtained, but more experiments may be required. The high-pressure X-ray diffraction work should be continued to establish directly whether the elastic properties of strained InGaAs are normal or anomalous. In conjunction with this, Raman spectroscopy could prove to be a useful tool in determining structural properties of strained materials, especially when they constitute quantum-wells or other heterostructures. If it turns out that the elastic behaviour is entirely normal then this would be a motivation for further theoretical work on the electronic band-structure of strained semiconductors.

6.9 References.

1. V.A.Wilkinson, A.D.Prins, J.D.Lambkin, E.P.O'Reilly, D.J.Dunstan and L.K.Howard, Phys. Rev. B, **42**, 3113 (1990)
2. P.J.A.Thijs, E.A.Montie, T.van Dongen and C.W.T.Bulle-Lieuwma, J. Crys. Growth, **105**, 339 (1990)
3. D.P.Bour, D.W.Treat, R.L.Thornton, T.L.Paoli, R.D.Bringans, B.S.Krusor, R.S.Geels, D.F.Welch and T.Y.Wang, J. Crys. Growth, **124**, 751 (1992)
4. J.S.Osinski, Y.Zou, P.Grodzinski, A.Mathur and P.D.Dapkus, IEEE Photonics Technol. Lett., **4**, 10 (1992)
5. I.Suemune, L.A.Coldren, M.Yamanishi and Y.Kan, Appl. Phys. Lett., **53**, 1378 (1988)
6. H.Q.Hou, L.J.Wang, R.M.Tang and J.M.Zhou, Phys. Rev. B, **42**, 2926 (1990)
7. Y.F.Tsay, S.S.Mitra and B.Bendow, Phys. Rev. B, **10**, 1 (1974)
8. W.Paul and D.M.Warschauer, *Solids Under Pressure*, (McGraw–Hill, New York, 1963)
9. A.D.Prins, J.D.Lambkin, E.P.O'Reilly, A.R.Adams, D.J.Dunstan, R.Pritchard, W.Truscott and K.E.Singer, *Proc. 20th Int. Conf. Phys. Semicond.*, Thessaloniki, Greece, 6th-11th August (1990)
10. R.J.Warburton, *Private Communication.*
11. H.Müller, R.Trommer, M.Cardona and P.Vogl, Phys. Rev. B, **21**, 4879 (1980)
12. C.S.Menoni, H.D.Hochheimer and I.L.Spain, Phys. Rev. B, **33**, 5896 (1986)
13. S.W.Tozer, D.J.Wolford, J.A.Bradley, D.Bour and G.B.Stringfellow, *19th Int.*

Conf. Phys. Semicond., ed. W.Zawadzki, 881 (1988)

14. M.Leroux, Semicond. Sci. Technol., **4**, 231 (1989)

15. J.D.Lambkin and D.J.Dunstan, Solid State Commun., **67**, 827 (1988)

16. A.R.Goñi, K.Strössner, K.Syassen and M.Cardona, Phys. Rev. B, **36**, 1581 (1987)

17. F.Murnaghan, *Proc. Nat. Acad. Sci. USA*, **30**, 244 (1944)

18. A.D.Prins and D.J.Dunstan, Datareview in *Properties of Indium Phosphide*, (EMIS Datareviews Series No.6, INSPEC), pg8 (1990)

19. A.D.Prins and D.J.Dunstan, Datareview in *Properties of Indium Phosphide*, (EMIS Datareviews Series No.6, INSPEC), pg373 (1990)

20. D.J.Wolford and J.A.Bradley, Solid State Commun., **53**, 1069 (1985)

21. Landolt-Börnstein, *Numerical Data and Functional Relationships in Science and Technology*, Group III, Vol. 17a, ed O.Madelung (Springer-Verlag, Berlin, 1982)

CHAPTER 7.

Conclusions.

The work described in this thesis has all been carried out using standard optical characterisation techniques in conjunction with high hydrostatic pressures generated using the diamond anvil cell. The DAC techniques that have been, and continue to be, developed here at Surrey have shown that high pressure is a perturbation technique that could be used as routinely, and by as many laboratories, as temperature-dependent studies are utilised currently. It is also worth noting that whilst this thesis is limited to investigations of III-V semiconductors, the potential applications of DAC techniques are numerous and span many disciplines outside physics.

During the course of this research high-pressure investigations have been carried out in a number of different III-V semiconductor systems.

The indirect band-gaps of a number of $In_xGa_{1-x}Sb$/GaSb quantum-wells have been measured. It has been shown that these results can be extrapolated to zero indium content (x=0) to give values for the indirect band-gaps of bulk GaSb. The values that we obtain agree, within experimental error, with currently accepted values but we cannot yet further refine these values due to errors associated with using ruby as a pressure calibrant. Suggestions are made for a method that will eliminate these errors.

In the AlGaInP materials system measurements have been made of both bulk and heterostructure properties. In bulk $(Al_xGa_{1-x})_{0.5}In_{0.5}P$ we have determined how the energies of the conduction band Γ and X minima vary with aluminium content (x). We have also put lower limits on the position of the L minima in this system and 1% compressively

strained $Ga_{0.38}In_{0.62}P$. Band-offsets have been measured in both the unstrained $Ga_{0.5}In_{0.5}P/(Al_xGa_{1-x})_{0.5}In_{0.5}P$ and 1% compressively strained $Ga_{0.38}In_{0.62}P/(Al_xGa_{1-x})_{0.5}In_{0.5}P$ systems as functions of x. Effects of atomic ordering on the Γ and X conduction band minima have also been investigated.

The phenomenon of anomalous pressure coefficients in strained $In_xGa_{1-x}As$ has been studied. Unexpectedly low direct band-gap pressure-coefficients, similar to those reported previously from InGaAs/GaAs quantum-wells, have been found in compressively strained InGaAs/InGaAsP quantum-wells grown on [001] InP substrates. It has been shown that the anomaly is a result of strain, rather than simply of composition. However, an InGaAs/GaAs quantum-well grown on a [111] oriented GaAs substrate showed no evidence of the anomaly. Results from InGaAs quantum-wells grown under tensile strain, whilst not definitive, suggest that tensile strain may give rise to an anomaly opposite in sign to that caused by compressive strain. The implications of these results on the precise nature of the cause of the anomaly have been discussed and a new technique of X-ray powder diffraction has been described which will be used to investigate one possible cause, namely anomalous elastic properties of strained InGaAs.

As the work described here demonstrates, in the field of semiconductor research high pressure is a powerful and versatile tool. It is worth pointing out, however, that the fundamental effect of hydrostatic pressure is simple and restricted; reducing the lattice-constant whilst maintaining the symmetry of the crystal. Much of the power and versatility of the technique comes from the careful design of suitable samples. In addition, the success of the technique is strongly dependent on the quality of the sample growth.